INSTITUTE OF PHYSICS PUBLISHING REPORTS ON PROGRESS IN PHYSICS

Rep. Prog. Phys. **69** (2006) 1–78 doi:10.1088/0034-4885/69/1/R01

Discrete-time modelling of musical instruments

Vesa Välimäki, Jyri Pakarinen, Cumhur Erkut and Matti Karjalainen

Laboratory of Acoustics and Audio Signal Processing, Helsinki University of Technology, PO Box 3000, FI-02015 TKK, Espoo, Finland

E-mail: Vesa.Valimaki@tkk.fi

Received 31 March 2005, in final form 1 September 2005
Published 17 October 2005
Online at stacks.iop.org/RoPP/69/1

Abstract

This article describes physical modelling techniques that can be used for simulating musical instruments. The methods are closely related to digital signal processing. They discretize the system with respect to time, because the aim is to run the simulation using a computer. The physics-based modelling methods can be classified as mass–spring, modal, wave digital, finite difference, digital waveguide and source–filter models. We present the basic theory and a discussion on possible extensions for each modelling technique. For some methods, a simple model example is chosen from the existing literature demonstrating a typical use of the method. For instance, in the case of the digital waveguide modelling technique a vibrating string model is discussed, and in the case of the wave digital filter technique we present a classical piano hammer model. We tackle some nonlinear and time-varying models and include new results on the digital waveguide modelling of a nonlinear string. Current trends and future directions in physical modelling of musical instruments are discussed.

Contents

1. Introduction

Musical instruments have historically been among the most complicated mechanical systems made by humans. They have been a topic of interest for physicists and acousticians for over a century. The modelling of musical instruments using computers is the newest approach to understanding how these instruments work.

This paper presents an overview of physics-based modelling of musical instruments. Specifically, this paper focuses on sound synthesis methods derived using the physical modelling approach. Several previously published tutorial and review papers discussed physical modelling synthesis techniques for musical instrument sounds [73, 129, 251, 255, 256, 274, 284, 294]. The purpose of this paper is to give a unified introduction to six main classes of discrete-time physical modelling methods, namely mass–spring, modal, wave digital, finite difference, digital waveguide and source–filter models. This review also tackles the mixed and hybrid models in which usually two different modelling techniques are combined.

Physical models of musical instruments have been developed for two main purposes: research of acoustical properties and sound synthesis. The methods discussed in this paper can be applied to both purposes, but here the main focus is sound synthesis. The basic idea of physics-based sound synthesis is to build a simulation model of the sound production mechanism of a musical instrument and to generate sound with a computer program or signal processing hardware that implements that model. The motto of physical modelling synthesis is that when a model has been designed properly, so that it behaves much like the actual acoustic instrument, the synthetic sound will automatically be natural in response to performance. In practice, various simplifications of the model cause the sound output to be similar to, but still clearly different from, the original sound. The simplifications may be caused by intentional approximations that reduce the computational cost or by inadequate knowledge of what is actually happening in the acoustic instrument. A typical and desirable simplification is the linearization of slightly nonlinear phenomena, which may avert unnecessary complexities, and hence may improve computational efficiency.

In speech technology, the idea of accounting for the physics of the sound source, the human voice production organs, is an old tradition, which has led to useful results in speech coding and synthesis. While the first experiments on physics-based musical sound synthesis were documented several decades ago, the first commercial products based on physical modelling synthesis were introduced in the 1990s. Thus, the topic is still relatively young. The research in the field has been very active in recent years.

One of the motivations for developing a physically based sound synthesis is that musicians, composers and other users of electronic musical instruments have a constant hunger for better digital instruments and for new tools for organizing sonic events. A major problem in digital musical instruments has always been how to control them. For some time, researchers of physical models have hoped that these models would offer more intuitive, and in some ways better, controllability than previous sound synthesis methods. In addition to its practical applications, the physical modelling of musical instruments is an interesting research topic for other reasons. It helps to resolve old open questions, such as which specific features in a musical instrument's sound make it recognizable to human listeners or why some musical instruments sound sophisticated while others sound cheap. Yet another fascinating aspect of this field is that when physical principles are converted into computational methods, it is possible to discover new algorithms. This way it is possible to learn new signal processing methods from nature.

2. Brief history

The modelling of musical instruments is fundamentally based on the understanding of their sound production principles. The first person attempting to understand how musical instruments work might have been Pythagoras, who lived in ancient Greece around 500 BC. At that time, understanding of musical acoustics was very limited and investigations focused on the tuning of string instruments. Only after the late 18th century, when rigorous mathematical methods such as partial differential equations were developed, was it possible to build formal models of vibrating strings and plates.

The earliest work on physics-based discrete-time sound synthesis was probably conducted by Kelly and Lochbaum in the context of vocal-tract modelling [145]. A famous early musical example is 'Bicycle Built for Two' (1961), where the singing voice was produced using a discrete-time model of the human vocal tract. This was the result of collaboration between Mathews, Kelly and Lochbaum [43]. The first vibrating string simulations were conducted in the early 1970s by Hiller and Ruiz [113, 114], who discretized the wave equation to calculate the waveform of a single point of a vibrating string. Computing 1 s of sampled waveform took minutes. A few years later, Cadoz and his colleagues developed discrete-time mass–spring models and built dedicated computing hardware to run real-time simulations [38].

In late 1970s and early 1980s, McIntyre, Woodhouse and Schumacher made important contributions by introducing simplified discrete-time models of bowed strings, the clarinet and the flute [173, 174, 235], and Karplus and Strong [144] invented a simple algorithm that produces string-instrument-like sounds with few arithmetic operations. Based on these ideas and their generalizations, Smith and Jaffe introduced a signal-processing oriented simulation technique for vibrating strings [120, 244]. Soon thereafter, Smith proposed the term 'digital waveguide' and developed the general theory [247, 249, 253].

The first commercial product based on physical modelling synthesis, an electronic keyboard instrument by Yamaha, was introduced in 1994 [168]; it used digital waveguide techniques. More recently, digital waveguide techniques have been also employed in MIDI synthesizers on personal computer soundcards. Currently, much of the practical sound synthesis is based on software, and there are many commercial and freely available pieces of synthesis software that apply one or more physical modelling methods.

3. General concepts of physics-based modelling

In this section, we discuss a number of physical and signal processing concepts and terminology that are important in understanding the modelling paradigms discussed in the subsequent sections. Each paradigm is also characterized briefly in the end of this section. A reader familiar with the basic concepts in the context of physical modelling and sound synthesis may go directly to section 4.

3.1. Physical domains, variables and parameters

Physical phenomena can be categorized as belonging to different 'physical domains'. The most important ones for sound sources such as musical instruments are the acoustical and the mechanical domains. In addition, the electrical domain is needed for electroacoustic instruments and as a domain to which phenomena from other domains are often mapped. The domains may interact with one another, or they can be used as analogies (equivalent models) of each other. Electrical circuits and networks are often applied as analogies to describe phenomena of other physical domains.

Quantitative description of a physical system is obtained through measurable quantities that typically come in pairs of variables, such as force and velocity in the mechanical domain, pressure and volume velocity in the acoustical domain or voltage and current in the electrical domain. The members of such dual variable pairs are categorized generically as 'across variable' or 'potential variable', such as voltage, force or pressure, and 'through variable' or 'kinetic variable', such as current, velocity or volume velocity. If there is a linear relationship between the dual variables, this relation can be expressed as a parameter, such as impedance $Z = U/I$ being the ratio of voltage U and current I, or by its inverse, admittance $Y = I/U$. An example from the mechanical domain is mobility (mechanical admittance) defined as the ratio of velocity and force. When using such parameters, only one of the dual variables is needed explicitly, because the other one is achieved through the constraint rule.

The modelling methods discussed in this paper use two types of variables for computation, 'K-variables' and 'wave variables' (also denoted as 'W-variables'). 'K' comes from Kirchhoff and refers to the Kirchhoff continuity rules of quantities in electric circuits and networks [185]. 'W' is the shortform for wave, referring to wave components of physical variables. Instead of pairs of across and through as with K-variables, the wave variables come in pairs of incident and reflected wave components. The details of wave modelling are discussed in sections 7 and 8, while K-modelling is discussed particularly in sections 4 and 10. It will become obvious that these are different formulations of the same phenomenon, and the possibility to combine both approaches in hybrid modelling will be discussed in section 10.

The decomposition into wave components is prominent in such wave propagation phenomena where opposite-travelling waves add up to the actual observable K-quantities. A wave quantity is directly observable only when there is no other counterpart. It is, however, a highly useful abstraction to apply wave components to any physical case, since this helps in solving computability (causality) problems in discrete-time modelling.

3.2. Modelling of physical structure and interaction

Physical phenomena are observed as structures and processes in space and time. In sound source modelling, we are interested in dynamic behaviour that is modelled by variables, while slowly varying or constant properties are parameters. Physical interaction between entities in space always propagates with a finite velocity, which may differ by orders of magnitude in different physical domains, the speed of light being the upper limit.

'Causality' is a fundamental physical property that follows from the finite velocity of interaction from a cause to the corresponding effect. In many mathematical relations used in physical models the causality is not directly observable. For example, the relation of voltage across and current through an impedance is only a constraint, and the variables can be solved only within the context of the whole circuit. The requirement of causality (more precisely the temporal order of the cause preceding the effect) introduces special computability problems in discrete-time simulation, because two-way interaction with a delay shorter than a unit delay (sampling period) leads to the 'delay-free loop problem'. The use of wave variables is advantageous, since the incident and reflected waves have a causal relationship. In particular, the wave digital filter (WDF) theory, discussed in section 8, carefully treats this problem through the use of wave variables and specific scheduling of computation operations.

Taking the finite propagation speed into account requires using a spatially distributed model. Depending on the case at hand, this can be a full three-dimensional (3D) model such as used for room acoustics, a 2D model such as for a drum membrane (discarding air loading) or a 1D model such as for a vibrating string. If the object to be modelled behaves homogeneously

enough as a whole, for example due to its small size compared with the wavelength of wave propagation, it can be considered a lumped entity that does not need a description of spatial dimensions.

3.3. Signals, signal processing and discrete-time modelling

In signal processing, signal relationships are typically represented as one-directional cause–effect chains. Contrary to this, bi-directional interaction is common in (passive) physical systems, for example in systems where the reciprocity principle is valid. In true physics-based modelling, the two-way interaction must be taken into account. This means that, from the signal processing viewpoint, such models are full of feedback loops, which further implicates that the concepts of computability (causality) and stability become crucial.

In this paper, we apply the digital signal processing (DSP) approach to physics-based modelling whenever possible. The motivation for this is that DSP is an advanced theory and tool that emphasizes computational issues, particularly maximal efficiency. This efficiency is crucial for real-time simulation and sound synthesis. Signal flow diagrams are also a good graphical means to illustrate the algorithms underlying the simulations. We assume that the reader is familiar with the fundamentals of DSP, such as the sampling theorem [242] to avoid aliasing (also spatial aliasing) due to sampling in time and space as well as quantization effects due to finite numerical precision.

An important class of systems is those that are linear and time invariant (LTI). They can be modelled and simulated efficiently by digital filters. They can be analysed and processed in the frequency domain through linear transforms, particularly by the Z-transform and the discrete Fourier transform (DFT) in the discrete-time case. While DFT processing through fast Fourier transform (FFT) is a powerful tool, it introduces a block delay and does not easily fit to sample-by-sample simulation, particularly when bi-directional physical interaction is modelled.

Nonlinear and time-varying systems bring several complications to modelling. Nonlinearities create new signal frequencies that easily spread beyond the Nyquist limit, thus causing aliasing, which is perceived as very disturbing distortion. In addition to aliasing, the delay-free loop problem and stability problems can become worse than they are in linear systems. If the nonlinearities in a system to be modelled are spatially distributed, the modelling task is even more difficult than with a localized nonlinearity. Nonlinearities will be discussed in several sections of this paper, most completely in section 11.

3.4. Energetic behaviour and stability

The product of dual variables such as voltage and current gives power, which, when integrated in time, yields energy. Conservation of energy in a closed system is a fundamental law of physics that should also be obeyed in true physics-based modelling. In musical instruments, the resonators are typically passive, i.e. they do not produce energy, while excitation (plucking, bowing, blowing, etc) is an active process that injects energy to the passive resonators.

The stability of a physical system is closely related to its energetic behaviour. Stability can be defined so that the energy of the system remains finite for finite energy excitations. From a signal processing viewpoint, stability may also be defined so that the variables, such as voltages, remain within a linear operating range for possible inputs in order to avoid signal clipping and distortion.

In signal processing systems with one-directional input–ouput connections between stable subblocks, an instability can appear only if there are feedback loops. In general, it is impossible

to analyse such a system's stability without knowing its whole feedback structure. Contrary to this, in models with physical two-way interaction, if each element is passive, then any arbitrary network of such elements remains stable.

3.5. Modularity and locality of computation

For a computational realization, it is desirable to decompose a model systematically into blocks and their interconnections. Such an object-based approach helps manage complex models through the use of the modularity principle. Abstractions to macro blocks on the basis of more elementary ones helps hiding details when building excessively complex models.

For one-directional interactions used in signal processing, it is enough to provide input and output terminals for connecting the blocks. For physical interaction, the connections need to be done through ports, with each port having a pair of K- or wave variables depending on the modelling method used. This follows the mathematical principles used for electrical networks [185]. Details on the block-wise construction of models will be discussed in the following sections for each modelling paradigm.

Locality of interaction is a desirable modelling feature, which is also related to the concept of causality. For a physical system with a finite propagation speed of waves, it is enough that a block interacts only with its nearest neighbours; it does not need global connections to compute its task and the effect automatically propagates throughout the system.

In a discrete-time simulation with bi-directional interactions, delays shorter than a unit delay (including zero delay) introduce the delay-free loop problem that we face several times in this paper. While it is possible to realize fractional delays [154], delays shorter than the unit delay contain a delay-free component. There are ways to make such 'implicit' systems computable, but the cost in time (or accuracy) may become prohibitive for real-time processing.

3.6. Physics-based discrete-time modelling paradigms

This paper presents an overview of physics-based methods and techniques for modelling and synthesizing musical instruments. We have excluded some methods often used in acoustics, because they do not easily solve the task of efficient discrete-time modelling and synthesis. For example, the finite element and boundary element methods (FEM and BEM) are generic and powerful for solving system behaviour numerically, particularly for linear systems, but we focus on inherently time-domain methods for sample-by-sample computation.

The main paradigms in discrete-time modelling of musical instruments can be briefly characterized as follows.

3.6.1. Finite difference models. In section 4 finite difference models are the numerical replacement for solving partial differential equations. Differentials are approximated by finite differences so that time and position will be discretized. Through proper selection of discretization to regular meshes, the computational algorithms become simple and relatively efficient. Finite difference time domain (FDTD) schemes are K-modelling methods, since wave components are not explicitly utilized in computation. FDTD schemes have been applied successfully to 1D, 2D and 3D systems, although in linear 1D cases the digital waveguides are typically superior in computational efficiency and robustness. In multidimensional mesh structures, the FDTD approach is more efficient. It also shows potential to deal systematically with nonlinearities (see section 11). FDTD algorithms can be problematic due to lack of numerical robustness and stability, unless carefully designed.

3.6.2. Mass–spring networks. In section 5 mass–spring networks are a modelling approach, where the intuitive basic elements in mechanics—masses, springs and damping elements—are used to construct vibrating structures. It is inherently a K-modelling methodology, which has been used to construct small- and large-scale mesh-like and other structures. It has resemblance to FDTD schemes in mesh structures and to WDFs for lumped element modelling. Mass–spring networks can be realized systematically also by WDFs using wave variables (section 8).

3.6.3. Modal decomposition methods. In section 6 modal decomposition methods represent another approach to look at vibrating systems, conceptually from a frequency-domain viewpoint. The eigenmodes of a linear system are exponentially decaying sinusoids at eigenfrequencies in the response of a system to impulse excitation. Although the thinking by modes is normally related to the frequency domain, time-domain simulation by modal methods can be relatively efficient, and therefore suitable to discrete-time computation. Modal decomposition methods are inherently based on the use of K-variables. Modal synthesis has been applied to make convincing sound synthesis of different musical instruments. The functional transform method (FTM) is a recent development of systematically exploiting the idea of spatially distributed modal behaviour, and it has also been extended to nonlinear system modelling.

3.6.4. Digital waveguides. Digital waveguides (DWGs) in section 7 are the most popular physics-based method of modelling and synthesizing musical instruments that are based on 1D resonators, such as strings and wind instruments. The reason for this is their extreme computational efficiency in their basic formulations. DWGs have been used also in 2D and 3D mesh structures, but in such cases the wave-based DWGs are not superior in efficiency. Digital waveguides are based on the use of travelling wave components; thus, they form a wave modelling (W-modelling) paradigm[1]. Therefore, they are also compatible with WDFs (section 8), but in order to be compatible with K-modelling techniques, special conversion algorithms must be applied to construct hybrid models, as discussed in section 10.

3.6.5. Wave digital filters. WDFs in section 8 are another wave-based modelling technique, originally developed for discrete-time simulation of analog electric circuits and networks. In their original form, WDFs are best suited for lumped element modelling; thus, they can be easily applied to wave-based mass–spring modelling. Due to their compatibility with digital waveguides, these methods complement each other. WDFs have also been extended to multidimensional networks and to systematic and energetically consistent modelling of nonlinearities. They have been applied particularly to deal with lumped and nonlinear elements in models, where wave propagation parts are typically realized by digital waveguides.

3.6.6. Source–filter models. In section 9 source–filter models form a paradigm between physics-based modelling and signal processing models. The true spatial structure and bi-directional interactions are not visible, but are transformed into a transfer function that can be realized as a digital filter. The approach is attractive in sound synthesis because digital filters are optimized to implement transfer functions efficiently. The source part of a source–filter model is often a wavetable, consolidating different physical or synthetic signal components needed to feed the filter part. The source–filter paradigm is frequently used in combination with other modelling paradigms in more or less ad hoc ways.

[1] The term digital waveguide is used also to denote K-modelling, such as FDTD mesh-structures, and source–filter models derived from travelling wave solutions, which may cause methodological confusion.

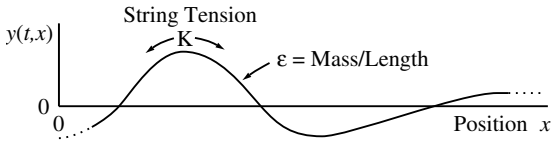

Figure 1. Part of an ideal vibrating string.

4. Finite difference models

The finite difference schemes can be used for solving partial differential equations, such as those describing the vibration of a string, a membrane or an air column inside a tube [264]. The key idea in the finite difference scheme is to replace derivatives with finite difference approximations. An early example of this approach in physical modelling of musical instruments is the work done by Hiller and Ruiz in the early 1970s [113, 114]. This line of research has been continued and extended by Chaigne and colleagues [45, 46, 48] and recently by others [25, 26, 29, 30, 81, 103, 131].

The finite difference approach leads to a simulation algorithm that is based on a difference equation, which can be easily programmed with a computer. As an example, let us see how the basic wave equation, which describes the small-amplitude vibration of a lossless, ideally flexible string, is discretized using this principle. Here we present a formulation after Smith [253] using an ideal string as a starting point for discrete-time modelling. A more thorough continuous-time analysis of the physics of strings can be found in [96].

4.1. Finite difference model for an ideal vibrating string

Figure 1 depicts a snapshot of an ideal (lossless, linear, flexible) vibrating string by showing the displacement as a function of position.

The wave equation for the string is given by

$$K y'' = \epsilon \ddot{y}, \tag{1}$$

where the definitions for symbols are $K \hat{=}$ string tension (constant), $\epsilon \hat{=}$ linear mass density (constant), $y \hat{=} y(t, x) =$ string displacement, $\dot{y} \hat{=} (\partial/\partial t)y(t, x) =$ string velocity, $\ddot{y} \hat{=} (\partial^2/\partial t^2)y(t, x) =$ string acceleration, $y' \hat{=} (\partial/\partial x)y(t, x) =$ string slope and $y'' \hat{=} (\partial^2/\partial x^2)y(t, x) =$ string curvature.

Note that the derivation of equation (1) assumes that the string slope has a value much less than 1 at all times and positions [96].

There are many techniques for approximating the partial differential terms with finite differences. The three most common replacements are the forward difference approximation,

$$f' \approx \frac{f(x + \Delta x) - f(x)}{\Delta x}, \tag{2}$$

the central difference approximation,

$$f' \approx \frac{f(x + \Delta x) - f(x - \Delta x)}{2\Delta x} \tag{3}$$

and the backward difference approximation,

$$f' \approx \frac{f(x) - f(x - \Delta x)}{\Delta x}. \tag{4}$$

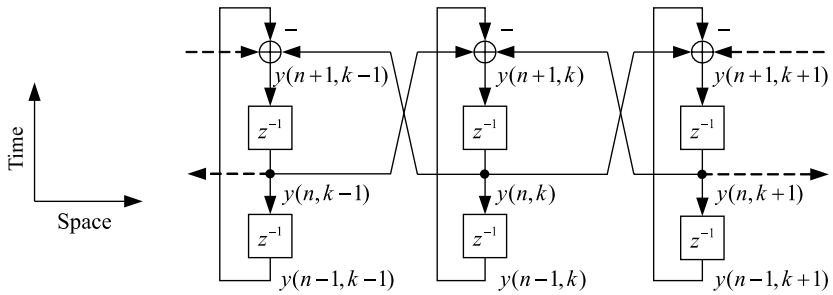

Figure 2. Block diagram of a finite difference approximation of the wave equation according to (8). The diagram shows how the next displacement value of the current position $y(n+1,k)$ is computed from the present values of its neighbours, $y(n,k-1)$ and $y(n,k+1)$, and the previous value $y(n-1,k)$. The block z^{-1} indicates a delay of one sampling interval.

Using the forward and backward difference approximations for the second partial derivatives and using indices n and k for the temporal and spatial points, respectively, yields the following version of the wave equation:

$$\frac{y(n+1,k)-2y(n,k)+y(n-1,k)}{T^2} = c^2\frac{y(n,k+1)-2y(n,k)+y(n,k-1)}{X^2}, \tag{5}$$

where T and X are the temporal and spatial sampling intervals, respectively, and

$$c = \sqrt{K/\epsilon} \tag{6}$$

is the propagation velocity of the transversal wave. We may select the spatial and the temporal sampling intervals so that

$$R = \frac{cX}{T} \leqslant 1, \tag{7}$$

that is, the waves in the discrete model do not propagate faster than one spatial interval at each time step. Here, R is called the Courant number and the inequality is known as the Courant–Friedrichs–Levy condition. Interestingly, the Von Neumann stability analysis (see, e.g. [264]) gives the same condition for R in the case of an ideal vibrating string. Now, by setting $R = 1$ it is easy to write (5) in the form that shows how the next displacement value $y(n+1,k)$ is computed from the present and the past values:

$$y(n+1,k) = y(n,k+1)+y(n,k-1)-y(n-1,k). \tag{8}$$

The recurrence equation (8) is also known as the leapfrog recursion. Figure 2 illustrates this update rule as a signal-processing block diagram, as suggested by Karjalainen [127]. The value of spatial index k increases to the right while the temporal index n increases upwards. The diagram shows how the next displacement value of the current position $y(n+1,k)$ is computed from the present values of its neighbours, $y(n,k-1)$ and $y(n,k+1)$, and the previous value $y(n-1,k)$. The diagram also indicates that the update rule is the same for all elements.

Equation (8) can conveniently be depicted using a spatio-temporal grid, a common illustration for FDTD schemes, depicted in figure 3. Here, the horizontal axis represents the spatial coordinate (i.e. position on the string) and the vertical axis represents the temporal coordinate (i.e. the time instant). Barjau and Gibiat have investigated the similarities and differences of the finite difference scheme and cellular automation schemes [18].

The finite difference model is a K method, i.e. it directly uses the physical variables as parameters, which can then be obtained from the physical system. Sound synthesis is possible, since the time-domain signal can be observed at one or several points in the system and then

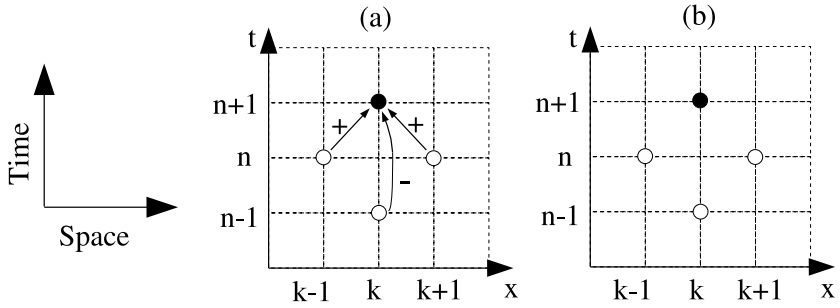

Figure 3. (*a*) Illustration of the 1D finite difference equation of an ideal string on a spatio-temporal grid. The vertical axis denotes the time, while the horizontal axis denotes the spatial location on the string. The left-hand side of equation (8) is presented with a black dot, while the values used in the right-hand side of equation (8) are presented as blank dots. The arrows in (*a*) denote the arithmetic operators of the equation and are usually left out, thus leading to a simplified form, illustrated in (*b*).

converted to an audio signal. Interaction at any discrete point or at many points along the spatial dimension is also allowed. A disadvantage is that the value of all points must be updated and stored individually for every sample time. This renders the model computationally expensive when there are many spatial sampling points.

4.2. Boundary conditions and string excitation

Since the spatial coordinate k of the string must lie between 0 and L_{nom}, which is the nominal length of the string, problems arise near the ends of the string when evaluating equation (8), because spatial points outside the string are needed. The problem can be solved by introducing boundary conditions that define how to evaluate the string movement when $k = 0$ or $k = L_{\mathrm{nom}}$. The simplest approach, introduced already in [113], would be to assume that the string terminations be rigid, so that $y(n, 0) = y(n, L_{\mathrm{nom}}) = 0$. This results in a phase-inverting termination, which suits perfectly the case of an ideal string. A noninverting termination of a finite difference system is discussed in [127].

For a more realistic string termination model, several solutions have been introduced. In [113], Hiller and Ruiz formulate boundary conditions for a lossy termination including reflection coefficients r_{l} and r_{r} for the left and right termination, respectively,

$$y(n+1, 0) = (1 - r_{\mathrm{l}})y(n, 1) + r_{\mathrm{l}}y(n-1, 0) \tag{9}$$

and

$$y(n+1, L_{\mathrm{nom}}) = (1 - r_{\mathrm{r}})y(n, L_{\mathrm{nom}} - 1) + r_{\mathrm{r}}y(n-1, L_{\mathrm{nom}}). \tag{10}$$

If the supports are lossless, i.e. if there is a perfect reflection at the boundaries, r_{l} and r_{r} will equal unity; in general, however, they will be numbers between 0 and 1. For a guitar-like string termination, where the string is clamped just behind the bridge, it is assumed [45] that the string termination point and the bridge share the same displacement, leading to

$$y(n, L_{\mathrm{nom}} - 1) = y(n, L_{\mathrm{nom}}). \tag{11}$$

The excitation of an FDTD string can also be implemented in several ways. If a plucked string is to be modelled, probably the simplest way to excite an FDTD string is to set its initial shape to match the displaced string prior to the release and then carry on with the simulation.

If the initial shape $y(0, k)$ of the FDTD string is set to resemble, e.g. the triangular form of a plucked string, and if we assume that the string has no initial velocity, the string displacement at time instant $n = 1$ must be set to [113]

$$y(1, k) = \begin{cases} y(0, k), & k = 0, 1, \ldots, L_{\text{nom}}, \quad k \neq j, j+1, \\ \frac{1}{2}[y(0, k-1) + y(0, k+1)], & k = j, j+1, \end{cases} \tag{12}$$

where j and $j+1$ denote the coordinates of the slope discontinuity (i.e. the peak of the triangle). In a way, this points out the 'correct direction' for the string vibration after the initialization. It must be noted, however, that if the spatial resolution of the string model is high, the vertex of the triangle must be smoothed to avoid slope discontinuities that might cause problems with high frequency partials and grid dispersion [45], an undesired property in FDTD models.

The plucking of a real string is, however, a more complex scheme than simply releasing the string from its initial shape. The properties of the finger or a plectrum alter the behaviour of the string, and measurements reveal that the release is rather gradual than instantaneous [192,193]. More advanced excitation models for FDTD strings have been suggested, e.g. in [45, 81]. A simple but useful FDTD string excitation method, which allows for interaction with the string during run-time has been proposed in [127]. There,

$$y(n, k) \leftarrow y(n, k) + \tfrac{1}{2}u(n) \tag{13}$$

and

$$y(n, k+1) \leftarrow y(n, k+1) + \tfrac{1}{2}u(n) \tag{14}$$

are inserted into the string, which causes a 'boxcar' block function to spread in both directions from the excitation point pair. Here, $u(n)$ denotes the external excitation signal.

4.3. Finite difference approximation of a lossy string

Frequency-independent losses can be modelled in a finite difference string by discretizing the velocity-dependent damping term in the lossy 1D wave equation

$$Ky'' = \epsilon\ddot{y} + d_1\dot{y} - d_2\dot{y}'', \tag{15}$$

where d_1 and d_2 are coefficients that represent the frequency-independent and frequency-dependent damping, respectively. Note that we have written the last term of equation (15) as a mixed time-space derivative instead of a third-order time derivative as, for example, in [45, 46, 113]. This is done because it can be shown [25] that having the third-order time derivative term in the lossy wave equation makes the system ill-posed and can lead into numerical instability, if the temporal and spatial sampling frequencies are high enough. It is also important to note that, in any case, the loss terms in equation (15) are only approximating the damping behaviour in a real string. A more sophisticated damping model is discussed, for instance, in [50, 156].

The first-order temporal derivative can be approximated using the central difference scheme (3), so that the recurrence equation (8) yields [45]

$$y(n+1, k) = g_k[y(n, k+1) + y(n, k-1)] - a_k y(n-1, k), \tag{16}$$

where

$$g_k = \frac{1}{1 + d_1 T/2} \tag{17}$$

and

$$a_k = \frac{1 - d_1 T/2}{1 + d_1 T/2}. \tag{18}$$

Note that in this case $d_2 = 0$ in equation (15). The string decay time can now be directly controlled via the damping coefficient d_1, since $d_1 = 1/(2\tau)$, where τ is the time constant for which the amplitude of the vibration decays to $1/e$ of its initial value.

Modelling the frequency-dependent losses is, however, a more demanding task. Discretizing equation (15) using the backward difference scheme for the temporal derivative in the last term and the central difference scheme for other terms, an explicit recurrence equation is obtained, as shown in [25].

4.4. Stiffness in finite difference strings

The dispersive behaviour of strings is best simulated in FDTD models by directly discretizing the stiff 1D wave equation

$$Ky'' = \epsilon\ddot{y} + \frac{E\pi r_s^4}{4} y'''', \tag{19}$$

where E is Young's modulus and r_s is the cross-sectional radius of the string. This leads to a recurrence equation containing three additional spatio-temporal terms in the discretized wave equation. The recurrence equation for stiff strings has been covered in several previous studies (e.g. [45, 113]).

5. Mass–spring networks

The mass–spring networks work primarily in the mechanical domain and use a dual-pair of K-variables, such as position and velocity or force and velocity. In this technique, the physical system to be modelled is divided into lumped mass elements which are connected by springs and dampers (links). The mass elements correspond to the nodes of a network and are the smallest modules representing inertia. The links represent physical interactions between them. The network of lumped mass elements, connected by links, approximates the behaviour of a distributed system. Each element is discretized using finite differences (see section 4) and operates locally. The fundamental difference between the finite difference and the mass–spring networks techniques is that a network is built by connecting the modules, rather than discretizing the governing equation for each case. Delay-free loops are avoided by imposing a causality in the ordering of the operations. Usually, a delay is inserted between the computation of a K-pair, and the two-way interactions are computed in an interleaved fashion.

The principles of mass–spring networks were introduced for musical instrument modelling by Cadoz and his colleagues within their system CORDIS-ANIMA [38, 98]. CORDIS-ANIMA is a physically-based formalism that allows modelling of objects prior to any sensory (audio, visual, gestural) modalities. The developments, achievements and results related to the CORDIS-ANIMA in a large time-span are outlined in a recent review paper by Cadoz and his colleagues [39].

The mass–spring networks are nowadays also referred to as 'mass-interaction','cellular' or 'particle' systems. Besides CORDIS-ANIMA, several other systems are built upon this basic idea by relying on similar concepts but by placing additional constraints on computation, sound generation or control. These systems are PhyMod [261], PMPD [109, 110], TAO [194, 195] and CYMATIC [116].

In this section, we first present the basic principles of the mass–spring network systems by considering a simple example in continuous time, then discuss the discretization and implementation of this mechanical system. Our primary focus is on CORDIS-ANIMA, and we consider other implementations by emphasizing their differences from CORDIS-ANIMA.

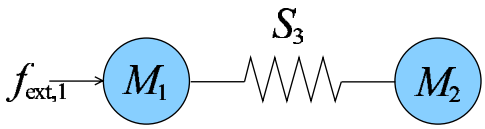

Figure 4. A simple, continuous time mechanical system of two masses and a spring. (This figure is in colour only in the electronic version)

5.1. Basic theory

A system is a collection of objects united by some form of interaction or interdependence, where each object is characterized by a finite number of attributes [322]. The interactions between the objects, as well as the interdependence between the object attributes, are usually expressed in a computable mathematical form. Consider a very simple 1D mechanical system composed of two particles M_1 and M_2, together with an ideal spring S_3 linking them, as illustrated in figure 4. The particles move along the x-axis and M_1 is subjected to an external force $f_{\text{ext},1}$.

The relevant attributes of a particle are its mass m, displacement $x(t)$, velocity $v(t)$, acceleration $a(t)$ and the total force $f(t)$ acting on the particle. The attributes of the spring are its spring constant k, length at rest l^0 and length under tension $l(t)$.

The relations between the attributes of the particles M_1 and M_2 are given by Newton's second law of motion:

$$f_1(t) = m_1 a_1(t), \tag{20}$$

$$f_2(t) = m_2 a_2(t). \tag{21}$$

The relation between the attributes of S_3 is given by Hooke's law:

$$f_3(t) = k(l_3^0 - l_3(t)). \tag{22}$$

Next, we formulate the relations representing interactions. The first one relates the time-varying length of the spring to the displacements of two masses

$$l_3(t) = x_2(t) - x_1(t), \tag{23}$$

whereas the next two relations impose force equilibria on the masses

$$f_1(t) = f_{\text{ext},1}(t) - f_3(t), \tag{24}$$

$$f_2(t) = f_3(t). \tag{25}$$

A typical simulation of this system may require calculation of the displacements $x_1(t)$ and $x_2(t)$ as a response to the external force $f_{\text{ext},1}(t)$. This simple system can easily be solved analytically by substituting the interaction relations into the attribute equations and by suppressing the non-relevant attributes. However, for numerical simulations involving a large number of particles, it is advantageous to keep the attribute and interaction relations separate, as will be explained further below.

5.1.1. Discretization. The objects of this system may be discretized using finite differences, as discussed in section 4. By applying forward differences twice to the acceleration in equation (20), we can obtain the displacement $x_1(n)$ as

$$x_1(n) = \frac{1}{m_1} f_1(n) + 2x_1(n-1) - x_1(n-2), \tag{26}$$

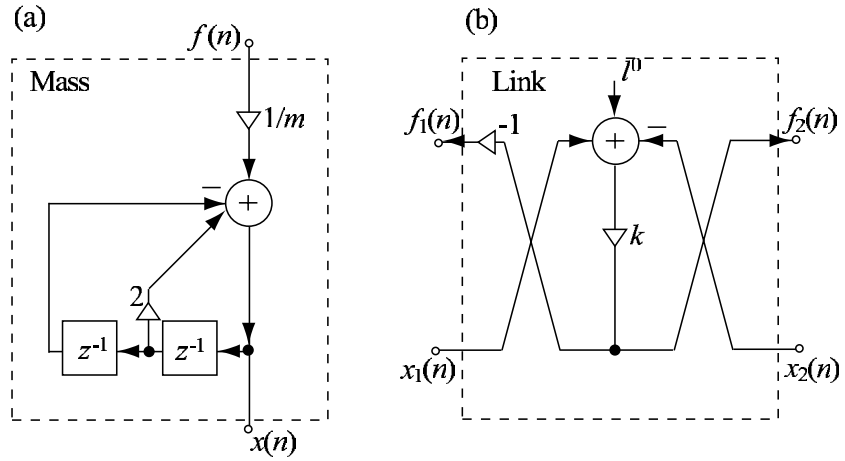

Figure 5. Basic elements of a mass–spring network. (*a*) A one-port mass element. (*b*) A two-port link element corresponding to an ideal spring.

where the sampling period ΔT is suppressed by normalization to unity and $f_1(n)$ is the total force acting on the mass at the discrete time instant n. The mass object is thus an LTI one-port, whose transfer function corresponds to the ratio of force and displacement. Similarly,

$$x_2(n) = \frac{1}{m_2} f_2(n) + 2x_2(n-1) - x_2(n-2). \tag{27}$$

The spring may be thought of as a two-port element that implements the interaction relations or that calculates the output forces as a function of the input displacements. Then,

$$f_3(n) = k(l_3^0 - x_2(n) + x_1(n)), \tag{28}$$

$$f_1(n) = f_{\text{ext},1} - f_3(n), \tag{29}$$

$$f_2(n) = f_3(n). \tag{30}$$

The one-port element corresponding to the mass object and the two-port element corresponding to the link element are illustrated in figure 5.

5.1.2. Implementation. The instantaneous interdependency of the displacements $x_1(n)$ and $x_2(n)$ and the forces $f_1(n)$ and $f_2(n)$ stands out as a problem for implementation. In other words, if the discrete one-port mass objects were interconnected by the two-port link element, a delay-free loop would occur. Mass–spring network systems typically impose a rule of causality in the ordering of operations to overcome this problem; for instance, the displacements at the instant n may be calculated using the forces defined at the instant $n-1$, as is done in CORDIS-ANIMA [38]. This practically means that the two-way interactions are computed in an interleaved fashion, with a delay inserted between the K-pair. The side effects of this delay are subject to numerous studies (see [10,33] for further discussion and improved techniques to eliminate the delay-free loops). However, we use the CORDIS-ANIMA solution to construct the mass–spring model corresponding to the basic mechanical system of figure 4. The resulting model is shown in figure 6, where the forces calculated by the link element acting on the masses M_1 and M_2 are designated as $f_{3,1}(n)$ and $f_{3,2}(n)$, respectively.

Models consisting of a large number of masses and links may be constructed by superposing the input forces of each mass and piping out their output displacements. However,

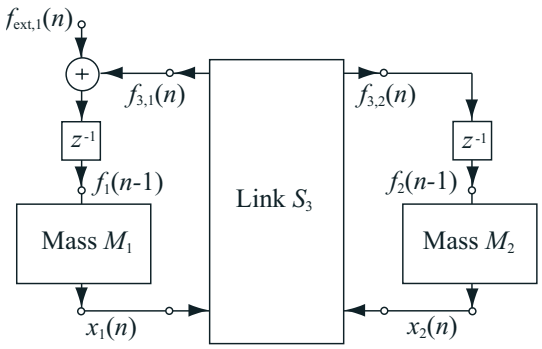

Figure 6. Discrete-time version of the mechanical system in figure 4.

more advanced models would require special elements for termination, damping, time-varying interactions and nonlinearities. Below, we discuss such elements within the CORDIS-ANIMA system.

5.2. CORDIS-ANIMA

In CORDIS-ANIMA, a network is constructed from three LTI basic modules and an additional 'conditional link'. The basic modules correspond to an ideal point 'mass', an ideal 'spring' and a 'damper' [98]. The basic LTI one-port mass element and the two-port spring element are the same as the ones previously shown in figure 5. The damper is a two-port, LTI element with a single parameter g corresponding to a viscous damping coefficient. The damping forces are calculated as

$$f_2(n) = g(x_1(n) - x_1(n-1) - x_2(n) + x_2(n-1)), \tag{31}$$

$$f_1(n) = -f_2(n). \tag{32}$$

The fourth element is a two-port 'conditional link' that combines the ideal spring and damping equations into one. This element is not LTI, as it can modify its variables in time or implement nonlinearities.

In CORDIS-ANIMA, these four elements are grouped according to the number of their ports, resulting in two main object groups: one-port mass (or material) objects (MAT) and the two-port objects that interconnect or link the mass objects (LIA). One-dimensional elements are extended to accept vector inputs and calculate vector outputs for simulations in higher dimensions; CORDIS-ANIMA thus supports higher-dimensional structures. In fact, within the formalism, there are no dimensionality restrictions on the physical variables. The basic library is extended by complementary elements [98]. For instance, a termination element is a special mass object that produces a constant displacement regardless of the applied force. Similarly, a gravity object is a special link element that always produces a constant force.

Besides the linear viscoelastic operations, two special link objects implement the time-varying or nonlinear interactions. The first special element contains a proximity detector: when two disconnected masses get closer, it implements a time-varying viscoelastic interaction between them. This object is most useful for modelling struck instruments. The second special element implements the nonlinear viscosity and elasticity by two table look-up operations. The tables define the output forces as a function of the relative distance and velocity of the interconnected mass objects.

The CORDIS-ANIMA library is further extended by prepackaged modules. Some of these modules support other synthesis paradigms, such as modal synthesis or basic digital waveguides. Constructing a detailed mass-interaction network is still a non-trivial task, since the objects and their interconnection topology require a large number of parameters. Cadoz and his colleagues, therefore, have developed support systems for mass-interaction networks. These systems include the model authoring environment GENESIS [42] (a user-interface dedicated to musical applications of CORDIS-ANIMA), the visualization environment MIMESIS [39] (an environment dedicated to the production of animated images) and tools for analysis and parameter estimation [270].

A large number of audio–visual modelling examples is reported in [39]. These examples include a model of a six-wheel vehicle interacting with soil, simple animal models such as frogs and snakes and models of collective behaviour within a large ensemble of particles. The most advanced model for sound synthesis by mass-interaction networks (and probably by any physics-based algorithm) is the model that creates the musical piece 'pico..TERA', which was developed by Cadoz using the CORDIS-ANIMA and GENESIS systems [36]. In this model, thousands of particles and many aggregate geometrical objects interact with each other. The 290 s of music is synthesized by running this model without any external interaction or post-processing.

5.3. Other mass–spring systems

PhyMod [261] is an early commercial software for visualization and sound synthesis of mass–spring structures. Besides the 1D mass and linear link objects, four nonlinear link elements are provided. The program uses a visual interface for building a *sound sculpture* from elementary objects. The basic algorithmic principles of this system (but not its visual interface) has been ported to the popular csound environment [56].

The system PMPD[2] [109, 110] closely follows the CORDIS-ANIMA formulation for visualization of mass-interaction networks within the pd-GEM environment [206]. In addition to the masses and links in one or more dimensions, PMPD defines higher-level aggregate geometrical objects such as squares and circles in 2D or cubes or spheres in 3D. The PMPD package also contains examples for 2D and 3D vibrations of a linear elastic string in its documentation subfolder (example 5: corde2D and example 7: corde3D). Although the package is a very valuable tool for understanding the basic principles or mass-interaction networks, it has limited support for audio synthesis.

TAO[3] specifically addresses the difficulty of model construction and the lack of a scripting language in the CORDIS-ANIMA system [194, 195]. It uses a fixed topology of masses and springs and provides pre-constructed 1D (string) or 2D (triangle, rectangle, circle and ellipse) modules, but 3D modules are not supported. Operations such as deleting the mass objects for constructing shapes with holes and joining the shapes are defined. For efficiency and reduction in the number of parameters, TAO constrains the spring objects by using a fixed spring constant. The system is driven by a score; the audio output is picked-up by virtual microphones and streamed to a file, which is normalized when the stream finishes.

A real-time synthesis software called CYMATIC was recently developed by Howard and Rimell [116]. The synthesis engine of CYMATIC is based on TAO, but it introduces two important improvements. The first improvement is the replacement of the forward differences

[2] PMPD has multi-platform support and it is released as a free software under the GNU Public License (GPL). It can be downloaded from http://drpichon.free.fr/pmpd/.

[3] TAO is an active software development project and it is released as a free software under the GPL. It resides at http://sourceforge.net/projects/taopm/.

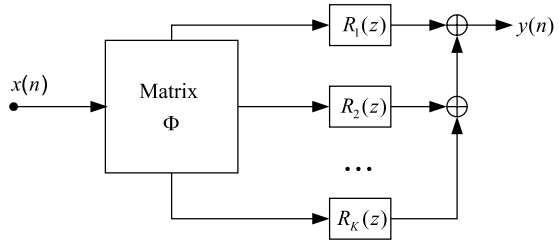

Figure 7. Schematic presentation of the modal synthesis method.

common in all previous systems by central differences. The central difference scheme results in a more stable model and reduces the frequency warping. The second improvement in CYMATIC over TAO is the support for 3D structures, as in CORDIS-ANIMA and PMPD.

6. Modal decomposition methods

Modal decomposition describes a linear system in terms of its modes of vibration. Modelling methods based on this approach look at the vibrating structure from the frequency point of view, because modes are essentially a spectral property of a sound source. Nevertheless, physical models based on modal decomposition lead to discrete-time algorithms that compute the value of the output signal of the simulation at each sampling step. In this sense, modal methods have much in common with other discrete-time modelling techniques discussed in this paper. In this section, we give an overview of the modal synthesis, some filter-based modal decomposition methods and the FTM.

6.1. Modal synthesis

An early application of the modal decomposition method to modelling of musical instruments and sound synthesis was developed by Adrien at IRCAM [2, 3]. In his work, each vibrating mode had a resonance frequency, damping factor and physical shape specified on a discrete grid. The synthesis was strongly related to vibration measurements of a specific structure or instrument, and this is where the modal data was obtained. A software product called Modalys (formerly MOSAIC) by IRCAM is based on modal synthesis [78, 178]. Bisnovatyi has developed another software-based system for experimenting with real-time modal synthesis [32].

Figure 7 shows the block diagram of a modal synthesis system. The input signal $x(n)$ can be interpreted as the force signal applied to a certain spatial point of a physical system. Matrix Φ maps the force into a parallel resonator bank. The sum of their output signals, $y(n)$, can be interpreted as a velocity caused by the input force that is observed at one point. Each resonator $R_k(z)$ represents a single mode of the physical system that is modelled. The resonance frequency, bandwidth and gain of these resonators define the modal synthesis model. Stability of a modal synthesis system like this is easy to ensure, because it suffices to make sure that each of the resonant filter has a stable pair of poles.

Alternatively, modal data can be derived analytically for simple structures, such as strings or membranes. This requires spatial discretization, which leads to a decrease in the amount of modes. As shown by Trautmann and Rabenstein [279], modal data obtained in this way suffers from underestimation of modal frequencies. The error can be reduced by rendering the spatial sampling grid denser, but this solution is undesirable for synthesis purposes, since it

increases the number of modes and thus the computational cost becomes larger. An obvious way to reduce the computational cost of real-time modal synthesis is to prune the number of modes by leaving out some resonant filters.

6.2. Filter-based modal methods

Another approach to modal synthesis that is well suited for percussive sounds, such as drums or bells, is to extract modal data from a recorded signal. Various signal-processing methods are known that can estimate a digital filter transfer function for a given sampled signal. Sandler used linear prediction techniques [223, 224] and Mackenzie *et al* applied the balanced model truncation method [166] to obtain a digital filter model for drum sounds. Laroche [158] and Macon *et al* [167] applied parametric methods on various frequency bands for the same task. The frequency-zooming ARMA method [133] can yield a high-resolution parametric filter model for acoustic signals even if they have a large number of modes located close to each other in frequency. While all such filter models allow accurate modelling and flexible modification of each resonance, they are less meaningful physically than analytically derived or measurement-based modal synthesis models, since they lack information about the spatial distribution of the modes.

Laroche and Meillier [159] proposed a parametric synthesis model for the piano based on a modal resonator bank. This approach allows exact adjustment of the frequency, the level and the decay rate for each mode of a vibrating string, which is helpful for imitating the inharmonicity and complex temporal decay patterns of partials observed in piano tones. State–space modelling discussed by Matignon *et al* [170, 171] and by Depalle and Tassart [74] is another approach to derive filter-based models. The resulting transfer function can be implemented with modal resonant filters or as a high order digital filter. The coupled mode synthesis technique introduced by Van Duyne [297] is another filter-based approach to modal synthesis. It has a special filter structure in which allpass filters are used as building blocks and they are all fed back through the same filter. Banded waveguides introduced by Essl *et al* [86–90] combine characteristics from modal synthesis and digital waveguides, which we discuss in section 7.

Cook has extended the idea of modal synthesis to parametric synthesis of percussive sounds with noisy excitation [63, 66]. This method is called physical inspired sonic modelling or PhISM. Based on parametric spectral analysis, the PhISM method derives a resonator bank and an associated excitation signal. From analysis of several types of excitation it is possible to parametrize the strike position and style, which can then be used for real-time control. The input signal for synthesis can be obtained, for example, by inverse filtering and by simplifying the residual signal. Inverse filtering in this case refers to the process of filtering a recorded signal using the inverted transfer function of the resonant filter bank.

The filter-based modal synthesis methods can be called source–filter models, since they consist in essence of a filter transfer function and a properly chosen input signal. Source–filter models are discussed in section 9 of this paper.

6.3. The functional transform method

A novel technique related to modal synthesis is the FTM introduced by Trautmann and Rabenstein [207, 278, 279], which also describes a linear system in terms of its modes. This method allows the derivation of accurate models based directly on physics for simple geometries, just as can be done with finite difference models. The main novelty in functional transform modelling is to apply two different integral transforms to remove partial derivatives.

The Laplace transform operates on the temporal and the Sturm–Liouville transform on the spatial terms of the partial differential equation. The multidimensional transfer function can then be implemented using digital filters. For linear systems, this results in a set of second-order resonators connected in parallel, just as shown in figure 7. The method can also be extended for nonlinear systems [279, 280]. The FTM can be used for constructing accurate physical models of vibrating strings and membranes without conducting physical measurements, if the necessary numerical values of physical variables are known. Advantages of this modelling method are that spatial discretization is unnecessary, that there is no systematic error in mode frequencies and that the signal phase is correct with respect to both the input and the output locations [279].

7. Digital waveguides

The digital waveguide (DWG) method is based on discrete-time modelling of the propagation and scattering of waves. The principle was used already in the Kelly–Lochbaum speech synthesis model [145, 266], in which the human vocal tract was simulated by unit-sample delay lines and wave scattering junctions between them. Such modelling has often been called 'transmission-line modelling', but in computer music it is better known by the term 'digital waveguide modelling'. This term was proposed by Smith [245, 247] because of an analogy to the concept of waveguide that has been used, for example, in microwave technology. For almost two decades, DWGs have been the most popular and successful physics-based modelling methodology, particularly for efficient sound synthesis applications [249, 253, 254].

In this section, we present an overview of digital waveguide modelling, deriving from the behaviour of plucked strings and acoustic tubes, but also discussing modelling of other instruments. Relations of DWGs to other modelling paradigms are mentioned briefly. Some structures, such as extensions of the Karplus–Strong model, can be seen as intermediate cases between DWGs and source–filter models. Although they may seem to belong more to the source–filter category (section 9), in this presentation they are discussed primarily in the present section on digital waveguides.

7.1. From wave propagation to digital waveguides

A vibrating string is a good example of one-dimensional wave propagation that can serve for derivation of the digital waveguide principle. Here we present a formulation after Smith [253] using an ideal string as a starting point for discrete-time modelling. A more thorough continuous-time analysis of the physics of strings can be found, for example, in [96].

The derivation of digital waveguides can be started from figure 1 and the same wave equation as for the finite difference models in section 4, i.e.

$$Ky'' = \epsilon \ddot{y}. \tag{33}$$

It can be readily checked that any string shape that travels to the left or right with speed $c = \sqrt{K/\epsilon}$ is a solution to the wave equation. If we denote right-going travelling waves by $y_\mathrm{r}(x - ct)$ and left-going travelling waves by $y_\mathrm{l}(x + ct)$, where y_r and y_l are arbitrary twice-differentiable functions, then the general class of solutions to the lossless, one-dimensional, second-order wave equation (33) can be expressed as

$$y(x, t) = y_\mathrm{r}(x - ct) + y_\mathrm{l}(x + ct), \tag{34}$$

or, when time is the primary variable for expressing the signals,

$$y(t, x) = y_\mathrm{r}(t - x/c) + y_\mathrm{l}(t + x/c). \tag{35}$$

These forms, composed of opposite-travelling wave components of arbitrary waveforms, are called the d'Alembert solution of the wave equation. Assuming that signals y_r and y_l in equation (35) are bandlimited to one half of the sampling rate, we may sample the travelling waves without losing any information. This yields

$$\begin{aligned} y(t_n, x_k) &= y_\mathrm{r}(t_n - x_k/c) + y_\mathrm{l}(t_n + x_k/c) \\ &= y_\mathrm{r}(nT - kX/c) + y_\mathrm{l}(nT + kX/c) \\ &= y_\mathrm{r}[(n-k)T] + y_\mathrm{l}[(n+k)T], \end{aligned} \tag{36}$$

where T is the time interval and X the spatial interval between samples so that $T = X/c$. Sampling is applied in a discrete space-time grid in which indices n and k are related to time and position, respectively. Since T multiplies all arguments, we suppress it by defining

$$y^+(m) \mathrel{\hat{=}} y_\mathrm{r}(mT) \qquad \text{and} \qquad y^-(k) \mathrel{\hat{=}} y_\mathrm{l}(mT). \tag{37}$$

The '+' superscript denotes a travelling wave component propagating to the right and '−' denotes propagation to the left. Finally, the left- and right-going travelling waves must be summed to produce a physical output according to the formula

$$y(t_n, x_k) = y^+(n-k) + y^-(n+k). \tag{38}$$

The next step is to make the model more realistic by including losses and dispersion that appear in real strings.

7.2. Modelling of losses and dispersion

By adding proper derivatives of time, space or mixed time and space of different orders to the wave equation, the damping and dispersion of travelling waves in the string can be specified. For example the first-order spatial derivative (velocity) can control losses and the fourth-order spatial derivative introduces dispersion, i.e. frequency-dependent wave velocity. Details on the physics of string vibration damping are analysed, for example, in [282].

Instead of starting from partial differential equations with various order terms, DWG models are typically designed by adding filtering operations to travelling wave signal paths in order to simulate losses and dispersion found in practice. Since every time-invariant, linear filter can be expressed as a minimum phase filter in cascade with an allpass filter, we may factor the filter into its lossy part and its dispersive part. The minimum phase part controls frequency-dependent gain (attenuation in a DWG) plus introduces minimal dispersion, while the allpass part implements most of dispersion (frequency-dependent delay). A discrete space-time simulation diagram appears in figure 8.

The discrete simulation of the travelling waves is exact, in principle, at the sampling positions and instants, even though losses and dispersion are included in the wave equation. The main requirement is that all initial conditions and excitations must be bandlimited to less than one half of the sampling rate. Note also that the losses which are distributed in the continuous solution have been consolidated, or lumped, at discrete position intervals of cT in the simulation. The z-transform expression yields the transmission filter $H_\mathrm{T}(z)$, which summarizes the distributed filtering incurred in one sampling interval, including losses and dispersion. Signal propagation to the right and left, respectively, is computed by

$$Y_k^+(z) = Y_{k-1}^+(z)\, H_\mathrm{T}(z) \qquad \text{and} \qquad Y_k^-(z) = Y_{k+1}^-(z)\, H_\mathrm{T}(z). \tag{39}$$

If the signal values between spatial or temporal sampling points are needed, bandlimited interpolation can yield them with arbitrary accuracy [154].

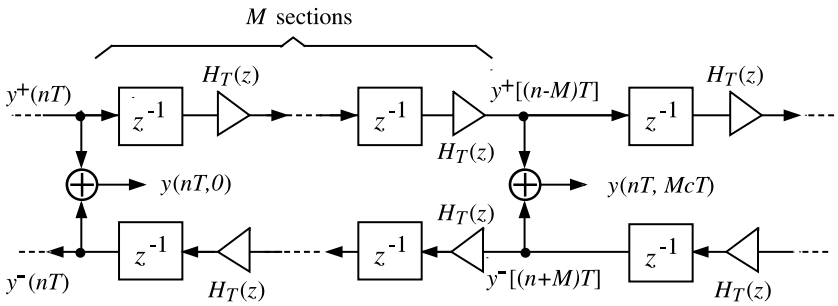

Figure 8. Wave propagation simulated by a digital waveguide consisting of two delay lines for wave components travelling in opposite directions. Each delay line is a sequence of unit delays (z^{-1}) and transmission filters $H_T(z)$ for losses and dispersion.

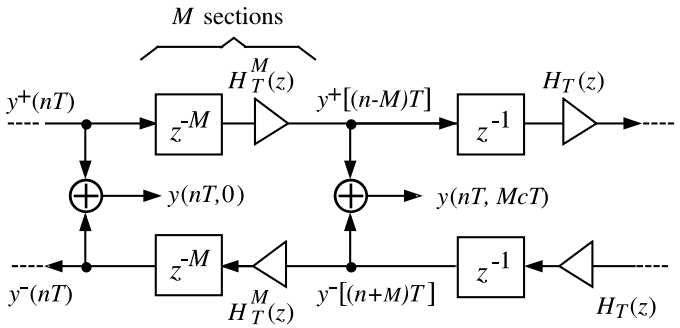

Figure 9. Digital waveguide obtained from the digital waveguide of figure 8 by consolidating M unit delays and transmission filters in each delay line.

For computational efficiency reasons, the digital waveguide can be simplified by further consolidation of elements between points of interest. Figure 9 shows how m consecutive delay-line sections can be combined into a single delay of M samples and transmission transfer function $H_T^M(z)$. This helps for time-domain simulation and sound synthesis, making the DWG approach highly efficient.

7.3. Modelling of waveguide termination and scattering

A wave entering an ideally rigid termination of a string reflects back with inverted polarity, i.e. the reflection can be represented by a constant coefficient equal to -1. A realistic termination adds frequency-dependent losses and dispersion that can be modelled using digital filters $R_a(z)$ and $R_b(z)$ as shown in figure 10. Excitation into and output from the DWG string model can be realized as characterized conceptually in the figure.

Figure 11 illustrates the behaviour of an ideal terminated string when a triangular-shaped displacement due to plucking is released. Several physical wave variables are characterized. The initial displacement is triangular in shape, while the velocity and string slopes are rectangular, and the acceleration as well as the curvature are impulse-like. From a sound synthesis point of view, the acceleration variable is favourable, because an impulse is useful as a single sample excitation. The radiated sound output of a string instrument is approximately proportional to bridge velocity (obtained by integrating acceleration) above a certain critical

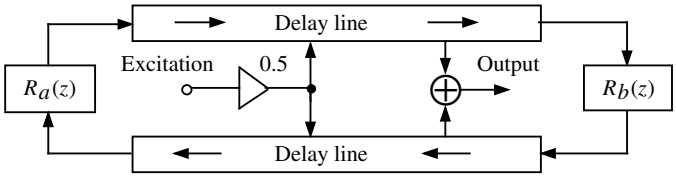

Figure 10. DWG model of a terminated string. Reflections of waves at terminations are represented by transfer functions $R_a(z)$ and $R_b(z)$. String input excitation and output probing are also shown conceptually.

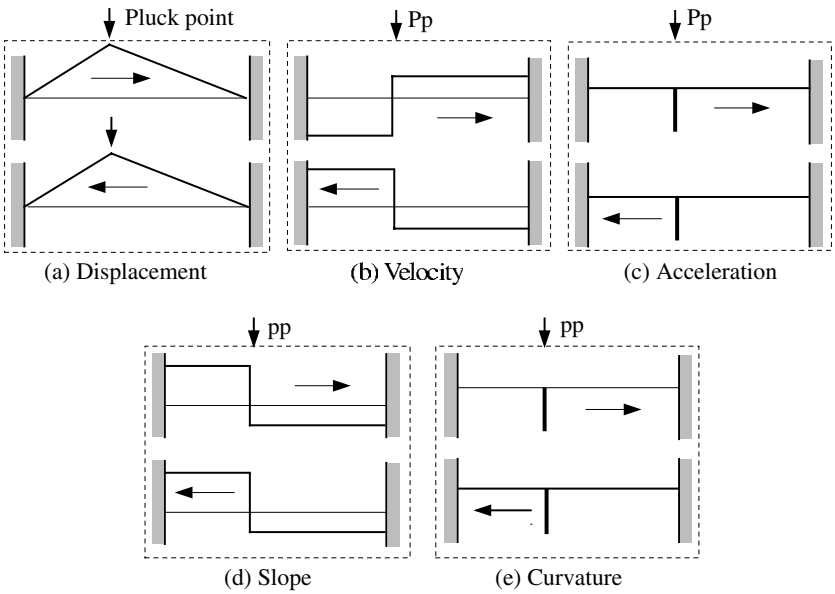

Figure 11. The behaviour of different mechanical waves in an ideal terminated string at the moment of plucking release: (*a*) displacement, (*b*) velocity, (*c*) acceleration, (*d*) slope and (*e*) curvature.

frequency, below which the radiation is proportional to acceleration. This is an idealized description, whereby the detailed instrument body effects are also omitted.

The string termination discussed above is a special case of wave scattering. In scattering, a part of wave energy entering a junction of connected waveguides is reflected back, and the rest of the energy is distributed to other waveguide branches. The general case with an arbitrary number of waveguides connected to a junction, including a direct excitation U_{ext}, is depicted in figure 12. In this case, we use the acoustic variables pressure P and volume velocity U instead of mechanical string variables, i.e. tube-like waveguides are connected together. (The capital letter symbols may be interpreted as Laplace, Fourier or Z-transforms.)

Junctions connecting elements must fulfil physical continuity constraints called the Kirchhoff rules in the electrical domain. For a parallel junction of acoustic components in figure 12, we may write

$$P_1 = P_2 = \cdots = P_N = P_{\text{J}}, \tag{40}$$

$$U_1 + U_2 + \cdots + U_N + U_{\text{ext}} = 0, \tag{41}$$

where P_i are pressures and U_i volume velocities at the ports of the junction, P_{J} is the common pressure of coupled branches and U_{ext} is an external volume velocity injected to the junction.

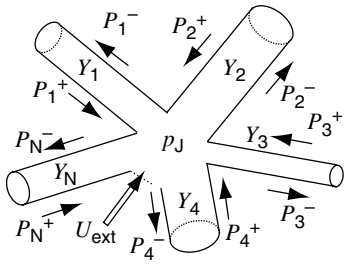

Figure 12. Parallel acoustic junction of admittances Y_i with associated pressure waves indicated. A direct volume velocity excitation U_{ext} is also attached.

When port pressures are represented by incident (incoming) wave components P_i^+ and scattered (outgoing) wave components P_i^-, acoustic admittances attached to each port by Y_i, and

$$P_i = P_i^+ + P_i^- \qquad \text{and} \qquad U_i^+ = Y_i P_i^+, \tag{42}$$

then the junction pressure P_J can be obtained as

$$P_J = \frac{1}{Y_{\text{tot}}} \left(U_{\text{ext}} + 2 \sum_{i=0}^{N-1} Y_i P_i^+ \right), \tag{43}$$

where $Y_{\text{tot}} = \sum_{i=0}^{N-1} Y_i$ is the sum of all admittances to the junction. Scattered pressure waves, obtained from equation (42), are then

$$P_i^- = P_J - P_i^+. \tag{44}$$

Figure 13 depicts the results of equations (41)–(44) as a signal flow diagram for the computation of an acoustic 3-port scattering junction. Due to the duality of variable pairs, the same diagram can be applied to a series connection and volume velocity waves so that pressures and volume velocities are interchanged and admittances are replaced by impedances.

In figure 13, port 1 is terminated by admittance Y_1 and port 2 is connected to a delay-line of admittance Y_2. Notice that for a passive termination Y_1 the incoming port signal is zero so that no computation is needed at that port. Port 3 is not connected. Dotted line regions show the groupings of signal processing elements for block-based (object-based) computation, and the bottom part of the figure depicts an abstraction diagram of these blocks. Arbitrary admittances can be given by their z-transforms as digital filters (FIR or IIR filters or just as real coefficients if all attached impedances are real). Note that each admittance is also represented in the block $1/\sum Y_i$. For real-valued admittances, the scattering junction computation can be optimized to minimize the number of operations needed [253].

An example of DWG string modelling in the mechanical domain is shown in figure 14, where velocity waves are used and series connected junctions have equal velocity at each port. A plucked string instrument with two strings is modelled by delay-line elements and termination impedances $Z = F/V$, which are ratios of force F to velocity V. Plucking is inserted as force to a point in the string and the output is the vibration velocity at the bridge. Both strings have a common bridge impedance so that there is coupling between them. This leads to 'sympathetic vibrations', whereby a vibrating string may transfer energy to another string, resulting in its vibration, too. For a full-scale model of the acoustic guitar, each string should have two subsystems, one for vertical and another for horizontal vibration with a matrix-like coupling of string polarities at the bridge, and six such string systems should be included.

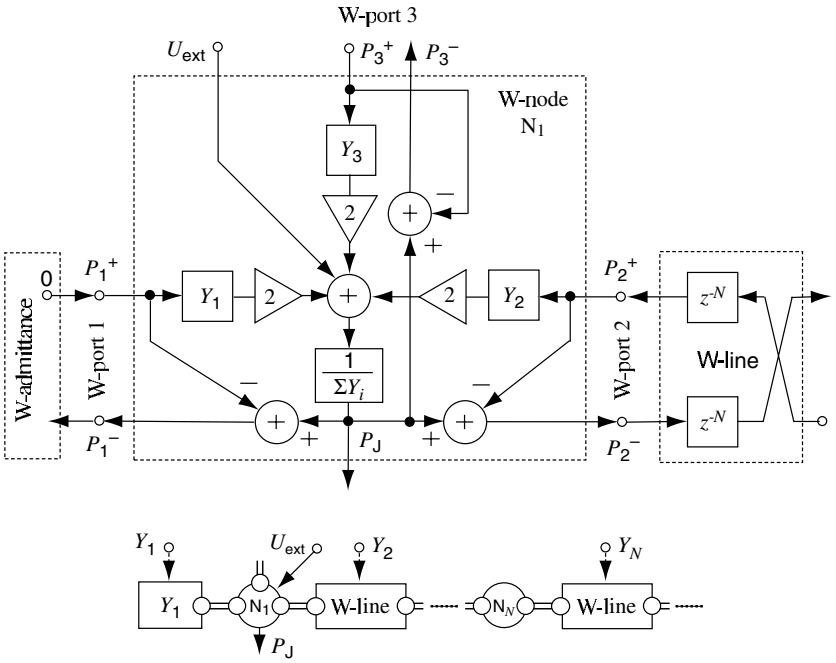

Figure 13. *Top*: a 3-port parallel scattering junction for acoustic pressure waves. Incoming pressures are P_i^+, outgoing ones P_i^- and P_J is common junction pressure. Port 1 (left) is terminated by admittance Y_1, port 2 (right) is connected to a delay-line having wave admittance Y_2, and port 3 (top) is not connected. *Bottom*: block diagram with abstracted block notation and how the blocks can be connected to form a 1D digital waveguide.

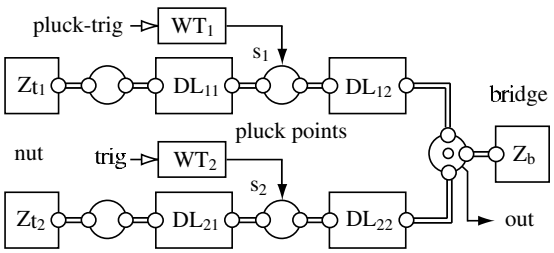

Figure 14. A DWG block diagram of two strings coupled through a common bridge impedance (Z_b) and terminated at the other end by nut impedances (Z_{t1} and Z_{t2}). Plucking points are for force insertion from wavetables (WT_i) into junctions in the delay-lines (DL_{ij}). Output is taken as the bridge velocity.

7.4. Digital waveguide meshes and networks

The DWG scattering junction of figure 13 allows for arbitrary network topologies to be formed as connections of delay lines and junction nodes. This is very flexible and useful particularly because the stability of the network can be easily guaranteed by keeping all elements passive (real part of each admittance positive at all frequencies). A special case of digital waveguide networks (DWN) is the 'digital waveguide mesh', which has a regular 2D or 3D mesh-like structure [299]. Figure 15 illustrates a part of a rectilinear 2D mesh, connecting each node to its four neighbours through bi-directional delay lines made of unit

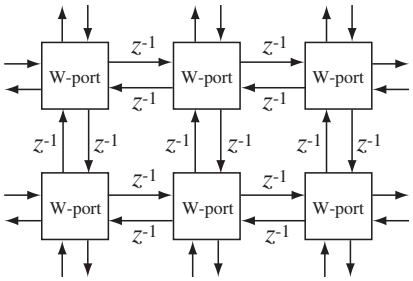

Figure 15. Part of a rectilinear 2D waveguide mesh structure. Bi-directional delay lines of unit delays z^{-1} connect scattering junctions (square blocks).

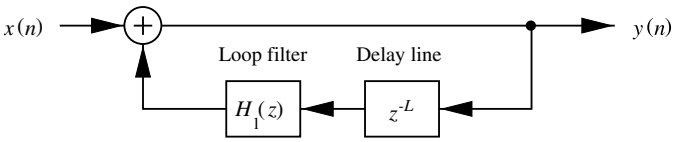

Figure 16. Single delay loop (SDL) structure containing loop filter $H_1(z)$ and delay z^{-L}.

delays. The 2D digital waveguide mesh can be used to model 2D resonators, such as percussion membranes [4, 100]. The 3D digital waveguide mesh is applicable to 3D resonators, such as rooms and enclosures [20, 117, 182, 226, 227, 230].

Digital waveguide meshes have the problem of dispersion in wave propagation, i.e. different frequencies have different propagation speeds, typically such that high frequencies propagate more slowly. In the rectilinear mesh it is also significantly direction-dependent, i.e. dispersion is stronger in axial directions, while diagonal directions are dispersion-free. This can be compensated by using interpolated meshes where the diagonal neighbours are taken into account in the computation of scattering junctions [228, 230]. Another way to obtain approximately direction-independent dispersion is to use triangular mesh structures in 2D modelling and tetrahedral mesh for 3D modelling [302]. Some dispersion remains both with interpolation and non-rectilinear meshes. It can be compensated for by frequency warping of the system impulse response off-line [228–230] or on-line [99, 101, 263]. This might not be needed in many cases, however, because the human auditory system is less sensitive to spectral details at high frequencies.

7.5. Reduction of a DWG model to a single delay loop structure

For efficient computation, the digital waveguide structure of figure 10 can be simplified further in the case when the input–output transfer function is of interest only. Instead of the dual delay-line signal loop, a single delay loop (SDL) structure [143] is used. Figure 16 illustrates the idea of the SDL structure. Note that this is a source–filter model (see section 9), rather than a strict physical model, because the signal variables in the single delay-line do not correspond to the K- or wave variables in the physical system anymore. In spite of this, the SDL structures have also been called digital waveguides.

A formal derivation of the SDL structure from the dual delay-line model has been presented in [143]. Figure 17 depicts both of these forms, the dual delay-line version on the top and the SDL structure in the bottom diagram. When considering signal paths E1→R1, E2→L2→L1→E1, R1→R2 and R2→E2, which make a feedback loop in the dual delay-line

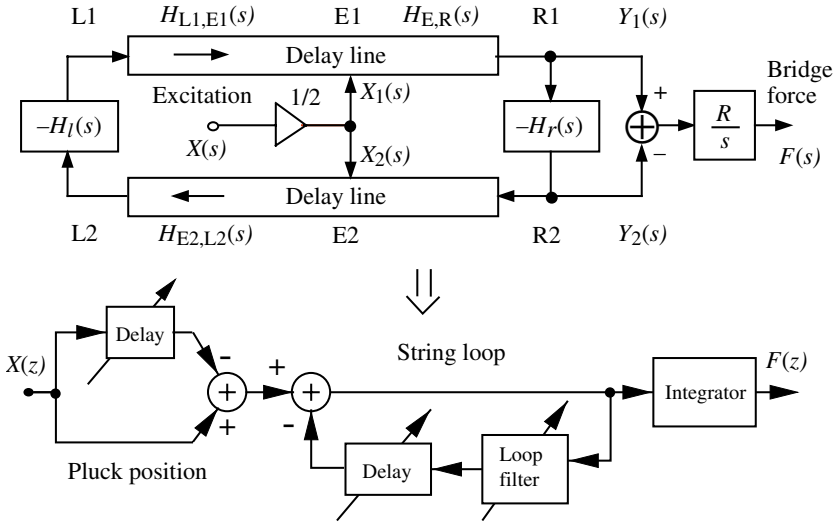

Figure 17. Reduction of bi-directional delay-line waveguide model (top) to a single delay line loop structure (bottom).

structure, the transfer function from excitation $X(s)$ to bridge force $F(s)$ can be derived in the Laplace transform domain. After minor simplifications and moving to the Z-transform domain, the following approximation results:

$$\frac{F(z)}{X(z)} \sim H_{\mathrm{E}}(z)H_{\mathrm{L}}(z)H_{\mathrm{B}}(z) = (0.5 + 0.5z^{-D_{\mathrm{p}}})\,\frac{1}{1 - H_{\mathrm{l}}(z)\,z^{-L}}\,I(z). \tag{45}$$

Here the first term $H_{\mathrm{E}}(z) = 0.5 + 0.5z^{-D_{\mathrm{p}}}$ corresponds to a comb filter that results from the plucking point effect, i.e. cancelling of frequencies for which the delay D_{p} is a half-wavelength. The second term $H_{\mathrm{L}}(z) = 1/[1 - H_{\mathrm{l}}(z)z^{-L}]$ is the SDL term as a feedback filter structure. The term $H_{\mathrm{B}}(z) = I(z)$ approximates integration ($1/s$ in the Laplace domain) to obtain the force at the bridge. In the form of a signal flow diagram, the SDL model obtained looks like the bottom part of figure 17.

7.6. Commuted DWG synthesis

In synthesizing string instruments, there is a further requirement to include the instrument body in the synthesis model. Different methods of body modelling will be discussed briefly in section 9, but for improved efficiency of string instrument synthesis by SDL structure 'commuted waveguide synthesis' is found particularly useful. Proposed independently in [250] and [142], commuted synthesis is based on the commutativity of linear systems connected in cascade.

Figure 18 shows the derivation of the commuted source–filter structure in (*c*) from a cascade of excitation $E(z)$, string model $S(z)$ and body model $B(z)$, as shown in (*a*). Plucking the string in (*a*) triggers feeding the excitation wavetable signal to the string model, the signal being filtered finally by the body model, while in (*c*) an aggregate signal of excitation and body response convolved into a wavetable is fed to the string model. Note that bi-directional interactions between physical objects are reduced into a unidirectional signal flow.

Mathematically, the commuted DWG synthesis is based on the equivalences

$$Y(z) = E(z)S(z)B(z) \equiv E(z)B(z)S(z) \equiv A(z)S(z), \tag{46}$$

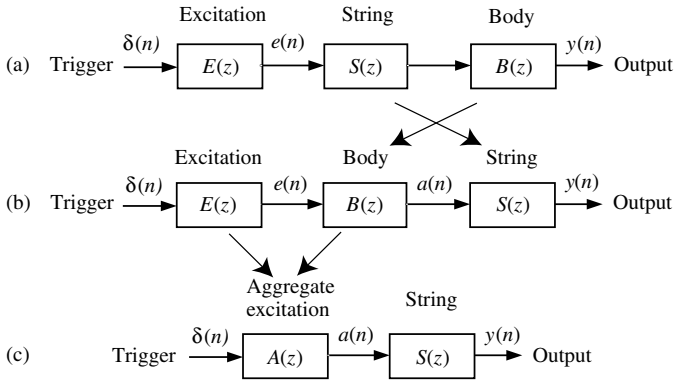

Figure 18. Principles of commuted DWG synthesis: (*a*) cascaded excitation, string and body, (*b*) body and string blocks commuted and (*c*) excitation and body blocks consolidated into a wavetable for feeding the string model.

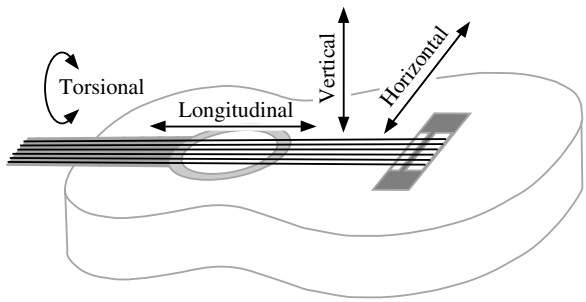

Figure 19. Degrees of freedom for string vibration in the guitar.

where $Y(z)$ is the model output and $A(z)$ is the consolidation of excitation and body model, i.e. a wavetable containing everything else in sound production except the string model. The advantage of the commuted structure is that the body block is reduced from a computationally expensive high-order digital filter to wavetable reading. This can reduce the computational cost of the whole synthesis model by orders of magnitude.

7.7. Case study: modelling and synthesis of the acoustic guitar

The acoustic guitar is an example of a musical instrument for which DWG modelling is found to be an efficient method, especially for real-time sound synthesis [134, 137, 142, 160, 286, 295]. The DWG principle in figure 14 allows for true physically distributed modelling of strings and their interaction, while the SDL commuted synthesis (figures 17 and 18) allows for more efficient computation. In this subsection we discuss the principles of commuted waveguide synthesis as applied to high-quality synthesis of the acoustic guitar.

There are several features that must be added to the simple commuted SDL structure in order to achieve natural sound and control of the playing features. Figure 19 depicts the degrees of freedom for the vibration of strings in the guitar. The transversal directions, i.e. the vertical and horizontal polarizations of vibration, are the most prominent ones. The vertical vibration connects strongly to the bridge, resulting in stronger initial sound and faster decay than the horizontal vibrations that start more weakly and decay more slowly. The effect of longitudinal

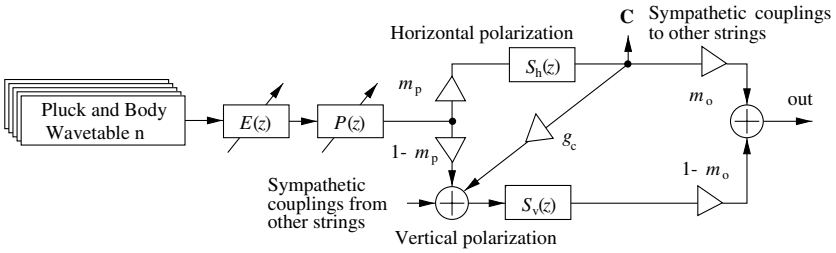

Figure 20. Dual-polarization string model with sympathetic vibration coupling between strings. Multiple wavetables are used for varying plucking styles. Filter $E(z)$ can control the detailed timbre of plucking and $P(z)$ is a plucking point comb filter.

vibration is weak but can be observed in the generation of some partials of the sound [320]. Longitudinal effects are more prominent in the piano [16, 58], but are particularly important in such instruments as the kantele [82] through the nonlinear effect of tension modulation (see section 11). The torsional vibration of strings in the guitar is not shown to have a remarkable effect on the sound. In the violin it has a more prominent physical role, although it makes virtually no contribution to the sound.

In commuted waveguide synthesis, the two transversal polarizations can be realized by two separate SDL string models, $S_v(z)$ for the vertical and $S_h(z)$ for the horizontal polarization in figure 20, each one with slightly different delay and decay parameters. The coefficient m_p is used to control the relative excitation amplitudes of each polarization, depending on the initial direction of string movement after plucking. The coefficient m_o can be used to mix the vibration signal components at the bridge.

Figure 20 also shows another inherent feature of the guitar, the sympathetic coupling between strings at the bridge, which causes an undamped string to gain energy from another string set in vibration. While the principle shown in figure 14 implements this automatically if the string and bridge admittances are correctly set, the model in figure 20 requires special signal connections from point C to the vertical polarization model of other strings. This is just a rough approximation of the physical phenomenon that guarantees the stability of the model. There is also a connection through g_c that allows for simple coupling from the horizontal polarization to excite the vertical vibration, with a final result of a coupling between the polarizations.

The dual-polarization model in figure 20 is excited by wavetables containing commuted waveguide excitations for different plucking styles. The filter $E(z)$ can be used to control the timbre details of the selected excitation, and the filter $P(z)$ is a plucking point comb filter, as previously discussed.

For solid body electric guitars, a magnetic pickup model is needed, but the body effect can be neglected. The magnetic pickup can be modelled as a lowpass filter [124, 137] in series with a comb filter similar to the plucking point filter, but in this case corresponding to the pickup position.

The calibration of model parameters is an important task when simulating a particular instrument. Methods for calibrating a string instrument model are presented, for example, in [8, 14, 24, 27, 137, 142, 211, 244, 286, 295, 320].

A typical procedure is to apply time-frequency analysis to recorded sound of plucked or struck string, in order to estimate the decay rate of each harmonic. Parametric models such as FZ-ARMA analysis [133, 138] may yield more complete information of the modal components in string behaviour. This information is used to design a low-order loop filter which approximates frequency-dependent losses in the SDL loop structure [14,17,79,244,286].

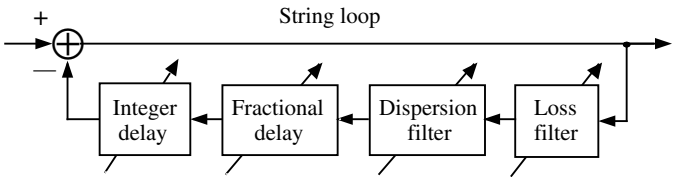

Figure 21. Detailed SDL loop structure for string instrument sound synthesis.

A recent novel idea has been to design a sparse FIR loop filter, which is of high order but has few non-zero coefficients [163, 209, 293]. This approach offers a computationally efficient way to imitate the large deviations in the decay rates of harmonic components. Through implementing a slight difference in the delays and decay rates of the two polarizations, the beating or two-stage decay of the signal envelope can be approximated. For the plucking point comb filter it is required to estimate the plucking point from a recorded tone [199, 276, 277, 286].

Figure 21 depicts a detailed structure used in practice to realize the SDL loop. The fundamental frequency of the string sound is inversely proportional to the total delay of the loop blocks. Accurate tuning requires the application of a fractional delay, because an integral number of unit delays is not accurate enough when a fixed sampling rate is used. Fractional delays are typically approximated by first-order allpass filters or first- to fifth-order Lagrange interpolators as discussed in [154].

When the loop filter properties are estimated properly, the excitation wavetable signal is obtained by inverse filtering (deconvolution) of the recorded sound by the SDL response. For practical synthesis, only the initial transient part of the inverse-filtered excitation is used, typically covering several tens of milliseconds.

After careful calibration of the model, a highly realistic sounding synthesis can be obtained by parametric control and modification of sound features. Synthesis is possible even in cases which are not achievable in practice in real acoustic instruments.

7.8. DWG modelling of various musical instruments

Digital waveguide modelling has been applied to a variety of musical instruments other than the acoustic guitar. In this subsection, we present a brief overview of such models and the features that need special attention in each case. For an in-depth presentation on DWG modelling techniques applied to different instrument families, see [254].

7.8.1. Other plucked string instruments. The acoustic guitar is particularly well suited to digital waveguide modelling and sound synthesis. Many other plucked string instruments are also relatively easy to model along the same guidelines, as long as there are no major nonlinearities; among such instruments are the mandolin and the banjo. From the keyboard string instrument family, the harpsichord also belongs to the plucked string category of relatively linear behaviour and has been synthesized by a DWG model [293].

Several plucked string instruments exhibit nonlinearities to a degree where it has an essential effect on the perceived sound. Good examples thereof are the Finnish kantele [82, 130, 275] and the Turkish tanbur [84]. In both instruments, a specific termination structure of the strings couples the longitudinal tension modulation, which originates in a nonlinear way from string displacement, to the body and strongly radiates even harmonic components [82]. This nonlinear phenomenon is distributed along the string so that no

commutation and consolidation is possible in accurate modelling. This requires a realization that is computationally much more expensive than a simple commuted DWG model.

Plucked string instruments that behave linearly in normal conditions can become highly nonlinear when played in specific ways. The so-called slap bass sound [208] is generated when a string is set into such a large amplitude that it touches frets or bounces back from the fretboard. Entirely different nonlinearities are met in electric guitar modelling and synthesis. The instrument itself is relatively straightforward to model [137], but it is often played through a distorting amplifier or device that requires different modelling techniques [137, 268].

Nonlinearities are discussed in more detail in section 11.

7.8.2. Struck string instruments. The piano is the most common musical instrument where strings are struck by a hammer that is accelerated by a key action mechanism [47, 46, 96]. Digital waveguide modelling of the piano has been studied actively in, for example [14–16, 22, 25, 27, 254, 258, 298, 301]. Modelling of the strings is basically similar to the acoustic guitar case, although there are many more strings that come in 1–3 string groups per key. Therefore, the coupling mechanism between strings and the soundboard is more complex.

One of the main challenges in struck string instruments and a clear difference from plucked strings is the interaction of the hammer and the string. This is an inherently nonlinear phenomenon, which makes the computationally efficient commuted synthesis more difficult than in the guitar. The hammer first makes an impact to displace the string, but when the string returns from displacement it makes another contact and possibly multiple further contacts with the hammer. The details of multiple contacts depend on the initial hammer velocity, so that the detailed time structure and therefore the spectrum of piano sound essentially varies from pianissimo to forte playing. In commuted synthesis, this variance can be simulated either by multiple wavetables for different hammer velocities or by using multiple application of wavetable(s), each one for a separate hammer contact [254].

Another method to model the hammer–string interaction is by wave digital techniques that are discussed in more detail in section 8. The so-called wave digital hammer [298] is a physically well-motivated way to deal with discrete-time modelling of nonlinear interaction in an energetically consistent manner.

In the piano, the longitudinal vibration of strings also has an effect that can be perceived. There are, for example, so-called phantom partials and a multitude of signal components that are due to nonlinear effects in the string [57]. Recently, these effects have also been added to waveguide modelling and synthesis of the piano [16].

Piano strings, particularly thick wound strings for the lowest notes, exhibit clearly perceptible inharmonicity, which originates from the stiffness of the strings [96]. Wave propagation in the string is therefore dispersive. The dispersion can be modelled using an allpass filter as a part of the feedback loop in the waveguide string algorithm [14, 22, 189, 216, 240, 244, 272, 300].

As another keyboard instrument belonging to the struck string category, the clavichord has also been modelled and synthesized using digital waveguide techniques [292].

7.8.3. Bowed string instruments. In the violin family of musical instruments, the strings are normally excited by bowing [96]. The complex behaviour of friction between the moving bow and the string results in so-called slip–stick alternation, and after a less regular attack period the string eigenmodes synchronize this phenomenon to periodic vibration. The slip–stick behaviour is highly nonlinear, which means that straightforward commuted waveguide synthesis is not possible.

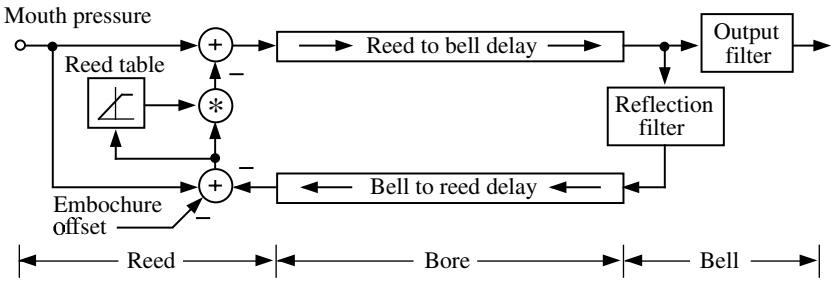

Figure 22. Digital waveguide model of a single-reed woodwind instrument with cylindrical bore. This can be applied, for example, to the clarinet.

Physical modelling of the dynamic behaviour of the violin was started by McIntyre, Woodhouse and Schumacher, although understanding the physics of the instrument had been of interest before (for a recent overview on the physics of the bowed string, see [321]). Particularly in [172, 236, 237, 243, 317, 318], the physical basis of violin behaviour has been developed and modelled.

Digital waveguide modelling of bowed string instruments towards real-time synthesis has been developed, since [244], from two starting points of view: modelling of the nonlinear bow–string interaction and special versions of commuted synthesis. The former case, which tries to duplicate the physical nonlinearity, is discussed further in section 11. For efficient sound synthesis purposes, another approach can be taken, where commuted waveguide synthesis is possible [252]. In it, each period of string vibration is given a separate wavetable excitation. Due to the nonlinearity of the physical phenomenon, inclusion of both the excitation and the body response in the wavetables becomes more problematic than, for example, in the guitar.

Other points of interest in DWG modelling of the violin are the torsional waves in string vibration [241], the impact of string stiffness [240] and the effect of finite bow width [115, 203–205, 238]. In addition to the violin family of musical instruments, bowing has also been modelled in the context of unusual objects [239], including the musical saw.

7.8.4. Wind instruments. Wind instruments are acoustic sound sources in which a linear tube-like resonator is combined with a nonlinear excitation system, i.e. mouthpiece and vibrating reed(s) or the player's lips [96]. The tube resonator can be modelled as a digital waveguide in a way similar to string modelling, while the mouthpiece and the player's lips require nonlinear lumped element modelling. Wind instruments can be categorized by the mechanisms of excitation and pitch control as (a) woodwind instruments with a single or double reed vibrating and toneholes for length control, (b) brass instruments with player's lips vibrating and valve mechanism for tube length control and (c) 'air reed' instruments (flutes and organ pipes) where an air jet blown to a sharp edge starts to vibrate according to the modes of an attached tube.

The clarinet is a typical wind instrument with a cylindrical bore and a single reed. Figure 22 shows a digital waveguide model used for clarinet sound synthesis [173, 235, 254]. It consists of a bi-directional delay line as the bore waveguide, reflection and radiation output filters for the open end (bell) and a nonlinear reed model. Mouth pressure activates the oscillation that is sustained by positive feedback due to reed characteristics of flow versus pressure difference across the reed. This nonlinear characteristics curve is mapped to a lookup table. Wind instrument nonlinearities are discussed further in section 11.

The tube in wind instruments can be cylindrical or conical bore, and it can more or less expand in diameter towards the radiation end of the tube (called the bell for clearly

expanding cases). Modelling of the instrument bores has been studied in [19, 61, 70, 77, 231, 246, 248, 283, 287, 303, 304, 306, 307]. Conical and exponentially expanding bores are more demanding to simulate than the cylindrical ones [19, 70, 77, 231, 248, 267, 283, 287, 303, 304, 306, 307].

Another part of wind instruments that requires modelling effort are the toneholes, which are controllable side branch openings in the waveguide. Tonehole modelling is studied, for example, in [28, 231, 232, 283, 290, 305]. When open, a tonehole works similarly to an open end, and the rest of the bore towards the bell has little effect on sound production. When a tonehole is closed, it corresponds to a short closed tube that has a minor effect on the wave passing it.

Examples of brass instrument modelling are found, for example, in [312, 313]. Modelling of the player's lip vibration is similar to the case of vocal fold modelling in speech and singing, and it can be realized as a self-oscillating nonlinearity.

Yet another phenomenon of interest in brass instruments is the high pressure level of waves in the instrument bore, which exhibits slight nonlinearity in air compression, and results in the formation of shock waves [180, 181, 314]. This has to be taken into account in detailed modelling of loud sounds with their particular 'metallic' timbre, for example, in the trumpet and the trombone.

The flute and its air jet oscillation have been modelled by digital waveguide principles in [288, 309].

7.8.5. Percussion instruments. Percussive instruments, such as drums and gongs, have been studied from a physical point of view and with numerical methods, for example, in [49, 51, 52, 210], and they have been modelled and synthesized using 2D digital waveguide meshes in [299, 300]. (Actually those resonators are 3D objects if the air loading is taken into account.) For 2D (and 3D) digital waveguides there is no way to consolidate the structure of figure 15 as can be done in the 1D case (see figure 9). Therefore, the wave-based computation of digital waveguide meshes can become expensive for large structures. The losses can be commuted to waveguide terminations, which allows the mesh itself to be lossless and thus maximally simple.

Although the waveguide meshes are dispersive and therefore the higher modes do not have correct frequencies, it is acceptable due to the reduced frequency resolution of human auditory perception at high frequencies.

Many 2D resonators in percussive instruments exhibit nonlinear behaviour. This is particularly true for gong-like instruments [96]. Such nonlinearities make strong inter-mode coupling so that the vibration energy can spread, for example, from low to high frequencies with audible shift in timbre. The nonlinearities themselves are inherently lossless and require special techniques for simulation. Methods to realize such passive nonlinearities were proposed in [202, 296] and are briefly discussed in section 11. In a waveguide mesh synthesis of a gong, it may suffice to add passive nonlinearities only at the rim termination of the instrument model mesh, although in a real gong they are distributed. A further step in modelling complexity from gongs is the Caribbean steel pan (steel drum) [96], where the distribution of modal patterns creates regions tuned to different pitches and the nonlinearities make a rich timbre.

7.8.6. Speech and singing voice. As mentioned above, modelling of voice production was the early application of digital waveguide principle, at that time called the transmission line principle [145]. Since then, the same principle has been used in numerous simulations of

speech production, see for example [59, 128, 164, 267, 289], and in singing voice synthesis [59, 60, 64, 150, 151], although it has not become popular in practical speech synthesis, partly due to computational complexity compared with formant synthesis (see section 9) and concatenation methods based on samples from real speech.

In voice production, the DWG principle can be applied to the vocal (and nasal) tract by splicing it to short sections from the glottis to the lips. The admittance of each section is controlled proportionally to the cross-sectional area in that position. The method is well suited to articulatory modelling and synthesis whereby the movements of the articulators, particularly of the tongue, can be mapped to the area profile for vocal tract control.

7.8.7. Inharmonic SDL type of DWG models. Digital waveguides are most straightforward and efficient when applied to instruments producing harmonic spectrum of sound; this is what a simple terminated delay line does when excited. The majority of instruments used in western music produce fully or approximately harmonic sounds. DWGs needed for strongly inharmonic sounds are necessarily more complex.

An example on DWG modelling of highly inharmonic instruments is synthesis of bell sounds [140, 141]. By including a highly dispersive second-order allpass filter within a SDL feedback loop it was found that bell sounds can be synthesized by an efficient DWG model. Although only the lowest partials can be tuned relatively accurately, the perceptual quality of DWG bell models can be made close to real bells. Notice that in this case the model does not anyhow correspond to the spatial geometric structure and vibration distribution of a real bell. Rather, this is a generic DWG model tuned in its parameters to produce realistic bell sounds.

8. Wave digital filters

The purpose of this section is to provide a general overview of physical modelling using WDFs in the context of musical instruments. Only the essential basics of the topic will be discussed in detail; the rest will be glossed over. For more information about the subject, the reader is encouraged to refer to [254]. Also, another definitive work can be found in [94].

8.1. What are wave digital filters?

WDFs were developed in the late 1960s by Alfred Fettweis [93] for digitizing lumped analog electrical circuits. The travelling-wave formulation of lumped electrical elements, where the WDF approach is based, was introduced earlier by Belevitch [21, 254].

WDFs are certain types of digital filters with valid interpretations in the physical world. This means that we can simulate the behaviour of a lumped physical system using a digital filter whose coefficients depend on the parameters of this physical system. Alternatively, WDFs can be seen as a particular type of finite difference scheme with excellent numerical properties [254]. As discussed in section 4, the task of finite difference schemes in general is to provide discrete versions of partial differential equations for simulation and analysis purposes.

WDFs are useful for physical modelling in many respects. Firstly, they are modular: the same building blocks can be used for modelling very different systems; all that needs to be changed is the topology of the wave digital network. Secondly, the preservation of energy and hence also stability is usually addressed, since the elementary blocks can be made passive, and the energy preservation between blocks are evaluated using the Kirchhoff's laws. Finally, WDFs have good numerical properties, that is, they do not experience artificial damping at high frequencies.

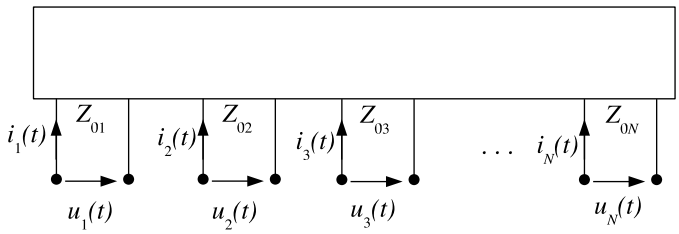

Figure 23. The N-port is a mathematical abstraction of a circuit element. It consists of N ports, which all have two terminals. To each port j, a port voltage $u_j(t)$ and a port current $i_j(t)$ are applied. A port is characterized by its port impedance Z_{0j}, which defines the ratio between the port voltage and current.

Physical systems were originally considered to be lumped in the basic wave digital formalism. This means that the system to be modelled, say a drum, will become a point-like black box, which has the functionality of the drum. However, its inner representation, as well as its spatial dimensions, is lost. We must bear in mind, however, that the question of whether a physical system can be considered lumped depends naturally not only on which of its aspects we wish to model but also on the frequency scale we want to use in the modelling (see section 3).

8.2. Analog circuit theory

This section introduces the analog elements that act as exemplars for the wave digital building blocks.

8.2.1. N-ports. An N-port can be seen as a mathematical abstraction of a circuit element. It is basically a 'black box' with N ports for interacting with other elements (see figure 23). Each port consists of two terminals, and a port voltage is applied across them. Also, a current is defined for each port, with the direction as shown in figure 23. The relationship between the port voltage and current is defined by port impedance Z_{0j} or its reciprocal, port admittance Y_{0j}, where j denotes the index of the port. For one-port elements, the index can be omitted. The port impedances can have arbitrary values, as long as they remain non-negative. We thus have an extra degree of freedom, which can be used later for simplifying the calculations.

Note that we could have used any other Kirchhoff pairs (force/velocity, pressure/volume velocity) as well, but we chose to work in the electrical domain, as is usually the case with WDFs. The domain under discussion can easily be changed at any point by replacing the Kirchhoff pair with the one originating from the desired domain.

We next switch to using wave variables instead of Kirchhoff variables, in order to study more thoroughly the one-port elements. This train of thought mostly follows the one provided by Smith in [254]. Formally, the change of variables is implemented by defining the new voltage wave variables a and b by

$$\begin{bmatrix} a \\ b \end{bmatrix} = \begin{bmatrix} 1 & Z_0 \\ 1 & -Z_0 \end{bmatrix} \begin{bmatrix} u(t) \\ i(t) \end{bmatrix}, \tag{47}$$

where a is the voltage wave travelling towards the port (also called the incident wave), while b is the voltage wave travelling away from the port (also called the reflected wave).

The original K-variables can be obtained by properly summing up the wave variables:

$$u(t) = \frac{a+b}{2} \qquad \text{and} \qquad i(t) = \frac{a-b}{2Z_0}. \tag{48}$$

It is worth noting that this differs from the wave decomposition often done in digital waveguides (see, e.g. [253]), where the K-variables are obtained by summing the wave variables without the scaling-by-two. We will discuss this in more detail in section 8.5.4.

Reflectance of a port is the transfer function that indicates the relation between an incoming and an outgoing wave to that port. Formally, it can be obtained from the Laplace transform of the reflected wave, divided by the Laplace transform of the incoming wave [254]:

$$S_{\mathrm{Z}}(s) = \frac{\mathcal{L}\{b\}}{\mathcal{L}\{a\}} = \frac{\mathcal{L}\{u(t) - Z_0 i(t)\}}{\mathcal{L}\{u(t) + Z_0 i(t)\}} = \frac{Z(s) - Z_0}{Z(s) + Z_0}, \tag{49}$$

where $\mathcal{L}$ is the Laplace operator. Note that here we used voltage waves in defining the reflectance; had we used current waves, we would have obtained another formulation for the reflectance. Therefore, this result can also be called the voltage-wave reflectance or the force-wave reflectance in the mechanical domain.

8.2.2. One-port elements. This section will discuss the basic one-port elements: capacitors, inductors, resistors, open- and short-circuits and voltage and current sources. We will derive their individual reflectances in a similar way as in [254]. Two-port elements, such as gyrators, transformers and QUARLs, are discussed, e.g. in [94].

For a capacitor, it holds that the current $i(t)$ flowing through the element is proportional to the time derivative of the voltage $u(t)$ across it:

$$i(t) = C\frac{\partial u(t)}{\partial t}, \tag{50}$$

where C is the capacitance in Farads. Using the Laplace transform, we have

$$I(s) = CsU(s), \tag{51}$$

where s is the complex frequency variable, and $I(s)$ and $U(s)$ stand for the current and voltage in the complex frequency domain, respectively. Using the generalized Ohm's law, the impedance of a capacitor can now be given as

$$Z_{\mathrm{C}}(s) = \frac{1}{Cs}. \tag{52}$$

Substituting $Z_{\mathrm{C}}(s)$ for $Z(s)$ in equation (49), we obtain the reflectance of the capacitor as

$$S_{\mathrm{C}}(s) = \frac{Z_{\mathrm{C}}(s) - Z_0}{Z_{\mathrm{C}}(s) + Z_0} = \frac{1 - Z_0 Cs}{1 + Z_0 Cs}. \tag{53}$$

For an inductor, the voltage is in turn proportional to the time derivative of the current:

$$v(t) = L\frac{\partial i(t)}{\partial t}, \tag{54}$$

where L denotes the inductance in Henrys. Similarly, taking the Laplace transform and calculating the impedance, we have

$$Z_{\mathrm{L}}(s) = Ls. \tag{55}$$

Substituting this result into equation (49), we obtain the reflectance of the inductor as

$$S_{\mathrm{L}}(s) = \frac{Z_{\mathrm{L}}(s) - Z_0}{Z_{\mathrm{L}}(s) + Z_0} = \frac{s - Z_0/L}{s + Z_0/L}. \tag{56}$$

For a resistor, we have

$$u(t) = Ri(t), \tag{57}$$

where R is the resistance (in Ohms), and for the impedance we get simply

$$Z_{\mathrm{R}}(s) = R. \tag{58}$$

Thus, the reflectance of the resistor becomes

$$S_{\mathrm{R}}(s) = \frac{1 - Z_0/R}{1 + Z_0/R}. \tag{59}$$

Obviously, for the open and short circuit impedances, we have

$$Z_{\mathrm{oc}}(s) = \infty \tag{60}$$

and

$$Z_{\mathrm{sc}}(s) = 0, \tag{61}$$

respectively. Hence, the reflectances become

$$S_{\mathrm{oc}}(s) = 1 \tag{62}$$

and

$$S_{\mathrm{sc}}(s) = -1. \tag{63}$$

Note that this corroborates with our knowledge of wave propagation. An open circuit reflects voltage waves without changing their phase, whereas the short circuit inverts the phase of the reflecting voltage. In mechanical terms, a rigid wall termination reflects force waves without phase inversion, while a free 'frictionless' termination inverts the phase of the reflecting force. For velocity waves, such as the ones observable in a vibrating string[4], the opposite is true: rigid terminations invert the phase, whereas free terminations preserve it.

We will consider voltage and current sources in their digitized form in section 8.3.3. These elements are needed if energy needs to be inserted into the system during run time. Otherwise, initializing the voltage and current of the circuit is sufficient.

8.3. Wave digital building blocks

This section discusses the digitized versions of the analog elements already introduced and provides rules for connecting them to form networks.

8.3.1. Discretization using the bilinear transform. The discretization of the network elements discussed in section 8.3.3 is implemented using the well-known bilinear transform:

$$s \to \psi = \frac{2}{T}\frac{1 - z^{-1}}{1 + z^{-1}} = \frac{2}{T}\tanh(sT/2), \tag{64}$$

where $z = \mathrm{e}^{sT}$ denotes the discrete complex frequency, while T stands for the sampling interval. By studying the real-valued discrete frequencies, we note that

$$Re[\psi] > 0 \;\Leftrightarrow\; Re\left[\frac{2}{T}\frac{\mathrm{e}^{sT} - 1}{\mathrm{e}^{sT} + 1}\right] > 0 \;\Leftrightarrow\; Re[s] > 0 \;\Leftrightarrow\; |z| > 1, \tag{65}$$

$$Re[\psi] < 0 \;\Leftrightarrow\; Re\left[\frac{2}{T}\frac{\mathrm{e}^{sT} - 1}{\mathrm{e}^{sT} + 1}\right] < 0 \;\Leftrightarrow\; Re[s] < 0 \;\Leftrightarrow\; |z| < 1 \tag{66}$$

and

$$Re[\psi] = 0 \;\Leftrightarrow\; Re\left[\frac{2}{T}\frac{\mathrm{e}^{sT} - 1}{\mathrm{e}^{sT} + 1}\right] = 0 \;\Leftrightarrow\; Re[s] = 0 \;\Leftrightarrow\; |z| = 1. \tag{67}$$

[4] Actually, looking at a vibrating string one observes the displacement waves, but comparing them to their time derivative, i.e. the velocity waves, one notices that they reflect similarly.

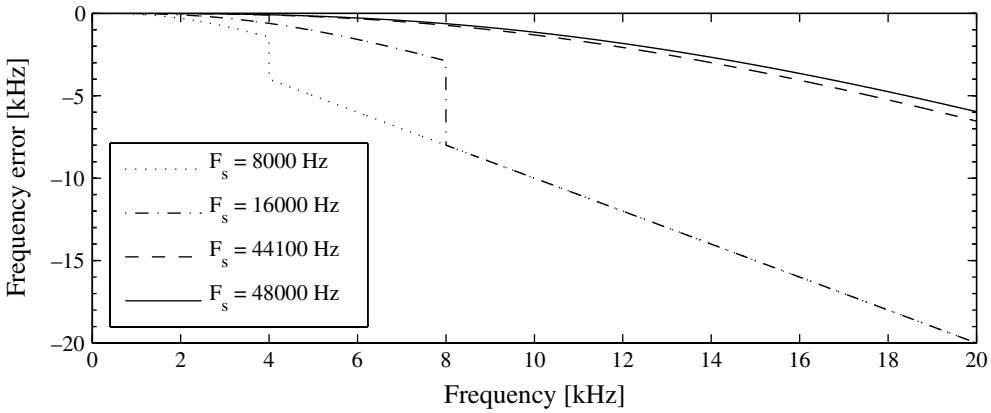

Figure 24. The frequency error, i.e. the difference between the desired analog frequency and the resulting digital frequency, caused by the bilinear transform as a function of the analog frequency. The different lines denote different sampling frequencies. The sudden increase of the negative error in sampling frequencies $F_s = 8000$ and $F_s = 16\,000$ takes place at the Nyquist frequency, and the following straight line denotes the fact that the error is 100%, since these frequencies cannot be generated.

This means that the bilinear transform applies a Möbius mapping for the imaginary s axis in the analog domain onto the unit circle in the digital domain. The frequency values with a positive real part are mapped to the outer disk, while the frequency values with a negative real part are mapped to the inner disk. By studying the inverse bilinear transform

$$z = \frac{1 + s(T/2)}{1 - s(T/2)}, \tag{68}$$

we see that the analog dc ($s = 0$) is mapped onto $z = 1$, which corresponds to the real digital frequency $\arg(z) = 0$ rad. Also, the highest analog frequency ($s = \infty$) is mapped onto $z = -1$, which corresponds to the highest digital frequency $\arg(z) = \pi$ rad.

Although the bilinear mapping is one-to-one so that aliasing does not occur, the frequency scale is not linear but warped, especially at the high frequencies. Figure 24 illustrates the digital frequency error as a function of analog frequency, with different sampling frequencies. Fortunately, in most audio synthesis applications the frequencies of interest are considerably lower than the Nyquist frequency, so this warping does not usually cause much trouble.

It is interesting to note that if z^{-1} is interpreted as the unit delay in the time domain, the bilinear transform of equation (64) is equivalent to the trapezoidal rule for approximating the time derivative [30]. We can now compare this approximation technique with the finite difference approximation, introduced in equation (2):

$$\frac{\partial y}{\partial t} \approx \frac{y(t) - y(t - T)}{T}. \tag{69}$$

If the temporal sampling interval is set to $T = 1$, as is often done in practice, we see that the transfer function of the FDA becomes $H_{\mathrm{FDA}}(z) = 1 - z^{-1}$, which is actually the (scaled) numerator part of the bilinear transform. It is easy to show [254] that the FDA in fact maps the imaginary axis onto a circle with radius $1/2$, centred at $z = 1/2$. Obviously, the warping of the frequencies is more severe in this case when compared with the bilinear transform. It must be noted that also other numerical integration schemes for solving PDEs, such as the Runge–Kutta method (see, e.g. [152]), can be interpreted as s-to-z mappings with different numerical properties.

8.3.2. Realizability. If the inductor element is now discretized using the bilinear transform, using equation (56), its reflectance becomes

$$S_{\mathrm{L}}\left(\frac{2}{T}\frac{1-z^{-1}}{1+z^{-1}}\right) = \frac{(2/T - Z_0/L) - (Z_0/L + 2/T)z^{-1}}{(2/T + Z_0/L) + (Z_0/L - 2/T)z^{-1}}. \tag{70}$$

Now, remembering that reflectance is actually the transfer function from the incident wave to the reflected one, we see that it has a delay-free term in the nominator. When this element is connected into a junction, we see that the incident wave (looking from the element's view) is evaluated using the reflected wave. Now, since there is a delay-free term in the reflectance of this element, the system becomes implicit, since we would need the instantaneous output of the system when calculating the input. Fortunately, we can solve this problem by utilizing the extra degree of freedom, the port impedance, by assigning an appropriate value for it.

8.3.3. One-port elements. Defining $Z_0 = Z_{\mathrm{L}} = 2L/T$ for the impedance of the wave digital inductor in equation (56), the reflectance simplifies to

$$S_{\mathrm{L}}(z) = -z^{-1}. \tag{71}$$

Similarly, selecting $Z_0 = Z_{\mathrm{C}} = T/(2C)$ for the impedance of the wave digital capacitor in equation (53) simplifies reflectance to

$$S_{\mathrm{C}}(z) = z^{-1}. \tag{72}$$

Since the reflectance of the resistor is memoryless, i.e. there is no s-term in equation (59), we can simply choose $Z_0 = Z_{\mathrm{R}} = R$ for the resistor's impedance in equation (59), and the reflectance goes to zero:

$$S_{\mathrm{R}}(z) = 0, \tag{73}$$

which means that there is no reflection from the one-port resistor element. We will later find out how connecting a wave digital resistor can still affect a system.

Voltage and current sources can also be implemented as wave digital elements. For the voltage source, we have [94]

$$S_{\mathrm{u}}(z) = 2e - 1, \tag{74}$$

and for the current source

$$S_{\mathrm{i}}(z) = 1 - 2e, \tag{75}$$

where e is the voltage generated by the source. Table 1 summarizes the one-port elements discussed thus far.

8.4. Interconnection and adaptors

The interconnection of different one-port elements is possible using adaptors. Adaptors are N-port interfaces that enable the connection of other N-port elements and implement the wave scattering resulting from the different port impedances. There are two types of adaptors: parallel and series. The parallel adaptor is the wave digital equivalent of the parallel connection from basic circuit theory. N-port elements connected in parallel share the same voltage, while their currents sum up to zero. Intuitively, the series adaptor is in turn the wave digital equivalent of the series connection. N-port elements connected in series share the current and the voltages sum up to zero.

In this section, we will derive the scattering rules first for two-port parallel and series adaptors, after which we will extend these results for obtaining the scattering rules for N-port adaptors. This derivation process follows the guidelines presented in the WDF literature [94, 254].

Table 1. Table of the basic analog elements (column 2) and their wave digital versions (column 5). Columns 3 and 4 contain the element impedances and the corresponding reflectances, respectively.

Element type	Analog element	Impedance	Reflectance	Wave digital element
Inductor	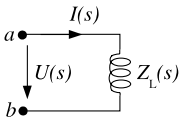	$Z_{\mathrm{L}} = 2L/T$	$S_{\mathrm{L}}(z) = -z^{-1}$	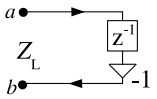
Capacitor	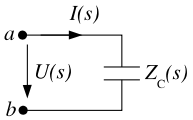	$Z_{\mathrm{C}} = T/(2C)$	$S_{\mathrm{C}}(z) = z^{-1}$	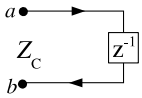
Resistor	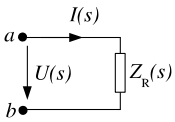	$Z_{\mathrm{R}} = R$	$S_{\mathrm{R}}(z) = 0$	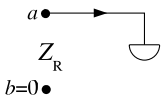
Open circuit	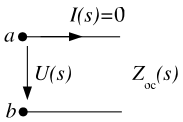	$Z_{\mathrm{oc}} = \infty$	$S_{\mathrm{oc}}(z) = 1$	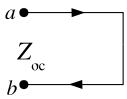
Short circuit	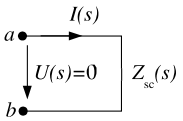	$Z_{\mathrm{sc}} = 0$	$S_{\mathrm{sc}}(z) = -1$	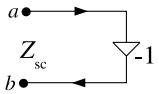
Voltage source	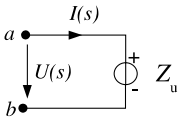	$Z_{\mathrm{u}} = 0$	$S_{\mathrm{u}}(z) = 2e - 1$	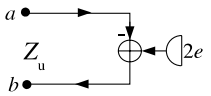
Current source	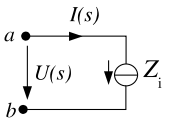	$Z_{\mathrm{i}} = \infty$	$S_{\mathrm{i}}(z) = 1 - 2e$	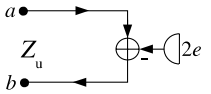

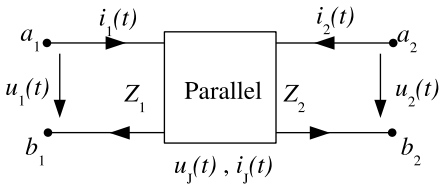

Figure 25. A two-port parallel adaptor. The subscripts of the K-variables $u(t)$ and $i(t)$ and the wave variables a and b correspond to the number of the port to which they are assigned. Variables $u_{\mathrm{J}}(t)$ and $i_{\mathrm{J}}(t)$ denote the voltage and current at the junction itself. The abstraction symbol for a two-port series adaptor is otherwise identical, but the text 'Parallel' is changed to 'Series' inside the adaptor.

8.4.1. Two-port adaptors. Let us consider a two-port parallel adaptor, illustrated in figure 25. For the parallel connection, the voltages must be equal and the currents must sum up to zero, i.e.

$$u_1(t) = u_2(t) \qquad \text{and} \qquad i_1(t) + i_2(t) = 0. \tag{76}$$

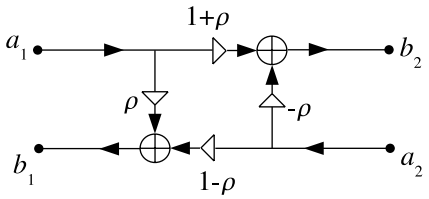

Figure 26. The Kelly–Lochbaum implementation of the two-port scattering junction. Coefficient ρ stands for the scattering coefficient.

Substituting equation (48) into equation (76), we have

$$\frac{a_1 - b_1}{2Z_1} + \frac{a_2 - b_2}{2Z_2} = 0, \tag{77}$$

and solving b_1 and b_2 from the first part of equation (48) we get

$$\frac{a_1 - u_1}{Z_1} + \frac{a_2 - u_2}{Z_2} = 0 \Leftrightarrow u_1 \left(\frac{1}{Z_1} + \frac{1}{Z_2} \right) = \frac{a_1}{Z_1} + \frac{a_2}{Z_2} \tag{78}$$

and finally

$$u_1 = u_2 = u_J = \frac{Y_1}{Y_1 + Y_2} a_1 + \frac{Y_2}{Y_1 + Y_2} a_2 = \frac{Y_1 a_1 + Y_2 a_2}{Y_1 + Y_2}, \tag{79}$$

where $Y_n = 1/Z_n$ is the admittance of port n. Now, for the reflected wave b_1, we have from equation (48)

$$b_1 = 2u_J - a_1 = \frac{2Y_1 a_1 + 2Y_2 a_2}{Y_1 + Y_2} - a_1 = \frac{Y_1 - Y_2}{Y_1 + Y_2} a_1 + \frac{2Y_2}{Y_1 + Y_2} a_2 \tag{80}$$

and similarly for b_2,

$$b_2 = 2u_J - a_2 = \frac{2Y_1}{Y_1 + Y_2} a_1 + \frac{Y_2 - Y_1}{Y_1 + Y_2} a_2. \tag{81}$$

Let us now think of connecting a wave digital one-port element to the first port of this adaptor (see figure 25). If the reflectance of the one-port has a delay-free term; i.e. if a_1 depends directly on b_1 as in equation (70), a delay-free loop is formed between the one-port and the adaptor. This is the reason why we chose such values for the port impedances so that the delay-free terms were eliminated in the reflectances in section 8.3.3.

Note also, that if we define a reflection coefficient as $\rho = (Y_1 - Y_2)/(Y_1 + Y_2)$, equations (80) and (81) simplify to the familiar form

$$\begin{bmatrix} b_1 \\ b_2 \end{bmatrix} = \begin{bmatrix} \rho & 1 - \rho \\ 1 + \rho & -\rho \end{bmatrix} \begin{bmatrix} a_1 \\ a_2 \end{bmatrix}, \tag{82}$$

called the Kelly–Lochbaum implementation of the scattering junction. This junction is illustrated in figure 26.

For the two-port series adaptor, we have that the current is common and the voltages must sum up to zero, i.e.

$$i_1(t) = i_2(t) \qquad \text{and} \qquad u_1(t) + u_2(t) = 0. \tag{83}$$

Substituting equation (48) into equation (83) and solving b_1 and b_2 from the latter part of equation (48), we have

$$i_J(t) = \frac{a_1 + a_2}{Z_1 + Z_2}, \tag{84}$$

which denotes the current at the junction. Again, from equation (48), we get

$$b_1 = \frac{Z_2 - Z_1}{Z_1 + Z_2} a_1 - \frac{2Z_1}{Z_1 + Z_2} a_2 \tag{85}$$

and

$$b_2 = -\frac{2Z_2}{Z_1 + Z_2} a_1 + \frac{Z_1 - Z_2}{Z_1 + Z_2} a_2. \tag{86}$$

Since

$$Y_j = 1/Z_j \Rightarrow \rho = \frac{Y_1 - Y_2}{Y_1 + Y_2} = \frac{Z_2 - Z_1}{Z_1 + Z_2}, \tag{87}$$

we can denote equations (85) and (86) simply as

$$\begin{bmatrix} b_1 \\ b_2 \end{bmatrix} = \begin{bmatrix} \rho & -(1-\rho) \\ -(1+\rho) & -\rho \end{bmatrix} \begin{bmatrix} a_1 \\ a_2 \end{bmatrix}. \tag{88}$$

8.4.2. N-port adaptors. The scattering rules from the two-port adaptors can directly be extended for defining the scattering of the N-port adaptors [254]. For the parallel connection, we have

$$\sum_{j=1}^{N} i(t) = 0 \Leftrightarrow \sum_{j=1}^{N} \frac{a_j - b_j}{2Z_j} = 0, \tag{89}$$

which becomes

$$\sum_{j=1}^{N} \frac{a_j - u(t)}{Z_j} \tag{90}$$

after substituting $b_j = 2u(t) - a_j$. Note that the voltage $u(t)$ is common in the parallel connection. Now, we can formulate the total junction voltage as

$$u(t) = u_J(t) = \frac{\sum_{j=1}^{N} a_j Y_j}{\sum_{k=1}^{N} Y_k}. \tag{91}$$

From equation (48), we now have the reflected voltage wave as

$$b_m = \frac{2\sum_{j=1}^{N} a_j Y_j}{\sum_{k=1}^{N} Y_k} - a_m \qquad \text{for the parallel connection.} \tag{92}$$

For the series connection, we have

$$\sum_{j=1}^{N} u(t) = 0 \Leftrightarrow \sum_{j=1}^{N} \frac{a_j + b_j}{2} = 0 \Leftrightarrow \sum_{j=1}^{N} a_j - Z_j i(t) = 0, \tag{93}$$

so the total junction current is

$$i(t) = i_J(t) = \frac{\sum_{j=1}^{N} a_j}{\sum_{k=1}^{N} Z_k}. \tag{94}$$

Again, from equation (48) we have

$$b_m = a_m - \frac{2Z_m}{\sum_{k=1}^{N} Z_k} \sum_{j=1}^{N} a_j \qquad \text{for the series connection.} \tag{95}$$

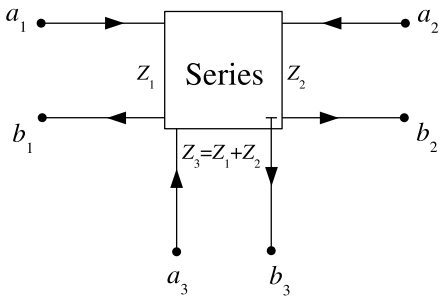

Figure 27. A three-port series adaptor with a reflection-free third port. No delay-free loops can then occur between the third port and the element connected to it, regardless of implementation of that element.

It is interesting to note that the N-port wave digital adaptors perform the exactly same computation as the N-port digital waveguide junctions [254], provided that the wave definitions are compatible. We will return to this topic in section 8.5.4.

8.4.3. Reflection-free ports. In section 8.3.3 we defined the port impedances of the one-port elements so that no delay-free loops could be formed when the one-ports were interconnected. Optionally, we can make one of the ports of an N-port adaptor reflection-free by assigning suitable values for the port impedances. More specifically, if we define the impedance of port m to equal the sum of all other port impedances connected in series with it, i.e.

$$Z_m = \sum_{j=1,\, j\neq m}^{N} Z_j, \tag{96}$$

the impedance match from branch m to the junction becomes exact and no reflection occurs. This can be checked by substituting equation (96) to equation (95) and obtaining

$$b_m = a_m - 2\frac{\sum_{j=1,\, j\neq m}^{N} Z_j}{\sum_{j=1}^{N} Z_j} \sum_{j=1}^{N} a_j = a_m - 2\frac{\sum_{j=1,\, j\neq m}^{N} Z_j}{2\sum_{j=1,\, j\neq m}^{N} Z_j} \sum_{j=1}^{N} a_j = -\sum_{j=1,\, j\neq m}^{N} a_j \tag{97}$$

for the series reflection-free port.

In the same manner, for the parallel connection, we can define the admittance of port m to equal the sum of all other port admittances, i.e.

$$Y_m = \sum_{j=1,\, j\neq m}^{N} Y_j, \tag{98}$$

and obtain the wave leaving the parallel adaptor at port m from

$$b_m = \frac{2}{\sum_{j=1}^{N} Y_j} \sum_{j=1,\, j\neq m}^{N} Y_j a_j. \tag{99}$$

Equations (97) and (99) now reveal that since the reflected wave at port m does not depend on the incident wave a_m, no delay-free loop can be formed between the one-port and the adaptor, regardless of implementation of the one-port element.

Figure 27 illustrates a three-port series adaptor, where the third port is reflection-free. Note that the b_3 terminal has a T-shaped ending to emphasize the fact that it does not depend on a_3.

Table 2. Table of the analogies between different domains: electrical (first column), mechanical (second column) and acoustical (third column). In the acoustic domain, ρ_{air} denotes the air density, l denotes the length of a short, open tube, while a stands for the cross-sectional area of the tube. V and c are the volume of a cavity and the speed of sound, respectively.

Electrical domain	Mechanical domain	Acoustical domain
voltage, $u(t)$	force, $f(t)$	air pressure, $p(t)$
current, $i(t)$	velocity, $v(t)$	volume velocity, $u(t)$
inductance, L	mass, m	acoustic inductance (in a tube), $\rho_{\text{air}} l/a$
capacitance, C	inverse of the spring constant, $1/k$	acoustic capacitance (inside a cavity), $V/\rho_{\text{air}} c^2$
resistance, R	mechanical resistance, R	fluid-dynamic resistance, R

8.5. Physical modelling using WDFs

The modelling process of a physical system using WDFs can be summarized in the following steps:

(i) Analyse the physical system to be modelled. Express a mechanical system using masses, springs and dampers or an acoustic system using acoustic inductances, capacitances and losses. Remember that if the elements share the same force (air pressure) they are connected in parallel. If they share the same velocity (volume velocity) they are connected in series. Find out which parameters are given and which must be obtained.

(ii) Move the system into the electrical domain using analogies between different domains. (See table 2. For a more thorough discussion between the analogies between domains, see, e.g. [10].)

(iii) Substitute the analog elements with the wave digital one-ports and their connections with adaptors. Substitute the given parameters and use the equations presented in the previous section to evaluate the desired quantities.

We will look more deeply into connecting the WDFs to form networks in the following section. Section 8.5.2 will consider implementing nonlinearities in wave digital networks.

8.5.1. Wave digital networks. The one-port elements and the N-port adaptors discussed in section 8.3 can now be connected for modelling physical structures. The connections between the one-ports and adaptors should comply with the following rules.

- A terminal can be connected to no more than one other terminal only.
- The grouping of terminals must be preserved; i.e. if a terminal a_n of port n is connected to a terminal b_m of port m, the remaining terminals of these ports, namely b_n and a_m, must be connected also.
- The wave flow directions must be preserved within the terminals. This means that after connecting a wave digital element into an adaptor the wave b_n leaving the element must become the wave a_m entering the adaptor [254].
- The impedances of connected ports must be equal. This is necessary since wave scattering can be properly implemented only by the adaptor element, not by the port impedance itself.
- No delay-free loops can occur. We have demonstrated two techniques for accomplishing this: choosing the element impedances properly or using reflection-free ports.

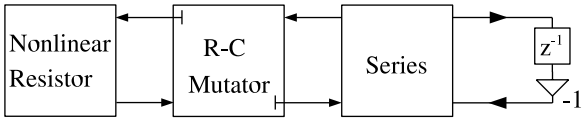

Figure 28. A nonlinear capacitance connected in series with a linear inductance. The reactive part of the capacitance is implemented by the mutator, while the resistive part is implemented by the nonlinear resistor. Both terminals of the mutator are reflection-free, since there is no instantaneous dependence between the incident and reflected waves.

8.5.2. Modelling of nonlinearities. We have so far discussed only linear systems. Although many physical systems can indeed be considered linear, the characteristic tones of many musical instruments are due to nonlinearities. This section briefly discusses modelling of nonlinearities via WDFs. We will first consider the simulation of nonlinear resistors, after which we will generalize our system to cover also nonlinear capacitors and inductors using special mutator elements, as done in [225]. An overview on nonlinearities in WDFs can be found in [197].

Let us consider a simple nonlinear resistor whose value depends on the voltage applied over it. This means that there is a nonlinear dependency between the voltage and the current. In practice, we can obtain samples of this dependency, e.g. by measurements, and the values can be stored in a lookup table. Using this table, we can implement a wave digital version of the nonlinear resistor in the following way [225].

- First, a K-variable at the port connected to the resistor, $u(t)$ for example, is needed. This can be obtained by evaluating the Thevenin equivalent of the rest of the circuit, for instance.
- Next, read the value of the other K-variable, $i(t)$ in this case, from the lookup table using its dual variable.
- Finally, use equation (47) to get the wave leaving the nonlinear resistor.

Note that in order to avoid delay-free loops, the nonlinear resistor must be connected to a reflection-free port of an adaptor. This also means that the incident wave at the resistor does not affect the reflected wave. A more analytical formulation of a nonlinear resistor can be found in [175].

When the nonlinearity is reactive, i.e. it involves integrals or derivatives, the above procedure does not suffice. In fact, any classical wave digital modelling attempt fails due to computability problems [225], and special elements, called mutators, are needed. Basically, mutators are two-port adaptors with memory, and their task is to implement the reactive part of a general algebraic nonlinear element. A nonlinear capacitor, for example, is constructed by connecting an R–C mutator to a nonlinear resistor. The interaction with this nonlinear capacitor is then conducted using the remaining port of the mutator. A wave digital circuit with a nonlinear capacitor connected in series with a linear inductor is shown in figure 28.

Formally, implementing the reactive part of the nonlinearity is carried out by augmenting the reflection coefficient ρ of a two-port scattering junction with memory in order to obtain a reflection transfer function $\rho(z)$. For the R–C mutator, it can be shown, as in [225], that the reflection transfer function becomes simply

$$\rho(z) = z^{-1}. \tag{100}$$

For the R–L mutator, the reflection transfer function becomes [225]

$$\rho(z) = -z^{-1}. \tag{101}$$

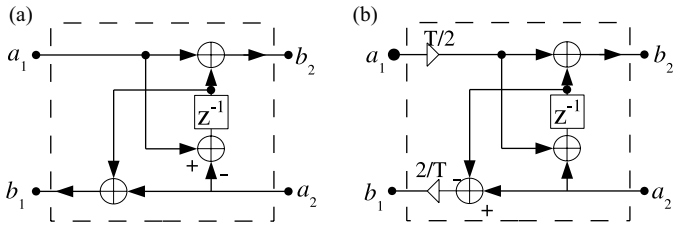

Figure 29. The signal flow graph of (*a*) the R–C mutator and (*b*) the R–L mutator. These graphs have been obtained from figure 26 by substituting $\rho \leftarrow z^{-1}$ in (*a*), and $\rho \leftarrow -z^{-1}$ in (*b*).

Note that this is in perfect agreement with our previous results; here the reflection coefficient ρ of a two-port junction (see, e.g. figure 26) has just been replaced by a reflection transfer function $\rho(z)$, which in the case of an R–C mutator equals the reflectance of a wave digital capacitor (equation (53)). Similarly, for the R–L mutator, we have $\rho(z) = S_{\mathrm{L}}(z^{-1})$. The signal flow graphs of the R–C and R–L mutators are illustrated in figure 29.

We will not consider time-varying WDFs here. Studies concerning them can be found, e.g. in [265] and [31].

8.5.3. Case study: the wave digital hammer. As a case study, we will consider a nonlinear wave digital piano hammer, introduced in [196]. This presentation of a piano hammer is a simplified one; the hammer is thought to consist of a mass and a nonlinear spring, corresponding to the compressing felt. Figure 30 shows the schematic diagram of the piano excitation mechanism, along with the simplified model. The string that the hammer excites can be modelled using a simple digital waveguide, attached to a damper, for modelling the losses. When the hammer is in contact with the string, they must share the same velocity. Also, the force that the hammer exerts on the string has an opposite but equal restoring force rising from the string, so that the total force is zero. Therefore, we can conclude that the connection between the string and the hammer is a series one.

For the losses, it is clear that the string and the damper share the same velocity since they are in motion together, and the force between them adds to zero. Therefore, the string–damper interaction is a series connection.

For the mass-to-spring connection, although the mass and the felt both share the same velocity when the hammer is 'in flight', they have different velocities when the hammer is in contact with the string, due to the felt compression. Also, since the same force is applied on both the mass and the spring, the connection between them is parallel. With these in mind, we can now present an electrical equivalent circuit of the nonlinear piano hammer with the damper in figure 31, and its wave digital version together with the string in figure 32.

Note that since there are no sources in this system, the wave digital hammer cannot be excited during run time. Instead, in order to move the hammer, we must set the initial parameter values so that the hammer is in motion already when the simulation begins.

8.5.4. Wave modelling possibilities. There are also alternative ways to perform the wave decomposition that we did in equation (47). As already stated, current (velocity) waves could be used instead, which would be equivalent to changing the inductors to capacitors and serial connections to parallel ones and vice-versa in our WDF networks. The behaviour of our model would still remain essentially the same, since this would mean only using the dual system in the Kirchhoffian sense.

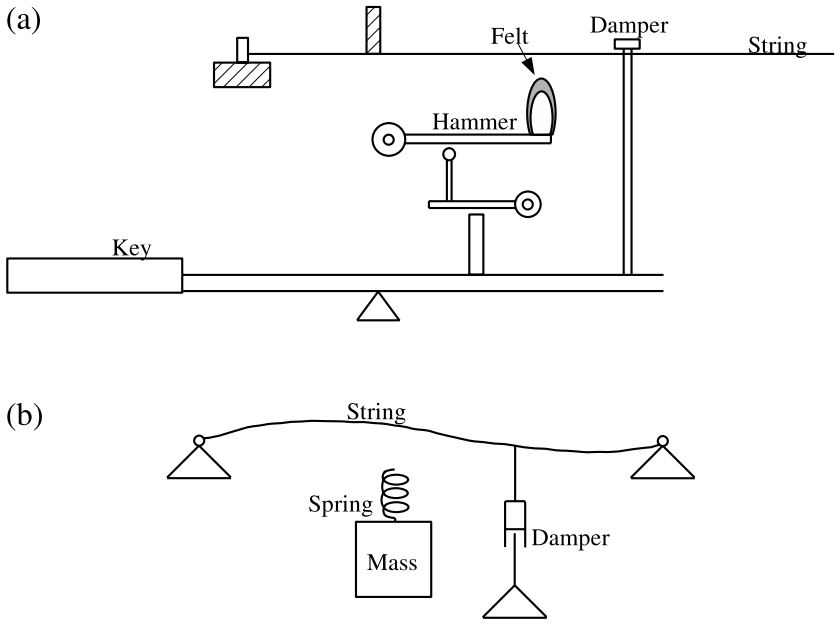

Figure 30. The schematic diagram of the excitation mechanism of a piano (*a*) (after [221]) and its simplified version (*b*) consisting of a mass, spring, damper and a string. In (*a*), when the key is pressed, energy is transferred via the lever mechanism to the hammer, which hits the string. The hammer is coated with a soft felt, which compresses in a nonlinear fashion.

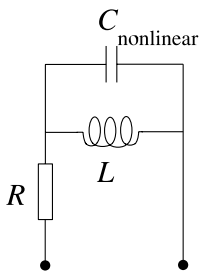

Figure 31. The electrical equivalent circuit of the nonlinear hammer with a damper. The resistance value of the damper is given as R, and the inductance corresponding to the hammer mass is denoted as L. The capacitor corresponding to the nonlinear spring is characterized by the capacitance $C_{\text{nonlinear}}$. The string element would be connected to the free terminals of the circuit.

Optionally, we could define the voltage waves similarly to what is often done in the digital waveguides:

$$\begin{bmatrix} a \\ b \end{bmatrix} = \frac{1}{2} \begin{bmatrix} 1 & Z_0 \\ 1 & -Z_0 \end{bmatrix} \begin{bmatrix} u(t) \\ i(t) \end{bmatrix}. \tag{102}$$

Note that here summing the wave variables a and b gives the K-variable $u(t)$ directly. This is traditionally the case with digital waveguides, where, e.g. the string displacement at a certain location is obtained by simply summing the wave components at that location. Therefore, if the wave variables are defined as in equation (102), the wave digital systems and digital waveguide structures become fully compatible. Otherwise, a scaling, like the one in figure 32,

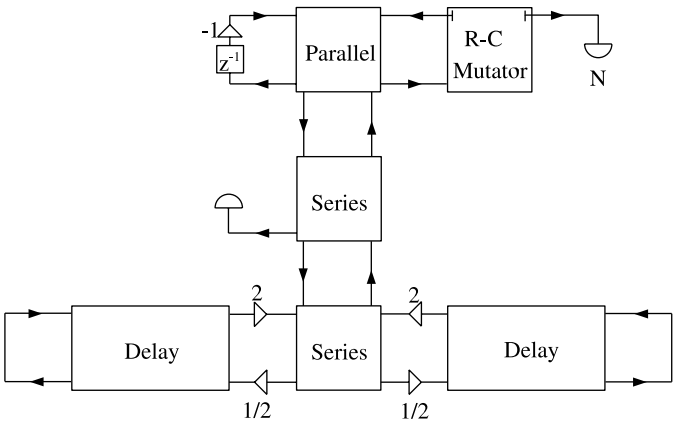

Figure 32. The wave digital presentation of the nonlinear piano hammer. The N near the top resistor denotes its nonlinearity. The nonlinear capacitor is obtained connecting the nonlinear resistor to an R–C mutator. The delay elements are bidirectional delay lines, implementing the digital waveguide string. The termination of the string from the rigid boundary is phase-preserving, since voltage (force) waves are used here. The reason for the scaling between the WDF and DWG blocks will be discussed in section 8.5.4.

must be made. It must be emphasized, however, that wave digital networks are generally *not* the same as digital waveguide networks, since in digital waveguides the impedance Z_0 is defined as the physical wave impedance [254], whereas in WDFs Z_0 is an additional degree of freedom that can be used for easing the calculations.

Another possibility for wave decomposition is to use power-normalized waves [94], where the wave components are defined as

$$\begin{bmatrix} a \\ b \end{bmatrix} = \frac{1}{2\sqrt{R}} \begin{bmatrix} 1 & Z_0 \\ 1 & -Z_0 \end{bmatrix} \begin{bmatrix} u(t) \\ i(t) \end{bmatrix}. \tag{103}$$

The advantage here is that the change in the wave impedances in different parts of the system does not change the power transmitted by the waves; i.e. the signal power does not depend on the impedances. This kind of behaviour is needed if time-varying wave digital networks are desired. Otherwise, changing the impedance of an element would result in changing the power and thus also the energy of the system. Power-normalized wave digital models have been used, e.g. in [23].

8.5.5. Multidimensional WDF networks. All models considered so far have been lumped, i.e. we have lost the spatial dimensions of the elements for obtaining simpler models. It is worth noting, however, that the spatial dimensions of the models can be preserved if they are modelled using multidimensional WDFs [94]. The procedure for deriving multidimensional WDF elements is somewhat similar to what is done in the lumped case, the main difference being the fact that the reference circuit must be presented by a multidimensional Kirchhoff circuit, since a simple electrical equivalent does not suffice.

This circuit is far more of a mathematical abstraction than its lumped version, and the state of the circuit depends on several variables, which may or may not include time [30]. A deeper discussion of the multidimensional WDFs is outside the scope of this paper, and the reader can find a thorough study of the topic in [30].

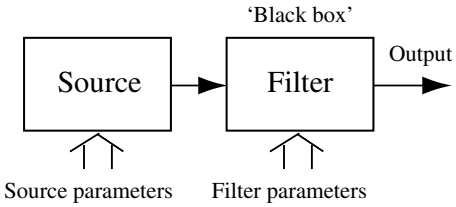

Figure 33. Black box representation of a source–filter model.

8.6. Current research

Wave digital filters are used in various musical instrument models. Nonlinear wave digital piano hammers have already been considered, e.g. in [23, 196, 298]. WDFs have also been used in woodwind modelling, where the tonehole is considered as a lumped system [304, 305]. Very recently, the energy-preserving abilities of WDFs have been used for designing energetically passive time-varying generalizations of allpass filters [31]. Furthermore, these allpass filters are used in generating an energetically well-behaving string model with time-varying tension [187].

9. Source–filter models

The source–filter paradigm for modelling of acoustic systems and for synthesizing related sounds dates back to early analog sound synthesis. Before computerized times, it was used extensively in speech synthesis and coding studies since the Voder synthesizer by Dudley (described in [95]) and many analog music synthesizers [281], such as the popular Minimoog [43].

Source–filter modelling and synthesis consist of a wide range of methods from abstract ad hoc signal processing techniques, which do not have any physical correspondence, to methods that have a clear physical interpretation. As a matter of fact, every model that includes an active excitation and a subsystem that processes the excitation can be seen as a source–filter model. In this sense, all physics-based modelling paradigms discussed in this paper exhibit the source–filter aspect; for example, a modal filterbank in the modal synthesis shows this aspect. Particularly, the single delay-line versions in DWG theory are clearly source–filter models.

There is no strict dividing line between truly physics-based modelling and abstract source–filter models. One way to categorize systems is to refer to the simple black box representation in figure 33. To be a true physical model, the source signal should be a physically relevant variable, and the inner structure of the filter should correspond to the physical structure of the system under study. Furthermore, the interaction of subsystems should be bi-directional in a physics-based manner. In spatially distributed structures, the variables used should correspond to the true spatial positions used for modelling. Such strict requirements can be essential if the modelling is intended to gain understanding of the physical details of a particular system, for example, in basic research of musical acoustics or virtual prototyping in instrument design. On the other hand, in sound synthesis the requirement of real-time efficiency can typically be fulfilled best by reducing the model to an abstract source–filter structure and uni-directional signal flow.

In source–filter modelling, referring to figure 33, the source can be an oscillator to generate a periodic or non-periodic waveform, such as a sine wave, sawtooth wave, impulsive signal,

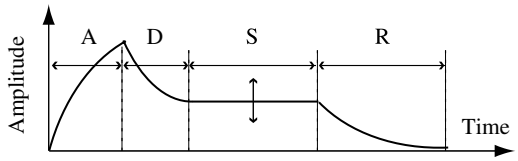

Figure 34. Typical ADSR envelope curve for controlling the signal level in sound synthesis.

noise or glottal waveform in speech synthesis. The source is often implemented as a wavetable, i.e. a stored synthetic or sampled signal is repeated in a loop and it is then modified by the filter.

The filter in discrete-time modelling can be any digital filter, linear or nonlinear, that is applicable to the task at hand. Basic resonant filters are presented below in section 9.2 as applied to the modelling of voice production and to speech synthesis. As a limit case we can see the memoryless nonlinear operations for waveshaping, such as the popular frequency modulation (FM) synthesis [54], which can be classified as an abstract synthesis algorithm but hardly as a source–filter model.

The source and particularly the filter in figure 33 are controlled by time-varying parameters in order to change the characteristics of sound as functions of time. A classical method in computer music, for both analog and digital synthesizers, is to apply so-called ADSR (attack, decay, sustain, release) characteristics to synthesis control. Figure 34 illustrates a typical ADSR curve for the amplitude level of synthesized sound.

9.1. Subtractive synthesis in computer music

The term 'subtractive synthesis' has been used often in computer music to describe techniques that are essentially source–filter modelling [5, 212]. The motivation to use this term probably comes from the fact that 'additive synthesis' is used as a paradigm where signal components, typically sinusoidal signals, are added to construct the desired signal spectrum. Therefore, it seems logical to define subtractive synthesis as a contrasting way to synthesize sounds, because it starts from a source signal and in a sense 'subtracts', i.e. attenuates some frequencies.

While the term 'subtractive synthesis' may seem logical, it can also be misleading as it does not fit into the model-based terminology. The filter part does not only attenuate (i.e. subtract) signal components, but it can amplify them as well. For this reason, we discourage using the term 'subtractive synthesis' unless it is used in the historical context.

9.2. Source–filter models in speech synthesis

An early application of the source–filter approach was the modelling of voice production and speech synthesis, first by analog and later by DSP [149]. It was found that the vocal tract transfer function could be realized as a proper set of second-order resonator filters, each one for a single formant resonance, i.e. eigenmode of the vocal tract [92, 95].

The formant resonators can be connected either in cascade (series) or in parallel. In the cascade model of figure 35, the resonators are second-order lowpass filters with a resonance peak that has a controllable frequency f_i. If a small number of resonators is used, for example $i = 1, \ldots, 4$ in figure 35, a correction filter (HPC) is needed to compensate for the missing higher formants. The source is a periodic excitation approximating the human glottal waveform [148], controllable in frequency (F_0) and amplitude. The cascade model is particularly well suited to vowel synthesis.

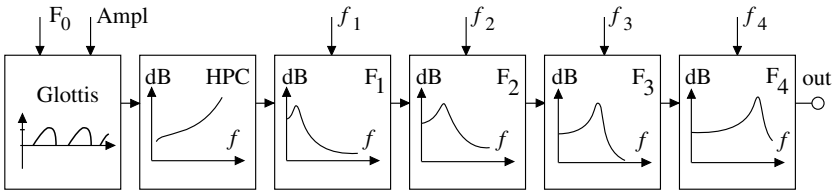

Figure 35. Cascade model of formant synthesizer.

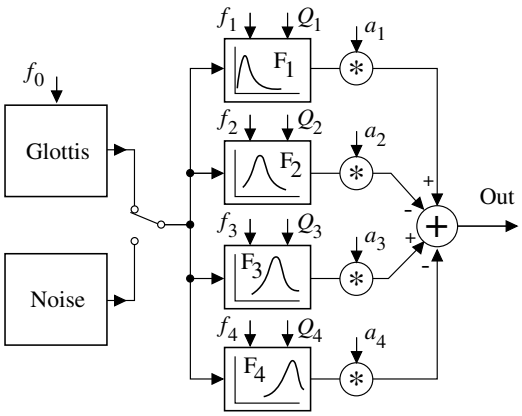

Figure 36. Parallel model of formant synthesizer.

A parallel formant synthesizer is characterized in figure 36. All formant resonators, which must have bandpass filter characteristics, are fed from the same source and the outputs are summed to obtain the synthetic speech signal. In this case, there are control parameters for the formant frequency f_i, the formant amplitude a_i and the Q value Q_i (resonance sharpness) of each formant. The filter part can be fed by a periodic glottal source with frequency control or by a noise source for frication sounds, and it can therefore also produce unvoiced sounds.

Many other digital filter configurations have been applied to speech synthesis. The development of digital filters and DSP was in fact greatly influenced by the needs of speech signal processing. An important further step was the introduction of linear prediction [169], which enabled the systematic analysis and synthesis of speech signals for coding (such as CELP coding, [233]) and synthesis applications. Linear prediction is also useful in musical signal processing applications.

In addition to speech synthesis and speech processing in general, the source–filter approach has been used in modelling and synthesizing the singing voice [9, 219, 269].

9.3. Instrument body modelling by digital filters

The body or the soundboard of a musical instrument is a multidimensional resonator. In the guitar, for example, the wooden box is a complex resonator structure that interacts with air resonances in the box's interior. Due to this multidimensionality, the body modelling is a computationally heavy task that requires spatially distributed modelling methods, such as the finite element, the boundary element or the finite difference method [75]. For real-time sound

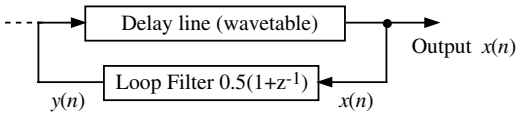

Figure 37. Signal flow diagram of Karplus–Strong algorithm.

synthesis, these methods are in most cases computationally too expensive. Thus, it is attractive to try to reduce the body effect to a single digital filter.

A number of filter-based body models were introduced in [139]. These include frequency-warped filters [108] and several basic techniques of filter decompositions. Since the models with full auditory accuracy tend to be expensive even for today's computers, simplifications are desirable. Higher frequency modes can be made sparse or totally discarded or they may be approximated by a reverberation algorithm [117, 198].

9.4. The Karplus–Strong algorithm

The Karplus–Strong algorithm is one of the basic inventions in computer music that later turned out to be an interesting and extremely simplified case of a physics-based model as well as a kind of source–filter. A wavetable is first filled with data, such as random numbers. Then it is circulated like the single delay-line loop with a simple loop filter, see figure 37. This method was proposed by Karplus and Strong [144], and soon thereafter it was extended to forms that have a closer relationship to physics-based modelling [120, 143, 244].

In the original Karplus–Strong algorithm, the loop filter is an averager of two succeeding samples, which corresponds to the transfer function $H(z) = 0.5\,(1 + z^{-1})$ and works as a lowpass filter. Thus, the filter attenuates high frequencies in the loop faster than low frequencies, which is exactly what happens, for example, in a plucked string. A new sound can be started by loading new content into the delay line. The fundamental frequency can easily be changed by controlling the sample rate of computation or the length of the delay line. Due to the extreme simplicity of the algorithm, it enabled real-time sound synthesis using the computers and processors of the early 1980s.

By feeding the excitation into the model from the dashed line input in figure 37 instead of loading the delay line all at once, the algorithm is converted into a source–filter structure. Through various extensions, it has been turned into different practical sound synthesis models, as discussed in section 7.

9.5. Virtual analog synthesis

Digital subtractive synthesis is called virtual analog synthesis, when reference is made to computational methods that imitate the sound generation principles of analog synthesizers of the 1960s and 1970s. The term 'virtual analog synthesis' became a popular and commercial term around 1995, when a Swedish company called Clavia introduced the Nord Lead 1 synthesizer, which was marketed as an analog-sounding digital synthesizer that used no sampled sounds. Instead, all of its sounds were generated by simulating analog subtractive synthesis using DSP techniques. Previously, the Roland D-50 synthesizer of the late 1980s worked in a similar way, although it also used sampled sounds. An early example of an attempt to design an analog-sounding digital synthesizer was the Synergy synthesizer [126].

What makes digital subtractive synthesis more demanding than is generally understood is that imitating analog electronics with digital processing is not as easy as it may seem.

Table 3. Hybrid modelling possibilities. The hybrid models encountered in the literature are marked by '●' symbols and the combinations that are currently untested are marked by '○' symbols.

	K-methods				Wave methods	
Method	Mass–spring	Modal	Finite difference	Source–filter	DWG	WDF
Mass–spring	●	●	○	●	●	○
Modal	●	●	○	○	●	●
Finite difference	○	○	●	●	●	●
Source–filter	●	○	●	●	●	●
DWG	●	●	●	●	●	●
WDF	○	●	●	●	●	●

One problem is aliasing caused by the sampling of analog waveforms that have sharp corners, such as the square wave or the sawtooth wave. The spectra of such waveforms continue infinitely high in frequency, and the signals are thus not bandlimited. Several algorithms have been proposed to generate discrete-time versions of analog waveforms so that aliasing is completely eliminated [177, 316] or is sufficiently suppressed [35, 157, 262, 285]. Another difficulty is that analog filters do not obey the linear theory exactly: at high signal levels they generate nonlinear distortion. This does not naturally occur in discrete-time signal processing, but it must be implemented, for example, by using a memoryless nonlinear function [118, 222].

Virtual analog synthesis can be seen to have similarities to the physical modelling synthesis research: in the latter case computational simulations of acoustic systems are designed, while in the former computational simulations are derived from electronic systems. Bandlimited oscillator algorithms are not usually based on the actual electronic circuit that was used in old music synthesizers, but instead on an imitation of their characteristic sound. However, some digital filters used in virtual analog synthesis are digitized versions of electric circuits, e.g. [118].

Another trend in audio and music processing is to simulate traditional analog electronics used in tube amplifiers, such as those used by electric guitar, bass and electric organ players. This problem is demanding due to nonlinearities in the tube behaviour. A simple model of a tube preamplifier for the electric guitar has been introduced in [137].

10. Hybrid models

Since both the wave models and K-models presented in earlier sections have their own pros and cons, it might be beneficial to combine their advantages in the same model. The results of combining different modelling schemes are known as hybrid or mixed models. Using hybrid approaches in sound synthesis to maximize strengths and minimize weaknesses of each technique is addressed in [119]. It has been pointed out that hybridization typically surfaces after a technique has been around for some time and its characteristics have been explored extensively. A corollary of this remark is that six commonly used techniques presented in previous sections result in 21 possible combinations. These combinations are schematically shown in table 3. Note that this table is redundant, as an upper-triangular 6×6 matrix would be sufficient to describe possible combinations. However, a full matrix presentation is preferred for ease of reading.

Combining discrete models, even those of the same technique, is a nontrivial task due to computability problems and thus deserves special attention. An exception is the source–filter

technique, because it is based on unidirectional signal flow as opposed to a dual pair of variables. It is therefore possible to combine the source–filter technique with any other technique, although such a combination is not common in modal synthesis.

The wave-based methods are more apt to hybrid modelling, as the WDF and DWG structures are mostly compatible. In addition, the adaptors in WDFs and the isomorphic scattering junctions in DWGs readily eliminate the delay-free loops in LTI cases. Because of these desirable properties, many WDF–DWG hybrids are reported in the literature (see, for instance, the hybrid model of a wave digital piano hammer and a DWG string in section 8 and the woodwind hybrid model reported in [304]). Moreover, the generalized theory of multivariable waveguides and scattering allows expression of DWG networks in a compact way [218]. The time-varying and nonlinear cases require special methods, as will be outlined in the next section.

The interconnected K-modules usually contain delay-free loops. We have already seen an example of how a delay-free loop occurs when linking two mass elements in section 5. The reported hybrid K-models usually restore computability by inserting a unit delay within the delay-free loop. This additional delay usually affects the accuracy and stability of the resulting hybrid structure, as demonstrated in a numerical model of hammer–string interaction in [33]. An exceptional case occurs when one of the interconnected K-modules has an impulse response that satisfies $h(0) = 0$. The output of such a module depends only on the past values of its inputs, which essentially means that a delay-free loop does not occur and the computability is restored without an additional delay, as reported in [105].

In this section we focus on systematic approaches for constructing hybrid models that inherently address the computability, accuracy, stability and efficiency of the resulting structure. A general method for solving computability problems due to the delay-free loops, especially those found when connecting nonlinear excitation blocks to linear resonator blocks, has been reported in [33]. This method is called the 'K-method' since it operates on the K-variables rather than the wave variables. The K-method transforms the state-variables of the linear part of the system in order to indicate all delay-free loops involving nonlinear maps and then operates a geometrical transformation on the nonlinearities in order to cut instantaneous dependences. Two possibilities are available for efficient numerical implementation of the K-method. The first is to pre-compute the new nonlinear map off-line and store it in a lookup table. Alternatively, it can be iteratively computed using the Newton–Raphson method. The iterative method has been used for combining two modal resonators and implementing their nonlinear interaction in [215].

10.1. KW-hybrids

In this section, we consider the connection of the wave models with K-models. We use the shorthand 'KW-hybrid' to refer to this kind of hybrid model.

The K-method can be used to form a KW-hybrid to couple a nonlinear lumped hammer model (consisting of a mass and a nonlinear spring) to a DWG [33]. In the case of LTI models, the K-method simplifies significantly, as the geometrical transformation can be solved analytically. Even simpler approaches have been reported for systematically constructed KW-hybrids.

One way of constructing KW-hybrids is to formulate a particular modular K-model with explicit instantaneous interaction elements and then use a special KW-converter. The KW-converter concept was developed in [80, 132] and formalized in [131]. The advantage of this approach is that the full dynamics of the K-model are preserved and its scheduling is made similar to that of the wave model. The disadvantage of this approach is that it is

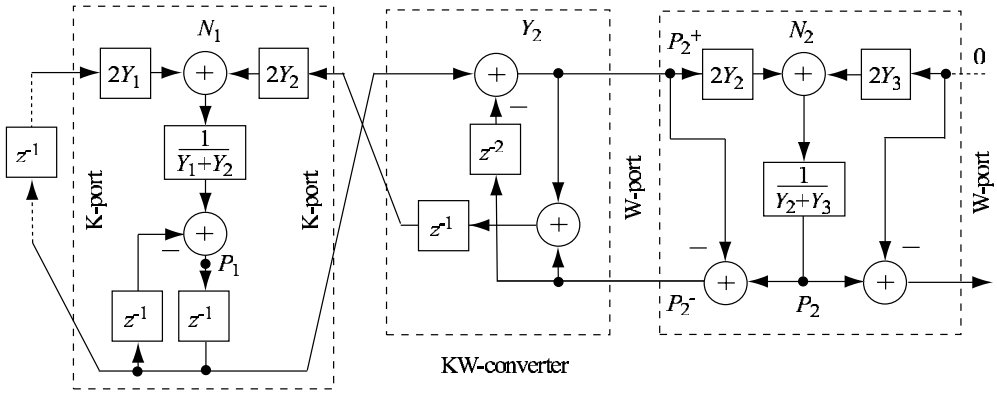

Figure 38. A FDTD node (left) and a DWG node (right) forming a part of a hybrid waveguide. There is a KW-converter between K- and wave models. Y_i are wave admittances of W-lines and K-pipes. P_1 and P_2 are the junction pressures of the K-node and wave node, respectively.

not general, as each K-model should be formulated separately for instantaneous modular interactions. Such a formulation is carried out in [131] for finite difference structures, as discussed in section 4. Here, the operation of a KW-hybrid model in the acoustical domain is outlined, as shown in figure 38.

The two-port K-node N_1 on the left-hand side of the figure is a generalization of the FDTD lattice element depicted in figure 2 of section 4.1. This K-node includes admittances Y_1 and Y_2 for connections between nodes through the K-ports. The figure also illustrates how a port of such a K-node can be terminated passively (Y_1 and feedback through z^{-1} on the left-hand side).

In figure 38, a K-node N_1 (left) and a wave node N_2 (right) are aligned with the spatial grids $i = 1$ and 2, respectively. The wave nodes (scattering junctions) were previously discussed in section 7. Note that the junction pressures are available in both types of nodes, but in the DWG case not at the wave ports. However, the similarity of operations may be used to obtain the following transfer matrix of the 2-port KW-converter element

$$\begin{bmatrix} P_2^+ \\ z^{-1}P_2 \end{bmatrix} = \begin{bmatrix} 1 & -z^{-2} \\ 1 & 1-z^{-2} \end{bmatrix} \begin{bmatrix} z^{-1}P_1 \\ P_2^- \end{bmatrix}. \tag{104}$$

The KW-converter in figure 38 essentially performs the calculations given in equation (104) and interconnects the K-type port of an FDTD node and the wave type port of a DWG node.

Another way of constructing KW-hybrids is to formulate the K-models within the state–space formalism (as a black box with added ports) and choose the port resistance to break instantaneous input–output path to avoid delay-free loops. The advantage of this approach is its generality, as any LTI K-model can be formulated as a state-space structure [254]. The disadvantage of this approach is that the dynamics of the K-model are hidden and its scheduling has to be separately authorized. A KW-hybrid modelling formulation based on the state-space formalism is presented in [201]. This formulation is used in [200] to construct a 1D KW-hybrid by mixing FDTD, FTM and WDF techniques. These techniques were discussed in sections 4, 6.3 and 8, respectively. Other KW-hybrid modelling examples are discussed in the next subsection.

10.2. KW-hybrid modelling examples

A practical application utilizing a KW-hybrid model is the RoomWeaver [20]; a software application used for building virtual 3D spaces and modelling their room impulse responses. RoomWeaver utilizes rectangular (2D) or cubic arrays (3D) of digital waveguide meshes to model the space with the desired geometry. Since multidimensional finite difference structures are computationally more efficient but do not provide as good implementations for boundary conditions as DWG schemes do, a mixed model is the proper choice for large meshes. In RoomWeaver, a KW-hybrid model (constructed by using the KW-converters in figure 38) is used to accomplish an efficient modelling solution. A comparison of the hybrid modelling and the conventional approaches is performed in [20]. A fan-shaped room was simulated at the sampling rate of 44.1 kHz using 260330 nodes in a mesh. The results showed a speed increase of 200% and a memory usage decrease of 50% when the hybrid mesh was compared with the standard one.

Other examples of FDTD/DWG hybrids include the string collision model of Krishnaswamy and Smith [153] and the finite width bow/string model of Pitteroff and Woodhouse [203–205]. These models are discussed in sections 11.1.4 and 7, respectively.

11. Modelling of nonlinear and time-varying phenomena

All musical instruments experience nonlinear behaviour. In some cases, the effect that the nonlinearity imparts on the sound of the instrument is so small that it can be considered negligible, and a linear synthesis model will suffice. For many instruments, however, this is not the case. All musical instruments also possess more or less time-variant properties. This is due to control by the player: the pitch or timbre of an instrument must usually vary in time in order for the sound to be considered musically interesting. Modelling of the time-varying phenomena can be achieved in two ways. The simplest choice is to use several copies of the same synthesis engine with different parameters to produce the different tones. This is especially well suited to the case in which the change in pitch or timbre is more instantaneous than gradual, e.g. in the case of a piano model. For instruments that experience a gradual change in sound characteristics, such as the slide guitar or a violin, a single synthesis model with time-varying properties must be used.

Modelling of nonlinear and time-varying phenomena will nearly always increase the computational complexity of the synthesis algorithm, since common simplifications, such as commuting, are no longer theoretically valid and thus usually cannot be applied. The following section will briefly discuss the modelling of different nonlinear phenomena in musical instruments. For an excellent overview of nonlinearities in musical instruments, see [97] and for the physics of musical instruments in general, see [96]. Section 11.2 will provide a more detailed case study in modelling the spatially distributed nonlinear string using a novel energy-preserving technique. Section 11.3 will discuss the modelling of time-varying properties of musical instruments with a special focus on energy conservation and stability issues.

11.1. Modelling of nonlinearities in musical instruments

11.1.1. Bowed strings. The nonlinearity in bowed string instruments is one of the most extensively studied musical instrument phenomena [68, 174, 203, 234, 236, 237, 321]. In bowed strings, as in all sustained tone instruments, the generation of harmonic tones requires nonlinear behaviour from the excitation mechanism [97]. In this case, the nonlinearity lies in the stick–slip contact between the bow and the string.

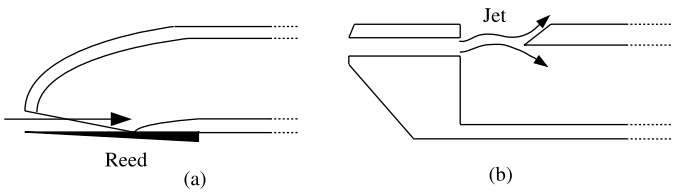

Figure 39. The reed generator (*a*) and the jet-flow generator (*b*) of wind instruments (after [96]).

Several computational algorithms for modelling the bowed string have been introduced; see [238] for a good overview. To model the bowed string with digital waveguides, Smith [246] used a waveguide string with a two-port scattering element representing the contact point between the bow and the string. The scattering element contains a simple lookup table where the appropriate string velocity can be read for a given bow velocity, force and position. Later, several refined waveguide models were introduced [115, 257, 271]. A simple and efficient bowed-string synthesis structure, the MSW-algorithm, is presented in [173]. It is based on the waveguide formalism and it uses digital filters to represent reflection, dispersion, losses and body responses. More recently, bowed string modelling has been studied in [236, 237, 318, 321].

A mass–spring model representing the bowed string was introduced in [37]. It is implemented using the CORDIS-ANIMA system [38] (see also section 5.2) as a series of masses linked together with visco-elastic elements. Also, a modal synthesis model of the nonlinear bow–string interaction was presented in [7]. A finite difference model simulating the behaviour of the bowed string has been discussed in [190].

11.1.2. Wind instruments. In reed-excited wind instruments, such as the clarinet or saxophone, the nonlinearity resides in the vibrational behaviour of the reed. The reed generator usually consists of a flat tapered reed held against an aperture, with a small opening between them. The reed generator is illustrated in figure 39(*a*). The aperture is connected to a resonator, which is a tube with an adjustable acoustic length. When a pressure source, such as the player's mouth, is connected to the input of the reed generator, the pressure difference between the source and the resonator tends to close the aperture. This pressure difference generates an air flow to the resonator through the aperture. When the positive pressure wave returns to the aperture from the resonator, the pressure difference decreases and the reed returns to near its starting position. The relation between the pressure difference and the static volume flow can be given as [96]

$$U(x(t), \triangle p(t)) = \gamma_1 |x(t)|^{\alpha} \triangle p(t)^{\beta}, \tag{105}$$

where $U(x(t), \triangle p(t))$ is the volume flow, γ_1 is a positive constant, $x(t)$ is the aperture opening, t is the time, $\triangle p(t)$ is the pressure difference and α and β are coefficients with typical values of $\alpha \approx 1$ and $\beta \approx \frac{1}{2}$. The relation (105) is not only nonlinear but also implicit, since the pressure difference $\triangle p(t)$ also actually depends on the volume flow. This implicitness clearly poses a problem for the discrete-time implementation of the algorithm.

A few different techniques for modelling the single reed have been proposed in the literature. In the simplest case, the reed behaviour is approximated using a simple linear oscillator [102]. For modelling the nonlinearity, Borin *et al* [33] and Avanzini and Rocchesso [11] have used the K-method approach already discussed in section 10. The K-method has been reported to model different nonlinearities accurately, even with

low sampling rates [15, 33]. A computationally demanding finite difference approach for directly discretizing the nonlinear reed equations was introduced in [291]. In 1986, Smith [246] proposed a conceptually straightforward waveguide method for synthesizing a reed instrument. In this model, the reed has been implemented as a simple lookup table, where the nonlinear relationship between the flow and the pressure has been stored in advance. This computationally efficient method is able to produce relatively high-quality synthesis. A spatially distributed reed model, that is, a model that does not consider the reed as a lumped, pointlike element, has been discussed in [13]. Very recently, Guillemain and co-workers [105] have shown that equation (105) can be solved explicitly in discrete time.

Modelling of the more complicated excitation mechanism, the nonlinear double reed, is discussed, for example, in [106, 311]. The double reed is used as an excitor in the oboe and bassoon, for example.

In brass instruments, such as the trumpet or trombone, the excitation mechanism, i.e. the player's lips, behaves somewhat differently from the reed. Several models for explaining the behaviour of the lip–valve excitors have been proposed. A review paper can be found in [40]. Sound synthesis based on such models has been discussed by several authors [1, 76, 180, 220, 313].

In jet-flow type wind instruments, such as the flute or the recorder, the resonator is excited by an air flow instead of a vibrating reed. When the pressure source is connected to the generator, the air jet emerges from a flue slit, passes the embouchure hole and finally reaches the bore edge, as illustrated in figure 39(*b*). The jet stream clearly generates a pressure wave inside the bore. When the pressure maximum returns to the slit end, it pushes the jet stream away from the bore. In other words, the moving air inside the bore modulates the transversal displacement of the jet stream, which in turn excites the air in the bore. With suitable bore lengths and jet velocities, this coupled air movement turns into a sustained oscillation. The air flow into the resonator can be given as [96]

$$U(\triangle h(t)) = WbV\left(\tanh\left(\frac{\triangle h(t)}{b}\right) + 1\right), \tag{106}$$

where W, b and V are parameters defining the shape of the jet stream and $\triangle h(t)$ is the time-varying transverse offset between the jet and the slit. As can be seen, equation (106) is also nonlinear. The behaviour of the jet flue is studied more thoroughly, for example, in [309]. A review paper about lumped jet flue models can be found in [91].

The flute synthesis models presented in the literature are surprisingly similar in nature. In almost all cases, digital waveguides have been used for modelling the instrument bore, while the nonlinearity has been realized with a lookup table or a simple polynomial. A signal delay is inserted prior to the nonlinearity for modelling the time it takes for the jet flow to travel across the embouchure hole.

The general requirements for a computational time-domain flute model were already discussed in [173]. The first real-time synthesis model was briefly presented by Karjalainen *et al* in [135]. It implemented the nonlinearity with a sigmoid function. A refined model was proposed in [288], where scaling coefficients for the pressure input and the feedback from the bore were added. Soon after that another waveguide model with a simple polynomial simulating the nonlinearity [61] and a conceptually similar model with a physically more rigorous approach were presented [55]. Chaotic variations in the jet offset due to turbulence have been simulated by slightly varying the coefficients of the polynomial nonlinearity with a noise generator [44, 62]. A waveguide-based flutelike instrument model, which takes into account the vortex shedding at the slit edge (labium) and the turbulence at the mouth of the instrument, has been proposed in [310].

11.1.3. The Piano. In a piano, the sound is generated when the player presses a key. The movement is transferred via a jack into the piano hammer, which hits the piano string (there are actually multiple strings for a hammer especially in the treble end, but here we will consider the case of a single string for the sake of simplicity). See figure 30 in section 8.5.3 for an illustration. For a more thorough discussion on piano acoustics, see, e.g. [96].

The piano hammer is basically a piece of wood covered with a layer of felt. The compression characteristics of the felt are inherently nonlinear, which affects the generated tone. This passive nonlinearity manifests itself when the piano is played with varying dynamics. When playing with greater intensity (*fortissimo*), the hammer seems harder than if the piano were played softly (*pianissimo*). This change of the effective stiffness results in greater amplitude of the higher harmonics, i.e. the sound is brighter if the piano is played with greater intensity.

When modelling the piano hammer, the core of the hammer is often simplified as a lumped mass while the felt is presented as a nonlinear spring connected to this mass. The force-to-compression relationship of this mass–spring system can be presented as [107]

$$F(\triangle y(t)) = C^{-1}\triangle y(t)^p, \tag{107}$$

when the hammer is in contact with the string. Here, $F(\triangle y(t))$ denotes the force applied to the string by the hammer, $\triangle y(t)$ is the compression of the spring (felt) and C is its generalized compliance. Note that with $p = 1$, equation (107) becomes Hooke's law for springs (22). Interestingly, the compression of the felt depends in turn on the hammer force, so equation (107) is implicit.

Several synthesis models for piano hammer–string interaction have been suggested; see [15] for a review. Chaigne and Askenfelt [46,47] have used the finite difference discretization of equation (107) with an additional delay between the compression and force terms in order to force the relation explicit. This artificial delay, however, makes the synthesis algorithm potentially unstable [15]. The K method [33] discussed earlier has also been utilized in removing the implicitness of equation (107). Very recently, Bensa and co-workers [26] have studied the parameter fitting for the hammer–string model.

As discussed in section 8, WDFs hold special means for removing the delay-free loops and have thus also been used in modelling the nonlinear piano hammer [23, 196, 225, 298]. Smith and Van Duyne [258, 301] have introduced a computationally efficient commuted waveguide model wherein the hammer is implemented as a linear filter. When the hammer hits the string, an impulse is fed to the string through this filter. The filter parameters are read from a pre-calculated table for a given hammer velocity.

There is also an additional physical phenomenon taking place in the compressing felt, namely the hysteresis. During interaction with the strings, the felt compresses and relaxes several times due to the travelling displacement wave in the string [34]. The hysteresis takes place when the temporal derivative of the felt compression changes its sign. In other words, when the compression of the felt starts to relax, the compression-to-force relationship does not follow the same trajectory as it did when the compression was increasing. In order to model the hysteresis effect also, Boutillon [34] suggested that a model

$$F(y) = \begin{cases} a_i \triangle y^{\alpha \mathrm{i}} & \text{when } y \text{ increases,} \\ a_d \triangle y^{\alpha \mathrm{d}} & \text{when } y \text{ decreases,} \end{cases} \tag{108}$$

be used. Here, $F(y)$ is the force applied by the hammer to a rigid string, $\triangle y$ is the hammer felt deformation and a and α represent a hypothetical series of coefficients, where each a and α must be larger than its predecessor.

11.1.4. Plucked string instruments. Plucked string instruments experience two main types of nonlinearities. The first is hard-limitation nonlinearity, which takes place when a freely vibrating string hits a spatial obstacle. The obstacle obviously limits the amplitude of the vibration, producing a nonlinear 'clipping' of the vibration. Usually, the obstacle is a part of the instrument itself, such as in the case of slapbass, where the string is 'popped' or struck so hard that it hits the frets on the fingerboard. A more complex manifestation of the hard-limitation nonlinearity takes place, e.g. in the Indian sitar or the tanpura. In these cases, the unilateral constraint caused by the curved bridge effectively shortens the string as it displaces towards the bridge [254]. A more thorough discussion of the effect is provided in [282].

The hard-limitation nonlinearity in the case of the slapbass was first modelled by Rank and Kubin in the late nineties [208]. They used a waveguide string model with displacement signals as wave variables. During the vibration, the displacement of the string is probed in certain given points on the string and then compared with the displacement limit y_{fret}, i.e. the distance between the string and the fret in equilibrium. If the string displacement exceeds the limit value at some of these locations, the displacement waves are reflected (with a sign change) into the delay line travelling in the opposite direction. When the displacement limit value is added to this, the string vibration amplitude at any of the given points is limited to y_{fret}.

Later, Karjalainen [127] suggested a technique where an impulse with a suitable amplitude is fed into the string when the collision with the obstacle occurs. This operation is in fact identical to what is described in [208], although it provides an alternative representation for the string by using so-called FDTD waveguides, illustrated already in figure 2. Soon after, Krishnaswamy and Smith [153] pointed out a nonphysical feature in the simulated string when this technique is used. They observed that the string release from the obstacle happens later than physical laws would predict, as if the string had artificial 'stickiness'. They formulated a refined waveguide model for the hard-limitation nonlinearity, which removed the constant offset differences between the two waveguide segments and thus resolved the physical validity problem. In addition to this computationally more expensive waveguide model, a FDTD/DWG hybrid approach was introduced in [153].

The other main nonlinearity in plucked strings resides in the variation of string tension due to transversal vibration. It has been extensively studied in the literature [6, 41, 179, 183, 184]. When a string is displaced, its tension is also increased. When the string moves near its equilibrium position, the tension is decreased. It is easy to see that the tension variation has twice the frequency of the transversal vibration, since both extreme displacements of the string produce a tension maximum, and the tension minimum is obtained when the string is near its steady-state location. With this in mind, it is also easy to understand that since a real string vibration decays in time, the average string tension also has a decaying form. As stated in equation (6), this tension decay leads into a decay in wave velocities and a descent in the fundamental frequency of the string.

This phenomenon, called the initial pitch glide, is most apparent in elastic strings with high vibrational amplitudes and relatively low nominal tension. In fact, the pitch glide is not the only effect caused by tension modulation. As is well known, the lack of certain modes in a plucked string vibration occurs due to the plucking location, which heavily attenuates all harmonics that would have a node at that point. In an ideal mid-plucked string, for example, all even modes are missing. However, the tension modulation nonlinearity does enable an energy transfer between the vibrational modes, so that the missing harmonics can be found in the spectrum. Typically, the missing harmonics gradually rise from the noise floor of the spectrum just after the plucking, reach their peak amplitude and decay off, just like all other modes. The generation of these missing harmonics is studied more thoroughly in [162].

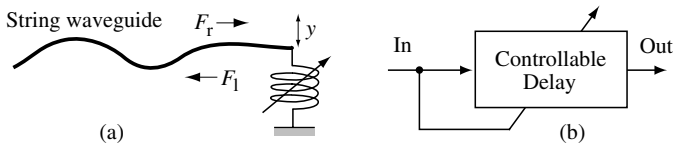

Figure 40. (*a*) Principle of passive nonlinearity for string termination and (*b*) realization using signal-dependent delay. In (*a*), F_r and F_l denote the force waves travelling right and left, respectively, while y is the displacement of the nonlinear spring.

There have been several attempts to model the tension modulation nonlinearity. The first one was introduced in the late nineties by Pierce and Van Duyne in [202], where they used a digital waveguide terminated with a nonlinear double spring. Figure 40 characterizes the principle by nonlinear spring in subview (*a*). A physically more motivated model was proposed in [275, 296], where the double spring had been replaced by a time-varying fractional delay filter. By varying the phase delay of the filter using the string elongation value, the initial pitch glide effect was reproduced in the synthesized string. The generation of missing harmonics was obtained as a by-product of the string elongation calculation. A waveguide model also implementing the direct coupling between the longitudinal string tension variation and the instrument body was proposed in [273].

All these nonlinear string models implement the nonlinearity as a lumped element at the termination of the waveguide. Physically, this corresponds to having a single elastic element at the end of an otherwise rigid string. Recently, a spatially distributed waveguide model of a nonlinear string was suggested in [188], where the delay lines of the waveguide were replaced by time-varying allpass filters. A finite difference model of a nonlinear string was also presented in [188]. It used interpolation in time for varying the time step in the linear FDTD recurrence equation (8), while the generation of missing harmonics was implemented by adding a force signal to the string termination. At the same time, Bilbao [29] introduced an energy-conserving finite difference model of a nonlinear string by directly discretizing the Kirchhoff–Carrier equation [41, 146]. In the next section, we will introduce a new energy-conserving waveguide model using power-normalized WDFs.

11.2. Case study: nonlinear string model using generalized time-varying allpass filters

In this section we propose a new hybrid modelling technique for simulating vibrating strings with tension modulation nonlinearity. The approach replaces unit delays with power-normalized WDFs (see section 8.5.4) in a waveguide loop in order to smoothly vary the waveguide pitch. The model consists of an energy-preserving varying tension string, introduced in [187], that is controlled using the string's elongation approximation.

11.2.1. Time-varying allpass filters. As stated in [31], certain power-normalized wave digital one-ports are realized as allpass filters, i.e. they apply a suitable phase delay for the signal without attenuating or boosting it. One such element is illustrated in figure 41. The filter coefficients are evaluated as [31]

$$a(n) = \frac{d(n) - 1}{d(n) + 1}, \qquad \beta = \pm 1, \qquad \phi(n) = \sqrt{\frac{1 - a(n+1)^2}{1 - a(n)^2}}, \tag{109}$$

where $d(n)$ is the desired phase delay as a function of time n for a single one-port.

The amount of delay this structure applies to the signal can be varied via parameter $a(n)$. If $a(n)$ is constant with respect to time, the one-port element actually reduces to a first-order

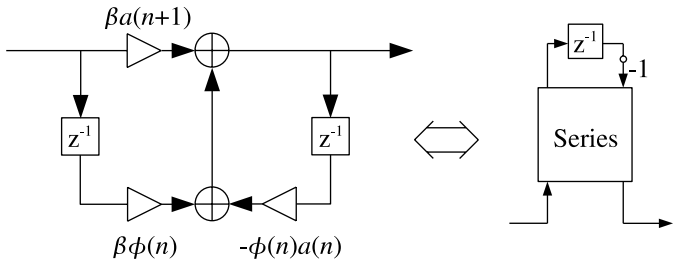

Figure 41. A signal flow diagram of a wave digital one-port implementation (left) and its abstraction (right). The one-port acts as an energy-preserving fractional delay even when $a(n)$ varies in time. If $a(n)$ is constant, the structure reduces to a first-order allpass filter. The filter coefficients are evaluated as in equation (109).

allpass filter. Interestingly, since the wave digital one-ports are power-normalized, the signal energy remains constant even when the phase delay (and thus the port impedance) is varied in time. This means that we can use the power-normalized WDF as a time-varying fractional delay which leaves the energy of the signal intact.

11.2.2. Nonlinear energy-conserving waveguide string. As shown in [187], a waveguide string can be constructed using the power-normalized one-ports. Conceptually, this can be done by replacing the unit delays in the waveguide loop (see figure 8) with the one-port elements shown in figure 41. This means also that the allpass filter parameter $a(n)$ becomes directly related to the string tension [187]. If the phase delay value $d(n)$ is now varied according to the elongation of the string [275]

$$L_{\text{dev}}(n) = \sum_{m=0}^{\hat{L}_{\text{nom}}} \sqrt{1 + [s_{\text{r}}(n,m) + s_{\text{l}}(n,m)]^2} - \hat{L}_{\text{nom}} \tag{110}$$

by

$$d(n) = 1 + \frac{D_{\text{dev}}}{\hat{L}_{\text{nom}}}, \tag{111}$$

an energy-preserving nonlinear string model is obtained. Here,

$$D_{\text{dev}}(n) \approx \frac{1}{2} \sum_{l=n-1-\hat{L}_{\text{nom}}}^{n-1} \left(1 + \frac{EA}{K_0}\right) \frac{L_{\text{dev}}(l)}{L_{\text{nom}}} \tag{112}$$

is the total delay variation in the waveguide loop, L_{nom} is the nominal string length in samples, $\hat{L}_{\text{nom}} = \text{floor}(L_{\text{nom}})$ and $s_{\text{r}}(n,m)$ and $s_{\text{l}}(n,m)$ are the right- and left-going slope waves, respectively. Symbols E, A and K_0 stand for the Young's modulus, cross-sectional area and the nominal tension of the string, respectively. This approach is similar in nature to the spatially distributed nonlinear string case [188] already mentioned in section 11.1.4, except now the tension variation does not alter the energy of the string.

For simulating the generation of missing harmonics, discussed in section 11.1.4, a method proposed in [188] can be used. This approach makes use of the fact that the vertical component of the tension is directly proportional to the string displacement near the termination. Thus, the tension modulation driving force (TMDF) [273] can be taken as the string elongation signal multiplied with the displacement of the string near termination, and it can be injected to the string through an appropriate scaling coefficient. Figure 42 illustrates the novel energy-preserving nonlinear string model.

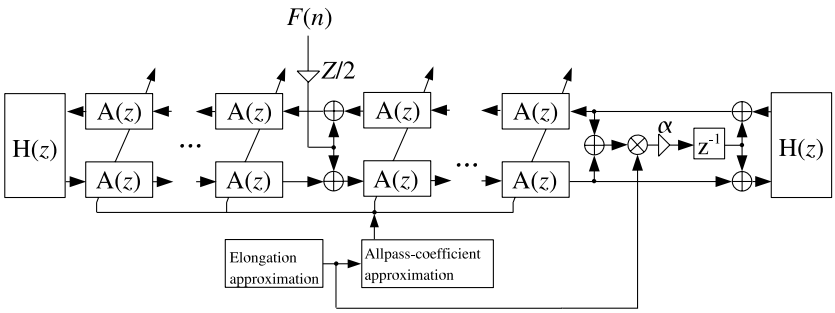

Figure 42. An energy-conserving digital waveguide model of a nonlinear string. Velocity waves are used as wave variables here. The generalized allpass filters are denoted by A(z), while H(z) stand for the loss filters. The exciting force signal (plucking) is denoted by $F(n)$, where n is the time index. The mechanic impedance of the string is denoted by Z, and the scaling coefficient α can be used for controlling the amplitude of the missing harmonics.

Preliminary experiments have revealed that this model performs well, that is, it simulates correctly the initial pitch glide phenomenon of nonlinear strings. It also seems to model the energetic behaviour of the nonlinear string more accurately than previous waveguide models. A proper comparison of the energetic behaviour between the nonlinear DWG string models is left for future work.

11.3. Modelling of time-varying phenomena

As discussed above, enabling the synthesis parameter variation in time is very important if a flexible and high quality synthesis is desired. However, when the parameter values are varied, an additional problem emerges. The passivity of the resonator structures or even the stability of the entire synthesis algorithm may become compromised if new parameters are suddenly used in calculating the next output from the previous signal values. Clearly, this is not a problem with memoryless algorithms. Another problem is whether the model behaves reasonably during the parameter change, i.e. does it behave like the real instrument it is trying to simulate?

Since it is extremely difficult, if not impossible, to find an answer to the latter problem by objective measurements (consider, e.g. a case where the mass density of a real string should be accurately varied during its vibration), we will consider only the passivity and stability criteria here. Remember that passivity always implies stability, and are both closely related to the conservation of energy in a system. In the following, we assume that the exciter parts of the synthesis algorithms will remain stable, i.e. that they will insert a finite amount energy into the resonator parts.

The means of checking the passivity of a system varies among different modelling techniques. For finite difference schemes, the Von Neumann analysis [264] has traditionally been used. The basic idea there is to evaluate the spatial Fourier spectrum of the system at two consecutive time steps and find an amplification function that describes how the spatial spectrum of the algorithm evolves with time. If the absolute value of this amplification function does not exceed unity, the system under consideration remains passive. Since this is a frequency-domain analysis method, it generally cannot be used for analysing nonlinear systems. For time-varying systems, the amplification function can become extremely complex even for simple systems, thus rendering the analysis method difficult to use [188]. It is important to note that for each system parameter varied in time, an additional degree of freedom is introduced in the amplification function.

For models whose implementation essentially consists of filters (modal decomposition, wave and source filter models), time-varying filter analysis methods [53] can be used. These methods are very similar to traditional filter analysis techniques, see, e.g. [176], except that the time-varying filters possess an additional time variable. As a consequence, the impulse- and frequency response functions determining the behaviour of the filter become two-dimensional.

For a linear time-varying filter to remain passive, the norm of its generalized impulse response cannot exceed unity. In mathematical terms this can be stated as [53]

$$h(m,n) = \frac{1}{a_0(n)}\left[-\sum_{k=1}^{K_1} a_k(n)h(m,n-k) + \sum_{k=0}^{K_2} b_k(n)\delta(n-k-m)\right] \leqslant 1, \tag{113}$$

where $h(m,n)$ is the output of the system measured at time instant n, when a unity impulse is inserted at the system's input at time instant m. Coefficients $a_k(n)$ and $b_k(n)$ correspond to the recursive and non-recursive parts of the system. For $K_1 > 0$, the system is said to be an infinite impulse response (IIR) filter of order K_1, while for $K_1 = 0$ it is said to be a finite impulse response (FIR) filter of order K_2.

By taking the z-transform of equation (113), we have the generalized transfer function of the system as

$$H(z,n) = \sum_{m=0}^{n} h(m,n)z^{m-n}, \tag{114}$$

which in the case of an IIR filter consists of a numerator (determined by $b_k(n)$) and a denominator (determined by $a_k(n)$). For ensuring the stability of system, the poles of the filter, i.e. the roots of the polynomial $\sum_{k=0}^{K_1} a_k(n)$, must remain inside the complex unit circle.

For a parallel filter structure, such as a modal synthesis scheme, it suffices to ensure the stability of the individual resonators. For cascaded filter structures, such as source–filter models or commuted waveguides, the transfer function of the whole system, i.e. the convolution of the individual filters, must be checked. It must also be noted that since the system is not LTI, the order of the cascaded structure cannot be changed in theory. In practice, however, the commutation process is often carried out without notable changes in the energetic properties (see, e.g. [250]).

If the system is both nonlinear and time-variant, the energetic analysis becomes even more difficult. For some modelling techniques, for example WDFs with power-normalized wave variables (see section 8.5.4), the correct energetic behaviour does not need to be addressed, since the definition of the variables already guarantees passivity. For other systems, ad hoc energy management methods should be used. One obvious approach is the so-called 'energy probing' (see, e.g. [187]), where the signal energy of a system is observed at some location and compared with pre-calculated limit values. The limit values can be, for example, the maximum and minimum energy levels allowed by physical laws for such a model. When the signal energy crosses the limit value, the signal must be attenuated or amplified so that it returns to a suitable energy level. This energy probing can be carried out at several locations in the model. Needless to say, energy probing can increase the computational load of the synthesis algorithm substantially.

12. Current trends and further research

Next we look at some current trends in physical modelling. Around the mid-1990s, the research reached the point where most Western orchestral instruments could be synthesized

based on a physical model [251]. More recently, many papers have been published on the modelling of ethnic and historical musical instruments. These include, for example, the Finnish kantele [82, 130, 186], various lutes [83, 84], the bowed bar [87], ancient Chinese flutes [71], an African flute [72], the Tibetan praying bowl [88, 89], the panpies [69] and the Japanese sho [111, 112]. We have also recently seen applications of physical modelling techniques to non-musical sound sources [213]. Some examples of these are physical modelling of bird song [125, 259, 260], various everyday sounds, such as those generated by wind chimes [63, 165], footsteps [65] and beach balls [214] and friction models that can be applied in many cases [12].

Another new direction is the subjective evaluation of perceptual features and parameter changes in physics-based synthesis, see [122, 123, 155, 217]. This line of research provides musically relevant information on the relation of timbre and the properties of human hearing. These results help in reducing the complexity of synthesis models because details that are inaudible need not be modelled.

The first attempts at audio restoration based on physical models were conducted recently [85]. While this can be successful for single tones, the practical application of such methods for recordings including a mix of several instruments is a challenge for future research. The main problem is high-quality source separation, which is required before this kind of restoration process. Sophisticated algorithms have been devised for this task, but, generally speaking, separation of a musical signal into individual source signals is still a difficult research problem (see, e.g. [147]).

The concept of Structured Audio introduced as part of the MPEG-4 international multimedia standard has opened a new application field for physical models [104, 308]: parametric coding of music, where a program for sound generation of the instruments and control data for playing the instrument are transmitted. The practical use of this idea remains a dream for the future.

Future work in the field includes, for example, highly accurate modelling of specific musical instruments. Currently, physics-based synthesis models still lack the excellent sound quality of sample-based digital instruments. A clear example of this defect in quality is seen in digital pianos; the most popular products use a large sample database to reproduce piano tones at all dynamic levels. Fully parametric physical models of the piano have not entered the market yet, probably because these imitations of the piano are still insufficient for professional players. Difficult subproblems related to this are parameter estimation and control of virtual instruments. For best sound quality, computational methods that automatically calibrate all the parameter values of a physical model according to the sound of a good instrument should exist. This is very challenging and almost hopeless for some methods, and relatively easy only for some special cases. The control, or playing, of physical models is another problem area where general solutions are unavailable. The piano, in fact, is one of the easiest cases, because the player only controls the fundamental frequency (which key) and dynamic level (velocity of key press) of tones. In the cases of string and wind instruments, the control issue requires clever technical solutions. The control of virtual musical instruments is currently a lively research field [61, 67, 116, 121, 136, 137, 161, 191, 315].

An ultimate dream of physical modelling researchers and instrument builders is virtual prototyping of musical instruments. This application will pre-eminently require physical models with excellent precision in the simulation of sound production, as stressed by Woodhouse [319]. A musical instrument designer should have the possibility to modify a computer model of a musical instrument and then play it to verify that the design is successful. Only after this would the designed instrument be manufactured. Naturally, fine details affecting the timbre of the instrument should be faithfully simulated, since otherwise this chain of events

would be fruitless. Current research is still far away from this goal. More research work is required.

13. Conclusions

Physical modelling of musical instruments has become one of the most active fields of musical acoustics research. There are six different main approaches to develop a computational model for any given instrument. These approaches were briefly overviewed. The digital waveguide method, together with its variations, is currently the most popular modelling technique, because it leads to computationally efficient algorithms that enable real-time synthesis of many simultaneous voices.

Some current research trends were listed, such as the modelling and synthesis of unusual musical instruments. It can be predicted that in the near future, the physical modelling techniques will be applied to numerous everyday sound sources in addition to synthesizing musical sounds. This research topic has become popular only a few years ago. Non-musical parametric sounds [66, 215] are of interest because they can be used in human–computer interfaces, computer games, electronic toys, sound effects for film and animation and virtual reality applications.

Acknowledgments

This work has been funded by the Academy of Finland (Projects 53537, 104934 and 105651) and by the Sixth EU Framework Programme for Research and Technological Development (FET-Open Coordination Action IST-2004-03773, 'Sound to Sense, Sense to Sound'). J Pakarinen's doctoral research is funded by the S3TK Graduate school and Tekniikan Edistämissäätiö. The authors wish to thank M Tikander for his help in mass–spring networks, K Pölönen for his help in hybrid modelling and S Bilbao, C Cadoz, A Chaigne, F Fontana, D T Murphy, S Petrausch, R Rabenstein, X Rodet, A Sarti, S Serafin and J Woodhouse for helpful discussions and suggestions.

References

[1] Adachi S and Sato M 1995 Time-domain simulation of sound production in the brass instrument *J. Acoust. Soc. Am.* **97** 3850–61

[2] Adrien J M 1989 Dynamic modeling of vibrating structures for sound synthesis, modal synthesis *Proc. Audio Engineering Socity 7th Int. Conf.: Audio in Digital Times (Toronto, ON, Canada, May 1989)* pp 291–9

[3] Adrien J-M 1991 The missing link: modal synthesis *Representations of Musical Signals* ed G De Poli *et al* (Cambridge: MIT Press) pp 269–97

[4] Aird M-L, Laird J and ffitch J 2000 Modelling a drum by interfacing 2-D and 3-D waveguide meshes *Proc. Int. Computer Music Conf. (Berlin, Germany, August 2000)* pp 82–5

[5] Alles H G 1980 Music synthesis using real time digital techniques *Proc. IEEE* **68** 436–49

[6] Anand G V 1969 Large-amplitude damped free vibration of a stretched string *J. Acoust. Soc. Am.* **45** 1089–96

[7] Antunes J, Tafasca M and Henrique L 2000 Simulation of the bowed string dynamics *5ème Conférence Française d'Acoustique (Lausanne, Switzerland, 3–7 September 2000)*

[8] Aramaki M, Bensa J, Daudet L, Guillemain P and Kronland-Martinet R 2001 Resynthesis of coupled piano string vibrations based on physical modeling *J. New Music Res.* **30** 213–26

[9] Arroabarren I and Carlosena A 2004 Vibrato in singing voice: the link between source-filter and sinusoidal models *EURASIP J. Appl. Signal Process.* **2004** 1007–20 Special issue on model-based sound synthesis

[10] Avanzini F 2001 Computational issues in physically-based sound models *PhD Thesis* Department of Computer Science and Electronics, University of Padova (Italy)

[11] Avanzini F and Rocchesso D 2002 Efficiency, accuracy and stability issues in discrete-time simulations of single reed wind instruments *J. Acoust. Soc. Am.* **111** 2293–301

[12] Avanzini F, Serafin S and Rocchesso D 2002 Modeling interactions between rubbed dry surfaces using an elasto-plastic friction model *Proc. COST G6 Conf. on Digital Audio Effects (Hamburg, Germany, September 2002)* pp 111–16

[13] Avanzini F and van Walstijn M 2004 Modelling the mechanical response of the reed-mouthpiece-lip system of a clarinet. Part I. One-dimensional distributed model *Acta Acust. united Acust.* **90** 537–47

[14] Bank B 2000 Physics-based sound synthesis of the piano *Master's Thesis* Budapest University of Technology and Economics, Department of Measurement and Information Systems, Budapest, Hungary

[15] Bank B, Avanzini F, Borin G, De Poli G, Fontana F and Rocchesso D 2003 Physically informed signal-processing methods for piano sound synthesis: a research overview *EURASIP J. Appl. Signal Process.* **2003** 941–52 Special Issue on Digital Audio for Multimeda Communications

[16] Bank B and Sujbert L 2005 Generation of longitudinal vibrations in piano strings: from physics to sound synthesis *J. Acoust. Soc. Am.* **117** 2268–78

[17] Bank B and Välimäki V 2003 Robust loss filter design for digital waveguide synthesis of string tones *IEEE Signal Process. Lett.* **10** 18–20

[18] Barjau A and Gibiat V 2003 Delay lines, finite differences and cellular automata: three close but different schemes for simulating acoustical propagation in 1D systems *Acta Acust. united Acust.* **88** 554–66

[19] Barjau A, Keefe D H and Cardona S 1999 Time-domain simulation of acoustical waveguides with arbitrarily spaced discontinuities *J. Acoust. Soc. Am.* **105** 1951–64

[20] Beeson M J and Murphy D T 2004 RoomWeaver: A digital waveguide mesh based room acoustics research tool *Proc. COST G6 Conf. Digital Audio Effects (Naples, Italy, October 2004)* pp 268–73

[21] Belevitch V 1962 Summary of the history of circuit theory *Proc. IRE* **50** 848–55

[22] Bensa J 2003 Analysis and synthesis of piano sounds using physical and signal models *PhD Thesis* Université de la Méditerranée, Marseille, France

[23] Bensa J, Bilbao S, Kronland-Martinet R and Smith J O 2003 A power normalized non-linear lossy piano hammer *Proc. Stockholm Music Acoustics Conf.* (*Stockholm, Sweden, 6–9 August 2003* vol I) pp 365–8

[24] Bensa J, Bilbao S, Kronland-Martinet R, Smith J O and Voinier T 2005 Computational modeling of stiff piano strings using digital waveguides and finite differences *Acta Acust. united Acust.* **91** 289–98

[25] Bensa J, Bilbao S, Kronland-Martinet R and Smith J O III 2003 The simulation of piano string vibration: from physical models to finite difference schemes and digital waveguides *J. Acoust. Soc. Am.* **114** 1095–107

[26] Bensa J, Gipouloux O and Kronland-Martinet R 2005 Parameter fitting for piano sound synthesis by physical modeling *J. Acoust. Soc. Am.* **118** 495–504

[27] Bensa J, Jensen K and Kronland-Martinet R 2004 A hybrid resynthesis model for hammer–string interaction of piano *EURASIP J. Appl. Signal Process.* **2004** 1021–35 Special issue on model-based sound synthesis

[28] Berners D and Smith J O 1994 Super-spherical wave simulation in flairing horns *Proc. Int. Computer Music Conf. (Aarhus, Denmark, 1994)* pp 112–13

[29] Bilbao S 2004 Energy-conserving finite difference schemes for tension-modulated strings *IEEE Int. Conf. on Acoustics Speech and Signal Processing (Montreal, Canada, May 2004)* pp 285–8

[30] Bilbao S 2004 *Wave and Scattering Methods for Numerical Simulation* (New York: Wiley) ISBN: 0-470-87017-6

[31] Bilbao S 2005 Time-varying generalizations of all-pass filters *IEEE Signal Process. Lett.* **12** 376–9

[32] Bisnovatyi I 2000 Flexible software framework for modal synthesis *Proc. COST G-6 Conf. on Digital Audio Effects (Verona, Italy, December 2000)* pp 109–14

[33] Borin G, De Poli G and Rocchesso D 2000 Elimination of delay-free loops in discrete-time models of nonlinear acoustic systems *IEEE Trans. Speech Audio Process.* **8** 597–605

[34] Boutillon X 1988 Model for piano hammers: experimental determination and digital simulation *J. Acoust. Soc. Am.* **83** 746–54

[35] Brandt E 2001 Hard sync without aliasing *Proc. Int. Computer Music Conf. (Havana, Cuba, September 2001)* pp 365–8

[36] Cadoz C 2002 The physical model as a metaphor for musical creation 'pico..TERA', a piece entirely generated by physical model *Proc. Int. Computer Music Conf. (Gothenburg, Sweden, 2002)* pp 305–12

[37] Cadoz C, Florens J-L and Gubian S 2001 Bowed string synthesis with force feedback gestural interaction *Proc. Int. Comput. Music Conf. (Havana, Cuba, 2001)*

[38] Cadoz C, Luciani A and Florens J-L 1983 Responsive input devices and sound synthesis by simulation of instrumental mechanisms: the CORDIS system *Comput. Music J.* **8** 60–73

[39] Cadoz C, Luciani A and Florens J-L 2003 Artistic creation and computer interactive multisensory simulation force feedback gesture transducers *NIME: Proc. Conf. on New Interfaces for Musical Expression (Montreal, Canada, May 2003)* pp 235–46

[40] Campbell M 2004 Brass instruments as we know them today *Acta Acust. united Acust.* **4** 600–10

[41] Carrier G F 1945 On the nonlinear vibration of an elastic string *Q. Appl. Math.* **3** 157–65
[42] Castagné N and Cadoz C 2002 Creating music by means of 'physical thinking': the musician oriented Genesis environment *Proc. COST G6 Conf. on Digital Audio Effects (Hamburg, Germany, September 2002)* pp 169–74
[43] Chadabe J 1997 *Electric Sound: the Past and Promise of Electronic Music* (New Jersey: Prentice-Hall)
[44] Chafe C 1995 Adding vortex noise to wind instrument physical models *Proc. Int. Computer Music Conf. (Banff, Canada, September 1995)* pp 57–60
[45] Chaigne A 1992 On the use of finite differences for musical synthesis. Application to plucked stringed instruments *J. Acoust.* **5** 181–211
[46] Chaigne A and Askenfelt A 1994 Numerical simulations of piano strings. I. A physical model for a struck string using finite difference methods *J. Acoust. Soc. Am.* **95** 1112–18
[47] Chaigne A and Askenfelt A 1994 Numerical simulations of piano strings. II. Comparisons with measurements and systematic exploration of some hammer–string parameters *J. Acoust. Soc. Am.* **95** 1631–40
[48] Chaigne A and Doutaut V 1997 Numerical simulations of xylophones. I. Time-domain modeling of the vibrating bars *J. Acoust. Soc. Am.* **101** 539–57
[49] Chaigne A, Fontaine M, Thomas O, Ferré M and Touzé C 2002 Vibrations of shallow spherical shells and gongs: a comparative study *Proc. Forum Acusticum (Sevilla, 2002)*
[50] Chaigne A and Lambourg C 2001 Time-domain simulation of damped impacted plates. Part I. Theory and experiments *J. Acoust. Soc. Am.* **109** 1422–32
[51] Chaigne A, Touzé C and Thomas O 2001 Nonlinear axisymmetric vibrations of gongs *Proc. Int. Symp. on Musical Acoustics (Perugia, 2001)*
[52] Chaigne A, Touzé C and Thomas O 2004 Mechanical models of musical instruments and sound synthesis: the case of gongs and cymbals *Proc. Int. Symp. on Musical Acoustics (Nara, Japan, 2004)*
[53] Cherniakov M 2003 *An Introduction to Parametric Digital Filters and Oscillators* (New York: Wiley) 2003 ISBN: 047085104X
[54] Chowning J 1973 The synthesis of complex audio spectra by means of frequency modulation *J. Audio Eng. Soc.* **21** 526–34
[55] Coltman J 1992 Time-domain simulation of the flute *J. Acoust. Soc. Am.* **92** 69–73
[56] Comajuncosas J M 2000 Physical models of strings and plates using a simplified mass-spring method *The Csound Book* ed R Boulanger (Cambridge: MIT Press) chapter 20 (CD-ROM)
[57] Conklin H A 1996 Design and tone in the mechanoacoustic piano. Part III. Piano strings and scale design *J. Acoust. Soc. Am.* **100** 1286–98
[58] Conklin H A 1999 Generation of partials due to nonlinear mixing in a stringed instrument *J. Acoust. Soc. Am.* **105** 536–45
[59] Cook P 1991 Identification of control parameters in an articulatory vocal tract model, with applications to the synthesis of singing *PhD Thesis* CCRMA, Stanford University
[60] Cook P 1996 Singing voice synthesis: history, current work and future directions *Comput. Music J.* **20**
[61] Cook P R 1992 A meta-wind-instrument physical model, and a meta-controller for real-time performance control *Proc. Int. Computer Music Conf. (San Jose, California, October 1992)* pp 273–6
[62] Cook P R 1995 Integration of physical modeling for synthesis and animation *Proc. Int. Computer Music Conf. (Banff, Canada, September 1995)* pp 525–8
[63] Cook P R 1997 Physically informed sonic modeling (PhISM): synthesis of percussive sounds *Comput. Music J.* **21** 38–49
[64] Cook P R 2001 SPASM: a real-time vocal tract physical model editor/controller and singer: the companion software synthesis system *Comput. Music J.* **17** 30–44
[65] Cook P R 2002 Modeling Bill's gait: analysis and parametric synthesis of walking sounds *Proc. AES 22nd Int. Conf. on Virtual, Synthetic and Entertainment Audio (Espoo, Finland, June 2002)* pp 73–8
[66] Cook P R 2002 *Real Sound Synthesis for Interactive Applications* (Wellesley: Peters A K) 2002 ISBN 1-56881-168-3
[67] Cook P R 2004 Remutualizing the musical instrument: co-design of synthesis algorithms and controllers *J. New Music Res.* **33** 315–20
[68] Cremer L 1983 *The Physics of the Violin* (Cambridge: MIT Press)
[69] Czyzewski A and Kostek B 2003 Waveguide modelling of the panpipes *Proc. Stockholm Music Acoustics Conf.* (*Stockholm, Sweden, August 2003* vol 1) pp 259–62
[70] de Bruin G and van Walstijn M 1995 Physical models of wind instruments: a generalized excitation coupled with a modular simulation platform *J. New Music Res.* **24** 148–63
[71] de la Cuadra P, Smyth T, Chafe C and Baoqiang H 2001 Waveguide simulation of neolithic Chinese flutes *Proc. Int. Symp. on Musical Acoustics (Perugia, Italy, September 2001)* pp 181–4

[72] de la Cuadra P, Vergez C and Caussé R 2002 Use of physical-model synthesis for developing experimental techniques in ethnomusicology—the case of the ouldeme flute *Proc. Int. Computer Music Conf. (Gothenburg, Sweden, 2002)* pp 53–6
[73] De Poli G and Rocchesso D 1998 Physically based sound modelling *Organised Sound* **3** 61–76
[74] Depalle P and Tassart S 1995 State space sound synthesis and a state space synthesiser builder *Proc. Int. Computer Music Conf. (Banff, Canada, September 1995)* pp 88–95
[75] Derveaux G, Chaigne A, Joly P and Bécache E 2003 Time-domain simulation of a guitar: model and method *J. Acoust. Soc. Am.* **114** 3368–83
[76] Dietz P H and Amir N 1995 Synthesis of trumpet tones by physical modeling *Proc. Int. Symp. on Musical Acoustics (Dourdan, France, 1995)* pp 472–7
[77] Ducasse E 2002 An alternative to the traveling-wave approach for use in two-port descriptions of acoustic bores *J. Acoust. Soc. Am.* **112** 3031–41
[78] Eckel G, Iovino F and Caussé R 1995 Sound synthesis by physical modelling with Modalys *Proc. Int. Symp. on Musical Acoustics (Dourdan, France, July 1995)* pp 479–82
[79] Erkut C 2001 Model order selection techniques for the loop filter design of virtual string instruments *Proc. 5th World Multi-Conf. on Systems, Cybernetics and Informatics* (*Orlando, FL, USA, July 2001* vol 10) pp 529–34
[80] Erkut C and Karjalainen M 2002 Finite difference method vs. digital waveguide method in string instrument modeling and synthesis *Proc. Int. Symp. on Musical Acoustics (Mexico City, Mexico, December 2002)* CD-ROM proceedings
[81] Erkut C and Karjalainen M 2002 Virtual strings based on a 1-D FDTD waveguide model: stability, losses, and travelling waves *Proc. AES 22nd Int. Conf. (Espoo, Finland, June 2002)* pp 317–23
[82] Erkut C, Karjalainen M, Huang P and Välimäki V 2002 Acoustical analysis and model-based sound synthesis of the kantele *J. Acoust. Soc. Am.* **112** 1681–91
[83] Erkut C, Laurson M, Kuuskankare M and Välimäki V 2001 Model-based synthesis of the ud and the Renaissance lute *Proc. Int. Computer Music Conf. (Havana, Cuba, September 2001)* pp 119–22
[84] Erkut C and Välimäki V 2000 Model-based sound synthesis of tanbur, a Turkish long-necked lute *IEEE Int. Conf. on Acoustics Speech and Signal Processing (Istanbul, Turkey, June 2000)* pp 769–772 Available online at http://lib.tkk.fi/Diss/2002/isbn95122619O1/
[85] Esquef P, Välimäki V and Karjalainen M 2002 Restoration and enhancement of solo guitar recordings based on sound source modeling *J. Audio Eng. Soc.* **50** 227–36
[86] Essl G 2002 Physical wave propagation modeling for real-time synthesis of natural sounds *PhD Thesis* Princeton University, Department of Computer Science, Princeton, NJ
[87] Essl G and Cook P R 2000 Measurements and efficient simulations of bowed bars *J. Acoust. Soc. Am.* **108** 379–88
[88] Essl G and Cook P R 2002 Banded waveguides on circular topologies and of beating modes: Tibetan singing bowls and glass harmonicas *Proc. Int. Computer Music Conf. (Gothenburg, Sweden, 2002) International Computer Music Association* pp 49–52
[89] Essl G, Serafin S, Cook P R and Smith J O 2004 Musical applications of banded waveguides *Comput. Music J.* **28** 51–63
[90] Essl G, Serafin S, Cook P R and Smith J O 2004 Theory of banded waveguides *Comput. Music J.* **28** 37–50
[91] Fabre B and Hirschberg A 2000 Physical modeling of flue instruments: a review of lumped models *Acta Acust. united Acust.* **86** 599–610
[92] Fant G 1970 *Acoustic Theory of Speech Production* (The Hague: Mouton)
[93] Fettweis A 1971 Digital filters related to classical structures *AEU: Archive für Elektronik und Übertragungstechnik* **25** 78–89
[94] Fettweis A 1986 Wave digital filters: theory and practice *Proc. IEEE* **74** 270–327
[95] Flanagan J 1972 *Speech Analysis, Synthesis and Perception* (Berlin: Springer)
[96] Fletcher N H and Rossing T D 1991 *The Physics of Musical Instruments* (New York: Springer)
[97] Fletcher N H 1999 The nonlinear physics of musical instruments *Rep. Prog. Phys.* **62** 723–64
[98] Florens J-L and Cadoz C 1991 The physical model: modeling and simulating the instrumental universe *Representations of Musical Signals* ed G De Poli *et al* (Cambridge: MIT Press) pp 227–68
[99] Fontana F 2003 Computation of linear filter networks containing delay-free loops, with an application to the waveguide mesh *IEEE Trans. Speech Audio Process.* **11** 774–82
[100] Fontana F and Rocchesso D 1998 Physical modeling of membranes for percussion instruments *Acta Acust. united Acust.* **84** 529–42
[101] Fontana F and Rocchesso D 2000 Online correction of dispersion error in 2D waveguide meshes *Proc. Int. Computer Music Conf. (Berlin, Germany, August 2000)* pp 78–81

[102] Gazengel B, Gilbert J and Amir N 1995 Time domain simulation of single-reed wind instruments. From the measured input impedance to the synthesis signal *Acta Acust.* **3** 445–72
[103] Giordano N and Jiang M 2004 Physical modeling of the piano *EURASIP J. Appl. Signal Process.* **2004** 926–33 Special issue on model-based sound synthesis
[104] Glass A and Fukudome K 2004 Warped linear prediction of physical model excitations with applications in audio compression and instrument synthesis *EURASIP J. Appl. Signal Process.* **2004** 1036–44 Special issue on model-based sound synthesis. Available online at: http://www.hindawi.com/journals/asp/volume-2004/S1110865704402078.html
[105] Guillemain P, Kergomard J and Voinier T 2005 Real-time synthesis of clarinet-like instruments using digital impedance models *J. Acoust. Soc. Am.* **118** 483–94
[106] Guillemain Ph 2004 A digital synthesis model of double-reed wind instruments *EURASIP J. Appl. Signal Process.* **2004** 990–1000 Special issue on model-based sound synthesis
[107] Hall D E 1992 Piano string excitation. VI: nonlinear modeling *J. Acoust. Soc. Am.* **92** 95–105
[108] Härmä A, Karjalainen M, Savioja L, Välimäki V, Laine U K and Huopaniemi J 2000 Frequency-warped signal processing for audio applications *J. Audio Eng. Soc.* **48** 1011–31
[109] Henry C 2004 Physical modeling for pure data (PMPD) and real time interaction with an audio synthesis *Proc. Sound and Music Computing (Paris, France, October 2004)*
[110] Henry C 2004 PMPD: physical modelling for Pure Data *Proc. Int. Computer Music Conf. (Coral Gables, Florida, November 2004)* (San Fransisco: International Computer Music Association)
[111] Hikichi T, Osaka N and Itakura F 2003 Time-domain simulation of sound production of the sho *J. Acoust. Soc. Am.* **113** 1092–101
[112] Hikichi T, Osaka N and Itakura F 2004 Sho-So-In: control of a physical model of the sho by means of automatic feature extraction from real sounds *J. New Music Res.* **33** 355–65
[113] Hiller L and Ruiz P 1971 Synthesizing musical sounds by solving the wave equation for vibrating objects: Part 1 *J. Audio Eng. Soc.* **19** 462–70
[114] Hiller L and Ruiz P 1971 Synthesizing musical sounds by solving the wave equation for vibrating objects: Part 2 *J. Audio Eng. Soc.* **19** 542–51
[115] Holm J-M and Toiviainen P 2004 A method for modeling finite width excitation in physical modeling sound synthesis of bowed strings *J. New Music Res.* **33** 345–54
[116] Howard D M and Rimell S 2004 Real-time gesture-controlled physical modelling music synthesis with tactile feedback *EURASIP J. Appl. Signal Process.* **2004** 1001–6 Special issue on model-based sound synthesis
[117] Huang P, Serafin S and Smith J O 2000 A 3-D waveguide mesh model of high-frequency violin body resonances *Proc. Int. Computer Music Conf. (Berlin, Germany, August 2000)* pp 86–9
[118] Huovilainen A 2004 Nonlinear digital implementation of the Moog ladder filter *Proc. Int. Conf. on Digital Audio Effects (Naples, Italy, October 2004)* pp 61–4
[119] Jaffe D A 1995 Ten criteria for evaluating synthesis techniques *Comput. Music J.* **19** 76–87
[120] Jaffe D A and Smith J O 1983 Extensions of the Karplus–Strong plucked-string algorithm *Computer Music J.* **7** 56–69
Also published in Roads C (ed) 1989 *The Music Machine* (Cambridge: MIT Press) pp 481–94
[121] Jordà S 2004 Instruments and players: some thoughts on digital lutherie *J. New Music Res.* **33** 321–41
[122] Järveläinen H and Tolonen T 2001 Perceptual tolerances for decay parameters in plucked string synthesis *J. Audio Eng. Soc.* **49** 1049–59
[123] Järveläinen H, Välimäki V and Karjalainen M 2001 Audibility of the timbral effects of inharmonicity in stringed instrument tones *Acoust. Res. Lett. Online* **2** 79–84
[124] Jungmann T 1994 Theoretical and practical studies on the behavior of electric guitar pick-ups *MSc Thesis* Helsinki University of Technology, Espoo, Finland
[125] Kahrs M and Avanzini F 2001 Computer synthesis of bird songs and calls *Proc. COST G6 Conf. on Digital Audio Effects (Limerick, Ireland, December 2001)* pp 23–7
[126] Kaplan S J 1981 Developing a commercial digital sound synthesizer *Comput. Music J.* **5** 62–73
[127] Karjalainen M 2002 1-D digital waveguide modeling for improved sound synthesis *IEEE Int. Conf. on Acoustics Speech Signal Processing (Orlando, FL, May 2002)* pp 1869–72
[128] Karjalainen M 2003 Mixed physical modeling techniques applied to speech production *8th European Conf. on Speech Communication and Technology (EuroSpeech 2003) (Geneva, Switzerland, 2003)* pp 2445–8
[129] Karjalainen M 2004 Discrete-time modeling and synthesis of musical instruments. *Proc. Baltic-Nordic Acoustics Meeting (Mariehamn, Finland, June 2004)* pp 1–20 Available online at: http://www.acoustics.hut.fi/asf/bnam04/webprosari/papers/i01.pdf
[130] Karjalainen M, Backman J and Pölkki J 1993 Analysis, modeling, and real-time sound synthesis of the kantele, a traditional Finnish string instrument *Proc. IEEE Int. Conf. on Acoustics, Speech and Signal Processing (Minneapolis, MN, 1993)* pp 229–32

[131] Karjalainen M and Erkut C 2004 Digital waveguides versus finite difference structures: equivalence and mixed modeling *EURASIP J. Appl. Signal Process.* **2004** 978–89

[132] Karjalainen M, Erkut C and Savioja L Compilation of unified physical models for efficient sound synthesis *Proc. ICASSP* (*Hong Kong, April 2003* vol 5) pp 433–6

[133] Karjalainen M, Esquef P A A, Antsalo P, Mäkivirta A and Välimäki V 2002 Frequency-zooming ARMA modeling of resonant and reverberant systems *J. Audio Eng. Soc.* **50** 953–67

[134] Karjalainen M and Laine U K 1991 A model for real-time sound synthesis of guitar on a floating-point signal processor *IEEE Int. Conf. on Acoustics Speech Signal Processing (Toronto, Canada, 1991)*

[135] Karjalainen M, Laine U K, Laakso T I and Välimäki V 1991 Transmission-line modeling and real-time synthesis of string and wind instruments *Proc. Int. Computer Music Conf. (Montreal, Quebec, Canada, 16–20 October 1991)* pp 293–6

[136] Karjalainen M and Mäki-Patola T 2004 Physics-based modeling of musical instruments for interactive virtual reality *Proc. Int. Workshop on Multimedia Signal Processing (Siena, Italy, September 2004)* pp 223–6

[137] Karjalainen M, Mäki-Patola T, Kanerva A, Huovilainen A and Jänis P 2004 Virtual air guitar *Proc. 117th AES Convention (San Francisco, California, 2004)*

[138] Karjalainen M and Paatero T 2005 High-resolution parametric modeling of string instrument sounds *Proc. European Signal Processing Conf. (Antalya, Turkey, 2005)*

[139] Karjalainen M and Smith J O 1996 Body modeling techniques for string instrument synthesis *Proc. Int. Computer Music Conf. (Hong Kong, 1996)* pp 232–9

[140] Karjalainen M, Välimäki V and Esquef P A A 2002 Efficient modeling and synthesis of bell-like sounds *DAFx: Proc. Int. Conf. on Digital Audio Effects (Hamburg, Germany, 2002)*

[141] Karjalainen M, Välimäki V and Esquef P A A 2003 Making of a computer carillon *Proc. Stockholm Music Acoustics Conf. (Stockholm, Sweden, 2003)*

[142] Karjalainen M, Välimäki V and Jánosy Z 1993 Towards high-quality sound synthesis of the guitar and string instruments *Proc. Int. Computer Music Conf. (Tokyo, Japan, 1993)* pp 56–63

[143] Karjalainen M, Välimäki V and Tolonen T 1998 Plucked-string models: from the Karplus–Strong algorithm to digital waveguides and beyond *Comput. Music J.* **22** 17–32

[144] Karplus K and Strong A 1983 Digital synthesis of plucked-string and drum timbres. *Computer Music J.* **7** 43–55
Also published in Roads C (ed) 1989 *The Music Machine* (Cambridge: MIT Press)

[145] Kelly J L and Lochbaum C C 1962 Speech synthesis *Proc. 4th Int. Congr. Acoustics (Copenhagen, Denmark, September 1962)* pp 1–4

[146] Kirchhoff G 1883 *Vorlesungen über Mechanik* (Leipzig: Tauber)

[147] Klapuri A 2003 Multiple fundamental frequency estimation based on harmonicity and spectral smoothness *IEEE Trans. Speech Audio Process.* **11** 804–16

[148] Klatt D 1980 Software for a cascade/parallel formant synthesizer *J. Acoust. Soc. Am.* **67** 971–95

[149] Klatt D 1987 Review of text-to-speech conversion for english *J. Acoust. Soc. Am.* **82** 737–93

[150] Kob M 2004 Analysis and modelling of overtone singing in the sygyt style *Appl. Acoust.* **65** 1249–59

[151] Kob M 2004 Singing voice modelling as we know it today *Acta Acust. united Acust.* **90** 649–61

[152] Kreyszig E 1992 *Advanced Engineering Mathematics* 7th edn (New York: Wiley) ISBN: 0471553808

[153] Krishnaswamy A and Smith J O 2003 Methods for simulating string collisions with rigid spatial objects *Proc. IEEE Workshop of Applications of Signal Processing to Audio and Acoustics, NY, USA (October 2003)* pp 233–6

[154] Laakso T I, Välimäki V, Karjalainen M and Laine U K 1996 Splitting the unit delay—Tools for fractional delay filter design *IEEE Signal Process. Mag.* **13** 30–60

[155] Lakatos S, Cook P R and Scavone G P 2000 Selective attention to the parameters of a physically informed sonic model *Acoust. Res. Lett. Online*
Lakatos S, Cook P R and Scavone G P 2000 Selective attention to the parameters of a physically informed sonic model *J. Acoust. Soc. Am.* **107** L31–6

[156] Lambourg C, Chaigne A and Matignon D 2001 Time-domain simulation of damped impacted plates. Part II. Numerical model and results *J. Acoust. Soc. Am.* **109** 1433–47

[157] Lane J, Hoory D, Martinez E and Wang P 1997 Modeling analog synthesis with DSPs *Comput. Music J.* **21** 23–41

[158] Laroche J 1989 A new analysis/synthesis system of musical signals using Prony's method—application to heavily damped percussive sounds *IEEE Int. Conf. on Acoustics Speech and Signal Processing (Glasgow, UK)* vol 3, pp 2053–6

[159] Laroche J and Meillier J-L Multichannel excitation/filter modeling of percussive sounds with application to the piano *IEEE Trans. Speech Audio Process.* **2** 329–44
[160] Laurson M, Erkut C, Välimäki V and Kuuskankare M 2001 Methods for modeling realistic playing in acoustic guitar synthesis *Comput. Music J.* **25** 38–49 Available at http://lib.hut.fi/Diss/2002/isbn9512261901/
[161] Laurson M, Norilo V and Kuuskankare M 2005 PWGLSynth: a visual synthesis language for virtual instrument design and control *Comput. Music J.* **29** 29–41
[162] Legge K A and Fletcher N H 1984 Nonlinear generation of missing modes on a vibrating string *J. Acoust. Soc. Am.* **76** 5–12
[163] Lehtonen H-M, Rauhala J and Välimäki V 2005 Sparse multi-stage loss filter design for waveguide piano synthesis *Proc. IEEE Workshop on Applications of Signal Processing to Audio and Acoustics (New Paltz, NY, October 2005)*
[164] Liljencrantz J 1985 Speech synthesis with a reflection-type vocal tract analog *PhD Thesis* Royal Institute of Technology, Stockholm, Sweden
[165] Lukkari T and Välimäki V 2004 Modal synthesis of wind chime sounds with stochastic event triggering *Proc. 6th Nordic Signal Processing Symp. (Espoo, Finland, June 2004)* pp 212–15
[166] Mackenzie J, Kale I and Cain G D 1995 Applying balanced model truncation to sound analysis/synthesis models *Proc. Int. Computer Music Conf. (Banff, Canada, September 1995)* pp 400–3
[167] Macon M W, McCree A, Lai W M and Viswanathan V 1998 Efficient analysis/synthesis of percussion musical instrument sound using an all-pole model *IEEE Int. Conf. on Acoustics Speech Signal Processing (Seattle, USA)* vol 6, pp 3589–92
[168] Marans M 1994 The next big thing *Keyboard* **20** 98–118
[169] Markel J D and Gray J H G 1976 *Linear Prediction of Speech Signals* (Berlin: Springer)
[170] Matignon D 1995 Physical modelling of musical instruments: analysis-synthesis by means of state space representations *Proc. Int. Symp. on Musical Acoustics (Dourdan, France, July 1995)* pp 497–502
[171] Matignon D, Depalle P and Rodet X 1992 State space models for wind-instrument synthesis *Proc. Int. Computer Music Conf. (San Jose California, October 1992)* pp 142–5
[172] McIntyre M E, Schumacher R T and Woodhouse J 1981 Aperiodicity in bowed-string motion *Acustica* **49** 13–32
[173] McIntyre M E, Schumacher R T and Woodhouse J 1983 On the oscillations of musical instruments *J. Acoust. Soc. Am.* **74** 1325–45
[174] McIntyre M E and Woodhouse J 1979 On the fundamentals of bowed string dynamics *Acustica* **43** 93–108
[175] Meerkötter K and Scholtz R 1989 Digital simulation of nonlinear circuits by wave digital filter principles *IEEE Proc. ISCAS '89 (New York, 1989)* (Piscataway: IEEE) pp 720–3
[176] Mitra S K 2002 *Digital Signal Processing: a Computer-Based Approach* 2nd edn (New York: McGraw-Hill)
[177] Moorer J A 1976 The synthesis of complex audio spectra by means of discrete summation formulae *J. Audio Eng. Soc.* **24** 717–27
[178] Morrison J and Adrien J M 1993 MOSAIC: a framework for modal synthesis *Comput. Music J.* **17** 45–56
[179] Morse P M and Ingard U K 1968 *Theoretical Acoustics* (Princeton: Princeton University Press)
[180] Msallam R, Dequidt S, Caussé R and Tassart S 2000 Physical model of the trombone including nonlinear effects. Application to the sound synthesis of loud tones *Acta Acust. united Acust.* **86** 725–36
[181] Msallam R, Dequidt S, Tassart S and Caussé R 1997 Physical model of the trombone including nonlinear propagation effects *Proc. Int. Symp. on Musical Acoustics (Edinburgh, Scotland)* pp 245–50
[182] Murphy D T, Newton C J C and Howard D M 2001 Digital waveguide mesh modelling of room acoustics: surround-sound, boundaries and plugin implementation *DAFx: Proc. Int. Conf. on Digital Audio Effects (Limerick, Ireland, 2001)*
[183] Srivinisa Murthy G S and Ramakrishna B S 1964 Nonlinear character of resonance in stretched strings *J. Acoust. Soc. Am.* **38** 461–71
[184] Narasimha R 1968 Non-linear vibration of an elastic string *J. Sound Vib.* **8** 134–46
[185] Nilsson J W and Riedel S A 1999 *Electric Circuits* 6th edn (Englewood Cliffs: Prentice-Hall)
[186] Pakarinen J, Karjalainen M and Välimäki V 2003 Modeling and real-time synthesis of the kantele using distributed tension modulation *Proc. Stockholm Music Acoustics Conf.* (*Stockholm, Sweden, August 2003* vol 1) pp 409–12
[187] Pakarinen J, Karjalainen M, Välimäki V and Bilbao S 2005 Energy behavior in time-varying fractional delay filters for physical modeling of musical instruments *Proc. Int. Conf. on Acoustics, Speech and Signal Processing* (*Philadelphia, PA, USA, 19–23 March 2005* vol 3) pp 1–4
[188] Pakarinen J, Välimäki V and Karjalainen M 2005 Physics-based methods for modeling nonlinear vibrating strings *Acta Acust. united Acust.* **91** 312–25

[189] Paladin A and Rocchesso D 1992 A dispersive resonator in real-time on MARS workstation *Proc. Int. Computer Music Conf. (San Jose, CA, October 1992)* pp 146–9
[190] Palumbi M and Seno L 1999 Metal string *Proc. Int. Computer Music Conf. (Beijing, China, 1999)*
[191] Paradiso J 1997 Electronic music interfaces: new ways to play *IEEE Spectrum* **34** 18–30
[192] Pavlidou M and Richardson B E 1995 The string-finger interaction in the classical guitar *Proc. Int. Symp. on Musical Acoustics (Dourdan, France, 1995)* pp 559–64
[193] Pavlidou M and Richardson B E 1997 The string–finger interaction in the classical guitar: theoretical model and experiments *Proc. Int. Symp. on Musical Acoustics (Edinburgh, UK)* pp 55–60
[194] Pearson M D 1995 TAO: a physical modelling system and related issues *Organised Sound* **1** 43–50
[195] Pearson M D 1996 Synthesis of organic sounds for electroacoustic music: cellular models and the TAO computer music program *PhD Thesis* Department of Electronics, University of York
[196] Pedersini F, Sarti A and Tubaro S 1999 Block-wise physical model synthesis for musical acoustics *Electron. Lett.* **35** 1418–19
[197] Pedersini F, Sarti A and Tubaro S 2000 Object-based sound synthesis for virtual environment using musical acoustics *IEEE Signal Process. Mag.* **17** 37–51
[198] Penttinen H, Karjalainen M, Paatero T and Järveläinen H 2001 New techniques to model reverberant instrument body responses *Proc. Int. Computer Music Conf. (Havana, Cuba, September 2001)* pp 182–5
[199] Penttinen H and Välimäki V 2004 Time-domain approach to estimating the plucking point of guitar tones obtained with an under-saddle pickup *Appl. Acoust.* **65** 1207–20
[200] Petrausch S, Escolano J and Rabenstein R 2005 A general approach to block-based physical modeling with mixed modeling strategies for digital sound synthesis *IEEE Int. Conf. on Acoustics Speech and Signal Processing* (*Philadelphia, PA, USA, March 2005* vol 3) pp 21–4
[201] Petrausch S and Rabenstein R 2005 Interconnection of state space structures and wave digital filters *IEEE Trans. Circuits Sys. II (Express Briefs)* **52** 90–3
[202] Pierce J R and Van Duyne S A 1997 A passive nonlinear digital filter design which facilitates physics-based sound synthesis of highly nonlinear musical instruments *J. Acoust. Soc. Am.* **101** 1120–6
[203] Pitteroff R and Woodhouse J 1998 Mechanics of the contact area between a violin bow and a string Part I: reflection and transmission behaviour *Acta Acust. united Acust.* 543–62
[204] Pitteroff R and Woodhouse J 1998 Mechanics of the contact area between a violin bow and a string Part II: simulating the bowed string *Acta Acust. united Acust.* 744–57
[205] Pitteroff R and Woodhouse J 1998 Mechanics of the contact area between a violin bow and a string Part III: parameter dependence *Acta Acust. united Acust.* 929–46
[206] Puckette M 1997 Pure data *Proc. Int. Computer Music Conf. (Thessaloniki, Greece, September 1997)* pp 224–7
[207] Rabenstein R and Trautmann L 2003 Digital sound synthesis of string instruments with the functional transformation method *Signal Process.* **83** 1673–88
[208] Rank E and Kubin G 1997 A waveguide model for slapbass synthesis *IEEE Int. Conf. on Acoustics Speech and Signal Processing (Munich, Germany)* pp 443–6
[209] Rauhala J, Lehtonen H-M and Välimäki V 2005 Multi-ripple loss filter for waveguide piano synthesis *Proc. Int. Computer Music Conf. (Barcelona, Spain, September 2005)*
[210] Rhaouti L, Chaigne A and Joly P 1999 Time-domain modeling and numerical simulation of a kettledrum *J. Acoust. Soc. Am.* **105** 3545–62
[211] Riionheimo J and Välimäki V 2003 Parameter estimation of a plucked string synthesis model using a genetic algorithm with perceptual fitness calculation *EURASIP J. Appl. Signal Process.* **3** 791–805 Special issue on Genetic and Evolutionary Computation for Signal Processing and Image Analysis
[212] Roads C 1996 *Computer Music Tutorial* (Cambridge: MIT Press)
[213] Rocchesso D 2004 Physically-based sounding objects, as we develop them today *J. New Music Res.* **33** 305–13
[214] Rocchesso D and Dutilleux P 2001 Generalization of a 3-D acoustic resonator model for the simulation of spherical enclosures *EURASIP J. Appl. Signal Process.* **2001** 15–26
[215] Rocchesso D and Fontana F (ed) 2003 *The Sounding Object* (Firenze: Edizioni di Mondo Estremo)
[216] Rocchesso D and Scalcon F 1996 Accurate dispersion simulation for piano strings *Proc. Nordic Acoustic Meeting (Helsinki, Finland, 1996)*
[217] Rocchesso D and Scalcon F 1999 Bandwidth of perceived inharmonicity for musical modeling of dispersive strings *IEEE Trans. Speech Audio Process.* **7** 597–601
[218] Rocchesso D and Smith J O 2003 Generalized digital waveguide networks *IEEE Trans. Speech Audio Process.* **11** 242–54
[219] Rodet X, Potard Y and Barriér J B 1984 The CHANT project: from the synthesis of the singing voice to synthesis in general *Comput. Music J.* **8** 15–31

[220] Rodet X and Vergez C 1999 Nonlinear dynamics in physical models: from basic models to true musical-instrument models *Comput. Music J.* **23** 35–49
[221] Rossing T D 1990 *Science of Sound* 2nd edn (Reading: Addison-Wesley)
[222] Rossum D 1992 Making digital filters sound analog *Proc. Int. Computer Music Conf. (San Jose, CA, October 1992)* pp 30–3
[223] Sandler M 1991 Algorithm for high precision root finding from high order lpc models *IEE Proc. I Commun. Speech Vision* **138** 596–602
[224] Sandler M 1992 New synthesis techniques for high-order all-pole filters *IEE Proc. G Circuits, Devices Sys.* **139** 9–16
[225] Sarti A and De Poli G 1999 Toward nonlinear wave digital filters *IEEE Trans. Signal Process.* **47** 1654–68
[226] Savioja L 1999 Modeling techniques for virtual acoustics *Doctoral Thesis, Report* TML-A3, Helsinki University of Technology
[227] Savioja L, Rinne T J and Takala T 1994 Simulation of room acoustics with a 3-D finite difference mesh *Proc. Int. Computer Music Conf. (Aarhus, Denmark, September 1994)* pp 463–6
[228] Savioja L and Välimäki V 2000 Reducing the dispersion error in the digital waveguide mesh using interpolation and frequency-warping techniques *IEEE Trans. Speech Audio Process.* **8** 184–94
[229] Savioja L and Välimäki V 2001 Multiwarping for enhancing the frequency accuracy of digital waveguide mesh simulations *IEEE Signal Process. Lett.* **8** 134–6
[230] Savioja L and Välimäki V 2003 Interpolated rectangular 3-D digital waveguide mesh algorithms with frequency warping *IEEE Trans. Speech Audio Process.* **11** 783–90
[231] Scavone G 1997 An acoustic analysis of single-reed woodwind instruments *PhD Thesis* Stanford University, CCRMA
[232] Scavone G and Smith J O 1997 Digital waveguide modeling of woodwind toneholes *Proc. Int. Computer Music Conf. (Thessaloniki, Greece, 1997)*
[233] Schroeder M R and Atal B S 1885 High-quality speech at very low bit rates *Proc. ICASSP (Tampa, Florida, 1885)* pp 937–40
[234] Schumacher R T 1979 Self-sustained oscillations of the bowed string *Acustica* **43** 109–20
[235] Schumacher R T 1981 Ab initio calculations of the oscillations of a clarinet *Acustica* **48** 72–85
[236] Schumacher R T and Woodhouse J 1995 Computer modelling of violin playing *Contemp. Phys.* **36** 79–92
[237] Schumacher R T and Woodhouse J 1995 The transient behaviour of models of bowed-string motion *Chaos* **5** 509–23
[238] Serafin S 2004 The sound of friction: real-time models, playability and musical applications *PhD Thesis* Stanford University
[239] Serafin S, Huang P, Ystad S, Chafe C and Smith J O III 2002 Analysis and synthesis unusual friction-driven musical instruments *Proc. Int. Comput. Music Conf. (Gothenburg, Sweden, 2002)*
[240] Serafin S and Smith J O 2001 Impact of string stiffness on digital waveguide models of bowed strings *Catgut Acoust. Soc. J.* **4** 49–52
[241] Serafin S, Smith J O and Woodhouse J 1999 An investigation of the impact of torsion waves and friction characteristics on the playability of virtual bowed strings. *Proc. IEEE Workshop of Applications of Signal Processing to Audio and Acoustics (New Paltz, NY, 1999)*
[242] Shannon C E 1948 A mathematical theory of communication *Bell Syst. Tech. J.* **27** 379–423
Shannon C E 1948 A mathematical theory of communication *Bell Syst. Tech. J.* **27** 623–56
[243] Smith J H and Woodhouse J 2000 The tribology of rosin *J. Mech. Phys. Solids* **48** 1633–81
[244] Smith J O 1983 Techniques for digital filter design and system identification with application to the violin *PhD Thesis* Stanford University, Stanford, CA
[245] Smith J O 1985 A new approach to digital reverberation using closed waveguide networks *Proc. 1985 Int. Computer Music Conf. (Vancouver, Canada, 1985)* pp 47–53
[246] Smith J O 1986 Efficient simulation of the reed-bore and bow–string mechanisms *Proc. Int. Computer Music Conf. (The Hague, Netherlands, 1986)* pp 275–80
[247] Smith J O 1987 Music applications of digital waveguides *Technical Report* STAN-M-39, CCRMA, Stanford University, CA
[248] Smith J O 1991 Waveguide simulation of non-cylindrical acoustic tubes *Proc. Int. Computer Music Conf. (Montreal, Canada, 1991)*
[249] Smith J O 1992 Physical modeling using digital waveguides *Comput. Music J.* **16** 74–91
[250] Smith J O 1993 Efficient synthesis of stringed musical instruments *Proc. Int. Computer Music Conf. (Tokyo, Japan, 1993)* pp 64–71
[251] Smith J O 1996 Physical modeling synthesis update *Comput. Music J.* **20** 44–56
[252] Smith J O 1997 Nonlinear commuted synthesis of bowed strings *Proc. Int. Computer Music Conf. (Thessaloniki, Greece, 1997)*

[253] Smith J O 1998 *Applications of Digital Signal Processing to Audio and Acoustics* chapter (Principles of digital waveguide models of musical instruments) (Dordrecht: Kluwer) pp 417–66
[254] Smith J O 2004 *Physical Audio Signal Processing: Digital Waveguide Modeling of Musical Instruments and Audio Effects* August 2004 Draft, http://ccrma.stanford.edu/~jos/pasp04/
[255] Smith J O 2004 Virtual acoustic musical instruments: review and update *J. New Music Res.* **33** 283–304
[256] Smith J O 2005 A history of ideas leading to virtual acoustic musical instruments *Proc. IEEE Workshop on Applications of Signal Processing to Audio and Acoustics (New Paltz, NY, October 2005)*
[257] Smith J O Nonlinear commuted synthesis of bowed strings *Proc. Int. Computer Music Conf. (Thessaloniki, Greece, 97)*
[258] Smith J O and Van Duyne S A 1995 Commuted piano synthesis *Proc. Int. Computer Music Conf. (Banff, Canada, September 1995)* pp 319–26
[259] Smyth T, Abel J S and Smith J O 2003 The estimation of birdsong control parameters using maximum likelihood and minimum action *Proc. Stockholm Musical Acoustics Conf. (Stockholm, Sweden, August 2003)* pp 413–16
[260] Smyth T and Smith J O 2002 The sounds of the avian syrinx—are they really flute-like? *Proc. Int. Conf. on Digital Audio Effects (Hamburg, Germany, September 2002)* pp 199–202
[261] Stelkens J and Jacobsen A 1997 Klangskulptur: Echtzeit Physical Modelling Synthese *c't: Magazin für Computer und Technik* (2) see also http://www.sonicspot.com/phymod/phymod.html
[262] Stilson T and Smith J O 1996 Alias-free digital synthesis of classic analog waveforms *Proc. Int. Computer Music Conf. (Hong Kong, China, August 1996)* pp 332–5
[263] Stoffels S 2000 Full mesh warping techniques *Proc. COST G-6 Conf. on Digital Audio Effects (Verona, Italy, December 2000)* pp 223–8
[264] Strikwerda J C 1989 *Finite Difference Schemes and Partial Differential Equations* (California: Wadsworth, Brooks & Cole)
[265] Strube H W 1982 Time-varying wave digital filters for modeling analog systems *IEEE Trans. Acoust. Speech, Signal Process.* **30** 864–8
[266] Strube H W 2000 The meaning of the Kelly–Lochbaum acoustic-tube model *J. Acoust. Soc. Am.* **108** 1850–5
[267] Strube H W 2003 Are conical segments useful for vocal-tract simulation? *J. Acoust. Soc. Am.* **114** 3028–31
[268] Sullivan C R 1990 Extending the Karplus–Strong algorithm to synthesize electric guitar timbres with distortion and feedback *Comput. Music J.* **14** 26–37
[269] Sundberg J 1991 Synthesizing singing *Representations of Musical Signals* ed G De Poli *et al* (Cambridge: MIT Press) pp 299–320
[270] Szilas N and Cadoz C 1998 Analysis techniques for physical modeling networks *Comput. Music J.* **22** 33–48
[271] Takala T, Hiipakka J, Laurson M and Välimäki V 2000 An expressive synthesis model for bowed string instruments *Proc. Int. Computer Music Conf. (Berlin, Germany, August 2000)* pp 70–3
[272] Testa I, Evangelista G and Cavaliere S 2004 Physically inspired models for the synthesis of stiff strings with dispersive waveguides *EURASIP J. Appl. Signal Process.* **2004** 964–77 Special issue on model-based sound synthesis
[273] Tolonen T, Erkut C, Välimäki V and Karjalainen M 1999 Simulation of plucked strings exhibiting tension modulation driving force *Proc. Int. Computer Music Conf. (Beijing, China, October 1999)* pp 5–8
[274] Tolonen T, Valimaki V and Karjalainen M 1998 *Evaluation of Modern Sound Synthesis Methods* Report 48 Helsinki University of Technology, Laboratory of Acoustics and Audio Signal Processing, Espoo, Finland Available online at http://www.acoustics.hut.fi/publications/
[275] Tolonen T, Välimäki V and Karjalainen M 2000 Modeling of tension modulation nonlinearity in plucked strings *IEEE Trans. Speech Audio Process.* **8** 300–10
[276] Traube C and Depalle P 2003 Extraction of the excitation point location on a string using weighted least-square estimation of a comb filter delay *Proc. Int. Conf. on Digital Audio Effects (London, UK, September 2003)* pp 188–91
[277] Traube C and Smith J O 2000 Estimating the plucking point on a guitar string *Proc. COST G-6 Conf. on Digital Audio Effects (Verona, Italy, December 2000)* pp 153–8
[278] Trautmann L and Rabenstein R 1999 Digital sound synthesis based on transfer function models *Proc. IEEE Workshop of Applications of Signal Processing to Audio and Acoustics (New Paltz, New York, October 1999)* pp 83–6
[279] Trautmann L and Rabenstein R 2003 *Digital Sound Synthesis by Physical Modeling Using the Functional Transformation Method* (New York: Kluwer Academic/Plenum)
[280] Trautmann L and Rabenstein R 2004 Multirate simulations of string vibrations including nonlinear fret-string interactions using the functional transformation method *EURASIP J. Appl. Signal Process.* **2004** 949–63
[281] Vail M 1993 *Vintage Synthesizers* (San Francisco: Miller Freeman Books)

[282] Valette C 1995 The mechanics of vibrating strings *Mechanics of Musical Instruments* ed A Hirschberg *et al* (Berlin: Springer) pp 115–83
[283] Välimäki V 1995 Discrete-time modeling of acoustic tubes using fractional delay filters *PhD Thesis* Helsinki University of Technology, Espoo, Finland
[284] Välimäki V 2004 Physics-based modeling of musical instruments *Acta Acust. united Acust.* **90** 611–17
[285] Välimäki V 2005 Discrete-time synthesis of the sawtooth waveform with reduced aliasing *IEEE Signal Process. Lett.* **12** 214–17
[286] Välimäki V, Huopaniemi J, Karjalainen M and Jánosy Z 1996 Physical modeling of plucked string instruments with application to real-time sound synthesis *J. Audio Eng. Soc.* **44** 331–53
[287] Välimäki V and Karjalainen M 1994 Digital waveguide modeling of wind instrument bores constructed of conical bores *Proc. Int. Computer Music Conf. (Aarhus, Denmark, 1994)* pp 423–30
[288] Välimäki V, Karjalainen M, Jánosy Z and Laine U K 1992 A real-time DSP implementation of a flute model *IEEE Int. Conf. on Acoustics Speech and Signal Processing* (*San Francisco, California, 23–26 March 1992* vol 2) pp 249–52
[289] Välimäki V, Karjalainen M and Kuisma T 1994 Articulatory speech synthesis based on fractional delay waveguide filters *Proc. IEEE Int. Conf. on Acoustics, Speech and Signal Processing (Adelaide, Australia, 1994)* pp 585–8
[290] Välimäki V, Karjalainen M and Laakso T I 1993 Modeling of woodwind bores with fingerholes *Proc. Int. Computer Music Conf. (Tokyo, Japan, 1993)* pp 32–9
[291] Välimäki V, Laakso T I, Karjalainen M and Laine U K 1992 A new computational model for the clarinet *Proc. Int. Computer Music Conf. (San Jose, California, October 1992)*
[292] Välimäki V, Laurson M and Erkut C 2003 Commuted waveguide synthesis of the clavichord *Comput. Music J.* **27** 71–82
[293] Välimäki V, Penttinen H, Knif J, Laurson M and Erkut C 2004 Sound synthesis of the harpsichord using a computationally efficient physical model *EURASIP J. Appl. Signal Process.* **7** 934–48 Special Issue on Model-Based Sound Synthesis
[294] Välimäki V and Takala T 1996 Virtual musical instruments—Natural sound using physical models *Organised Sound* **1** 75–86
[295] Välimäki V and Tolonen T 1998 Development and calibration of a guitar synthesizer *J. Audio Eng. Soc* **46** 766–78
[296] Välimäki V, Tolonen T and Karjalainen M Signal-dependent nonlinearities for physical models using time-varying fractional delay filters *Proc. Int. Computer Music Conf. (Ann Arbor, MI, October 1998)* pp 264–7
[297] Van Duyne S A 1997 Coupled mode synthesis *Proc. Int. Computer Music Conf. (Thessaloniki, Greece, September 1997)* pp 248–51
[298] Van Duyne S A, Pierce J R and Smith J O 1994 Traveling-wave implementation of a lossless mode-coupling filter and the wave digital hammer *Proc. Int. Computer Music Conf. (Aarhus, Denmark, 1994)* pp 411–18
[299] Van Duyne S A and Smith J O 1993 Physical modeling with the 2-D digital waveguide mesh *Proc. Int. Computer Music Conf. (Tokyo, Japan, 1993)* pp 40–7
[300] Van Duyne S A and Smith J O 1994 A simplified approach to modeling dispersion caused by stiffness in strings and plates *Proc. Int. Computer Music Conf. (Aarhus, Denmark, 1994)* pp 335–43
[301] Van Duyne S A and Smith J O 1995 Developments for the commuted piano *Proc. Int. Computer Music Conf. (Banff, Canada, September 1995)* pp 335–43 Available on-line at http://www-ccrma.stanford.edu/∼jos/pdf/svd95.pdf
[302] Van Duyne S A and Smith J O 1995 The tetrahedral digital waveguide mesh *Proc. IEEE Workshop on Applications of Signal Processing to Audio and Acoustics (New Paltz, NY, 1995)* pp 463–6
[303] van Walstijn M 2002 Discrete-time modelling of brass and woodwind instruments with application to musical sound synthesis *PhD Thesis* Unversity of Edinburgh, Faculty of Music, Edinburgh, UK
[304] van Walstijn M and Campbell M 2003 Discrete-time modeling of woodwind instrument bores using wave variables *J. Acoust. Soc. Am.* **113** 575–85
[305] van Walstijn M and Scavone G P 2000 The wave digital tonehole model *Proc. Int. Computer Music Conf. (Berlin, Germany, 2000)* pp 465–8
[306] van Walstijn M and Smith J O 1998 The use of truncated infinite impulse response TIIR filters in implementing efficient digital waveguide models of flared horns and piecewise conical bores with unstable one-pole filter elements *Proc. Int. Symp. on Musical Acoustics (Leavenworth, Washington, 1998)* pp 309–14
[307] van Walstijn M and Välimäki V 1997 Digital waveguide modeling of flared acoustical tubes *Proc. Int. Computer Music Conf. (Thessaloniki, Greece, 1997)* pp 196–9

[308] Vercoe B L, Gardner W G and Scheirer E D 1998 Structured audio: creation, transmission and rendering of parametric sound representations *Proc. IEEE* **86** 922–40
[309] Verge M-P 1995 Aeroacoustics of confined jets with applications to the physical modeling of recorder-like instruments *PhD Thesis* Technische Universiteit Eindhoven and Université du Maine
[310] Verge M-P, Hirschberg A and Caussé R 1997 Sound production in recorderlike instruments. II. A simulation model *J. Acoust. Soc. Am.* **101** 2925–39
[311] Vergez C, Almeida A, Caussé R and Rodet X 2003 Toward a simple physical model of double-reed musical instruments: influence of aero-dynamical losses in the embouchure on the coupling between the reed and the bore of the resonator *Acta Acust. united Acust.* **89** 964–73
[312] Vergez C and Rodet X 1997 Model of the trumpet functioning: real time simulation and experiments with artificial mouth *Proc. Int. Symp. on Musical Acoustics (Edinburgh, Scotland, 1997)* pp 425–32
[313] Vergez C and Rodet X 2000 Dynamic systems and physical models of trumpet-like instruments. Analytical study and asymptotical properties *Acta Acust. united Acust.* **86** 147–62
[314] Vergez C and Rodet X 2000 A new algorithm for nonlinear propagation of sound wave—Application to a physical model of a trumpet *J. Signal Process.* **4** 79–88
[315] Wanderley M M and Depalle P Gestural control of sound synthesis *Proc. IEEE* **92** 632–44
[316] Winham G and Steiglitz K 1970 Input generators for digital sound synthesis *J. Acoust. Soc. Am.* **47** 665–6
[317] Woodhouse J 1993 On the playability of violins: Part 1. Reflection functions *Acustica* **78** 125–36
[318] Woodhouse J 2003 Bowed string simulation using a thermal friction model *Acta Acust. united Acust.* **89** 355–68
[319] Woodhouse J 2004 On the synthesis of guitar plucks *Acta Acust. united Acust.* **90** 928–44
[320] Woodhouse J 2004 Plucked guitar transients: comparison of measurements and synthesis *Acta Acust. united Acust.* **90** 945–65
[321] Woodhouse J and Galluzzo P M 2004 The bowed string as we know it today *Acta Acust. united Acust.* **90** 579–89
[322] Zadeh L A and Desoer C A 1963 *Linear System Theory: the State Space Approach (Series in system science)* (New York: McGraw-Hill)